Charles University

Faculty of Science

Study programme: Biology

Branch of study: Cell and Developmental Biology

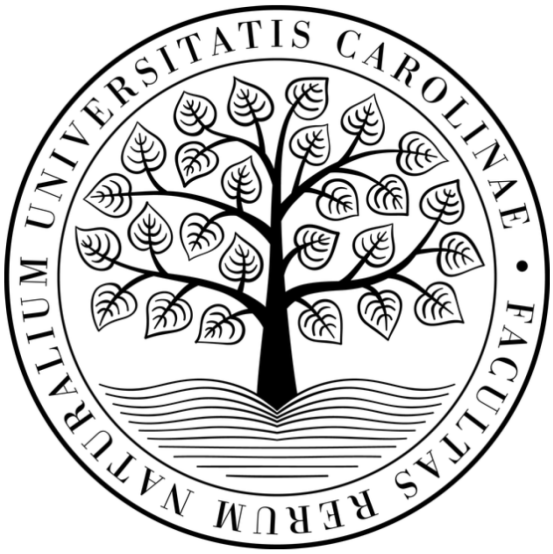

Bc. Ivan Šonský

Modulation of Mitophagy in Huntington Disease
Modulace mitofagie u Huntingtonovy choroby

Diploma thesis

Supervisor: RNDr. Hana Hansíková, CSc.

Consultant: Mgr. Vodička Petr, Ph.D.

Prague, 2022

Prohlášení:

Prohlašuji, že jsem závěrečnou práci zpracoval samostatně a že jsem uvedl všechny použité informační zdroje a literaturu. Tato práce ani její podstatná část nebyla předložena k získání jiného nebo stejného akademického titulu.

V Praze, 04.08.2022

Podpis

Acknowledgment

Foremost, I would like to thank my supervisor, RNDr. Hana Hansíková, CSc., for her time, support, and her advising. Next, I would like to express gratitude to my colleagues, namely then Nikol Volfová and Lucie Zdražilová, who supported me, while I was learning new methods, and without whom I wouldn't be able to finish this thesis. I would also like to thank my consultant Mgr. Vodička Petr, Ph.D. for his insight. Lastly, this endeavor would not have been possible without the support of my family, especially my fiancée.

This project was supported by research grant from the Ministry of Health of the Czech Republic (MZ CR AZV NU20-04-00136).

Abstract

Huntington diseases (HD) is a hereditary neurodegenerative disorder characterized by the presence of the aggregation prone mutated version of protein huntingtin (HTT). Mutation in huntingtin (mHTT) results in an aberrant expansion of the polyglutamine tract, thereby gaining toxic properties, which causes progressive loss of striatal medium spiny neurons. Neurons heavily rely on a healthy mitochondrial pool. Thereby, it is crucial to preserve biological mechanisms maintaining its turnover and quality control, such as mitophagy. However, mHTT impairs mitophagy, therefore preventing autophagosomes from engulfing mitochondria and resulting in an accumulation of dysfunctional mitochondria.

Our recent results showed that mHTT-caused mitochondrial impairments can be observed in more easily accessible extraneuronal cells such as skin fibroblasts. While mitophagy is considered a fundamental cellular process, there is a lack of compounds selectively modulating mitophagy. Thereby, the aim of this diploma thesis was to introduce a small-molecule compound, MIND4-17, which showed neuroprotective effects in HD, and to study its selective effect on mitophagy in cultivated fibroblasts from HD patients and controls.

Here we report that MIND4-17 increased the expression of specific autophagy markers in fibroblasts from HD patients, thereby allowing to bypass the perturbation of mitophagy caused by mHTT. MIND4-17 represents a pharmacological tool that could contribute to the investigation of mitophagy in HD.

Keywords: Mitophagy, mitochondrial quality control, Huntington disease, mHTT, NRF2, ARE, SQSTM1/p62

Abstrakt

Huntingtonova choroba (HD) je dědičné neurodegenerativní onemocnění charakterizované přítomností špatně se skládajícího mutovaného proteinu huntingtinu (HTT), který je náchylný k agregaci. Mutace v proteinu huntingtinu (mHTT) vede k nadměrnému prodloužení polyglutaminového řetězce, což způsobuje jeho toxicitu. Přítomnost mHTT následně vede k postupné ztrátě striatálních „medium spiny" neuronů. Správná funkce neuronů mj. závisí na stavu jejich mitochondrií. Je proto důležité, aby zůstaly zachovány biologické procesy, které zajišťují obrat a kontrolu kvality mitochondrií. Takovým procesem je především mitofagie. Mutovaný HTT má negativní dopad na mitofagii, což znemožňuje autofagozómům pohlcování mitochondrií a vede tak k akumulaci poškozených mitochondrií u HD. I když je mitofagie považována za základní buněčný proces, nejsou zatím známy téměř žádné látky, které by mitofagii specificky ovlivňovaly. Naše předchozí studie ukázaly, že mitochondriální defekty spojené s HD můžeme sledovat i ve snáze dostupných extraneuronálních tkáních, jakými jsou kožní fibroblasty.

Cílem předkládané práce bylo studovat mitofagii na modelu kultivovaných kožních fibroblastů od pacientů s HD a kontrol a testovat použití neuroprotektivní látky MIND4-17 pro selektivní ovlivnění mitofagie.

Výsledky práce ukázaly, že látka MIND4-17 mění expresi vybraných proteinů účastnících se dílčích kroků mitofagie a tím zvyšuje její míru, přičemž nedochází k negativnímu ovlivnění funkce mitochondrií. MIND4-17 představuje vhodný farmakologický nástroj ke studiu mitofagie s potencionálním využitím při hledání nových terapií u HD.

Klíčová slova: Mitofagie, kvalita kontroly mitochondrií, Huntingtonova choroba, mHTT, NRF2, ARE, SQSTM1/p62

Table of Contents

List of abbreviations

ARE	antioxidant response element
Atg	autophagy-related protein
BDNF	brain-derived neurotrophic factor
BNIP3	BCL2/adenovirus E1B 19 kDa protein-interacting protein 3
BNIP3L	BCL2 Interacting Protein 3 Like
CAG	cytosine-adenine-guanosine
CCCP	Carbonyl cyanide m-chlorophenyl hydrazone
CL	cardiolipin
DBH2	ubiquinol
DRP1	dynamin-1-like protein
DTNB	(5,5-dithio-bis-(2-nitrobenzoic acid)
ECAR	extracellular acidification ratio
HD	Huntington disease
HIP	HTT-interacting protein
HSF	human skin fibroblasts
HSF1	heat shock transcription factor 1
HTT	huntingtin protein
iFBS	inactivated fetal bovine serum
IMM	inner mitochondrial membrane
KEAP1	Kelch-like ECH-associated protein 1
LC3	microtubule-associated protein light chain 3
LIR	LC3 interacting region
L-OPA1	long, membrane bound version of OPA1
MFN 1 and 2	mitofusin 1 and 2
mHTT	mutated huntingtin protein
mTORC1	mammalian target of rapamycin complex 1
MTS	mitochondrial targeting sequence
NADH	Nicotinamide adenine dinucleotide
NDP52	nuclear dot protein 52 kDa
NEMO	NFκB essential modulator
NRF1	Nuclear Respiratory Factor 1
NRF2	Nuclear factor erythroid 2-related factor 2
NRP	NEMO related protein
OCR	oxygen consumption ratio
OMM	outer mitochondrial membrane
OPA1	optic atrophy 1
OPTN	optineurin
EGFP	enhanced green fluorescent protein
EM	electron microscopy
ER	endoplasmic reticulum
ERES	ER exit site
ETC	electron transport chain
FIS1	mitochondrial fission 1
FUNDC1	FUN14 Domain Containing 1
GABARAP	gamma aminobutyric acid receptor-associated protein
GAPDH	glyceraldehyde-3-phosphate dehydrogenase
HAP1	HTT-associated protein 1
HAP40	HTT-associated protein 40
HB299/PMI	p62-mediated mitophagy inducer
p53	Cellular tumor antigen p53
PARL	Presenilins-associated rhomboid like
PAS	phagophore assembly site
PE	phosphatidylethanolamine
PGC1α	peroxisome proliferator-activated receptor gamma coactivator 1α
PI3K	phosphatidylinositol 3-kinase
PINK1	PTEN-induced putative kinase 1
polyQ	polyglutamine
PPI	protein-protein interaction
PrP	Prion protein
ROS	reactive oxygen species
SDS-PAGE	sodium dodecyl sulfate–polyacrylamide gel electrophoresis
SFN	sulforaphane
S-OPA1	short form generated by cleavage of L-OPA1
SQSTM1/p62	sequestosome 1
BAC	bacterial artificial chromosome
TIM	translocase of the inner membrane
TNFα	tumor necrosis factor α
TOM	translocase of the outer membrane
TOR	target of rapamycin
UBA	ubiquitin-associated domain
UBL	ubiquitin-like domain

ULK1	UNC-51-like kinase 1	YAC	yeast artificial chromosome
UPS	ubiquitin-proteasome system	ΔΨm	mitochondrial membrane potential
WT	wild-type		

Introduction

1 Huntington Disease

Huntington disease (HD) is an autosomal dominant disease, which is clinically characterized by motor dysfunction accompanied by behavioral and cognitive decline. The disease is caused by an aberrant expansion of the cytosine-adenine-guanosine (CAG) trinucleotide repeat encoding a polyglutamine (polyQ) tract in the N-terminal part of the huntingtin (HTT) protein (MacDonald et al., 1993). Such elongated polyQ tract confers toxic gains of function and predisposes the protein to fragmentation and aggregation, leading to preferential atrophy and progressive loss of GABAergic medium spiny neurons in the striatum, and to a lesser extent, it also affects other regions, such as the cerebral cortex, which is affected mainly in later stages (Albin et al., 1990; Kowall et al., 1987).

There is a clear relationship between the CAG repeat length and the clinical phenotype. Huntingtin gene, which carries 36-39 repeats may lead to disease development, as the gene generates an aggregation prone misfolded HTT (mutant HTT, mHTT). However, if the gene carries more than 39 repeats, the mutation gets highly penetrant, thereby increasing the probability of disease manifestation (Rubinsztein et al., 1993).

Ultimately, HD results in death approximately 15 years after the onset of the first diagnosable symptoms, which usually get manifested at the age of 35-40 years. However, as the concentration threshold required for the aggregation of huntingtin protein decreases with the length of polyQ tract increasing, juvenile form of HD can be observed in individuals carrying longer CAG expansions (≥56 CAG) (Craufurd and Dodge, 1993; Tabrizi et al., 2022).

1.1 Huntingtin Protein

The HD locus is situated in chromosome 4p16.3 region and encodes a large protein of about 350 kDa. HTT is ubiquitously expressed throughout the whole body. However, its expression levels vary across different tissues depending on cell type. The protein can be found either in the nucleus and cytoplasm and can shuttle between these two compartments, depending on its form. While several physiological functions of HTT have been implied, the whole function of the protein has not yet been fully elucidated, as such a large protein comprises numerous points of interaction with other proteins. Having so many interactions results in many physiological functions being affected by the presence of mHTT. However, it is not the loss of physiological

functions, but the gain of toxicity represented by the polyQ stretch, which is generally believed to be the determining factor in the disease progression (Ikeda et al., 1996; Mangiarini et al., 1996; Ordway et al., 1997).

Although the physiological functions of HTT are still being uncovered, some of them have already been well defined, such as its determining role in the development of nervous system caused by the influence of HTT on the production and transport of brain-derived neurotrophic factor (BDNF) (Zuccato et al., 2001).

1.2 Impaired Mitochondria Play a Key Role in the HD Pathogenesis

Mitochondria have been described as a key regulator in a broad spectrum of pathways included in cellular homeostasis and aging ranging from cellular senescence to telomere maintenance and apoptosis (Sun et al., 2016). However, decline in mitochondrial function is well recognized as a contributing aspect in many neurodegenerative diseases, including Alzheimer's disease, Parkinson's disease, and HD.

Neurons have exceptionally high demand for energy in form of generated ATP, which is required to maintain mitochondrial membrane potential ($\Delta\Psi m$) and ion gradients, to generate synaptic vesicles, and for axonal transport. These features make neurons particularly vulnerable to mitochondrial damage.

In the past, various lines of evidence indicated that mitochondrial dysfunction plays a crucial role in the HD pathogenesis (Lin and Beal, 2006). While wild-type HTT even exhibits anti-apoptotic behavior, mHTT affects mitochondria on various levels (Fig. 1) (Rigamonti et al., 2000).

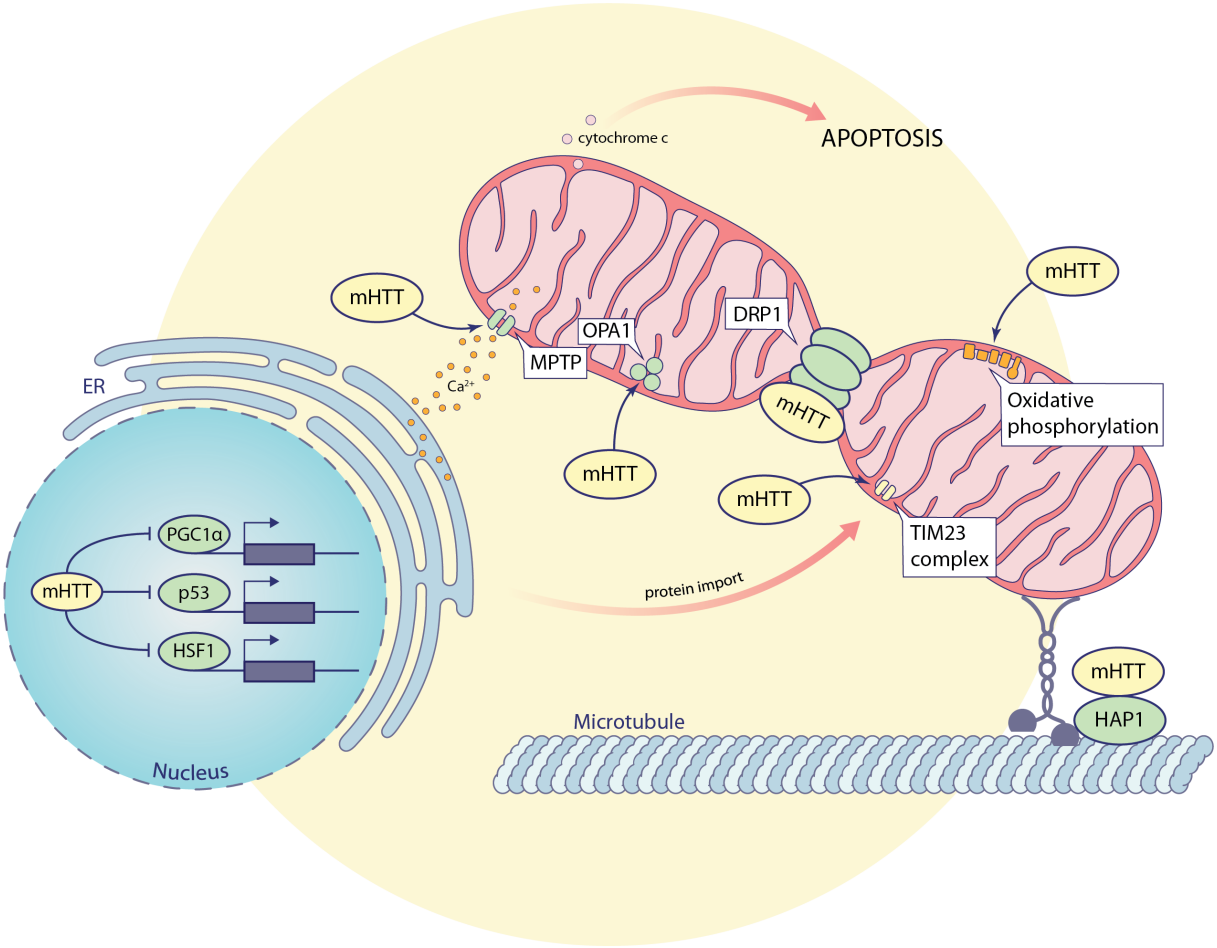

Fig. 1. A graphic summary showing negative impact of mutated huntingtin (mHTT) at various levels resulting in mitochondrial impairment. In Huntington disease, mHTT affects: oxidative phosphorylation, calcium handling, cristae morphology, dynamic processes fusion and fission, transport of mitochondria, import of proteins into mitochondria, and cell death. DRP1 – dynamin-related protein 1, ER – endoplasmic reticulum, HAP1 – huntingtin-associated protein 1, HSF - heat shock transcription factor 1, mHTT – mutant huntingtin, MPTP – mitochondrial permeability transition pore, p53 – cellular tumor antigen p53, PGC1α – peroxisome proliferator-activated receptor gamma, coactivator 1 alpha. Image taken from Sonsky et al., 2021 (Šonský et al., 2021).

1.2.1 Respiratory Chain

Magnetic resonance spectroscopy of brain showed marked decrease in glucose metabolism, whilst the corresponding production of lactate was increased in basal ganglia and the cerebral cortex of HD patients and HD mice model, pointing towards a bioenergetic defect (Jenkins et al., 2005; Koroshetz et al., 1997). Indeed, measurements in human *post mortem* brain tissue samples exhibited lower functionality of mitochondrial respiratory complexes II, III, and IV

(Gu et al., 1996). In addition, cases of selective loss of complex II/III activity in the brains of patients who died from HD have been described. Moreover, there is evidence suggesting that oxidative phosphorylation deficit occurs even in asymptomatic mutation carriers (Saft et al., 2005). Additional information supportive for the concept that respiratory-chain inhibition plays a crucial role in the pathogenesis of HD stems from studies that administered complex II inhibitors either locally, or systematically. Such application accurately replicated the pathology of HD (Beal et al., 1993; Brouillet et al., July 18; Tabrizi et al., 1999). Besides, an overexpression of Ip or Fp subunit restored complex II activity and acted protectively against Htt171-82Q-induced cell death in striatal neurons (Benchoua et al., 2006).

1.2.2 Calcium Handling

Another important role of mitochondria is Ca^{2+} buffering and thereby controlling concentration of cytoplasmic Ca^{2+} concentrations after neurotransmission (Budd and Nicholls, 1996). Lymphoblast mitochondria from HD patients had a lower membrane potential and required lower calcium loads for depolarization than control cells, possibly due to the interaction of mHTT and mitochondria. Similar results were observed in mitochondria from YAC72 mouse brain, where the defect preceded pathological and behavioral anomalies by a margin of several months (Panov et al., 2002).

1.2.3 Trafficking

Another major contribution to the pathology of HD arises from insufficient distribution of mitochondria in neurons, which is, in general, caused by impaired mitochondrial trafficking along axons and dendrites. Medium spiny neurons are polarized cells with long projections and might therefore be more susceptible to trafficking defects. In healthy neurons, mitochondria arrange into filamentous structures varying in length (~2–25 μm), which move along microtubules, either anterogradely – in the direction from cell body – or retrogradely – in the direction towards the cell body. Such trafficking is secured by ATP-dependent motor proteins. Anterograde movement is regulated by kinesins, and retrograde movement is regulated by dynein-dynactin complex (Hollenbeck and Saxton, 2005).

HTT interacts with several proteins involved in axonal transport, secretion, and endocytosis, such as adaptin, HTT-interacting protein (HIP), HTT-associated proteins (HAP), endophilin 3, dynamin, and clathrin (Borrell-Pagès et al., 2006; Kaltenbach et al., 2007; Li et al., 1995; Pal et al., 2006; Sittler et al., 1998; Wanker, 2002). A rescue experiment performed on human HD fibroblasts and STHdhQ^{111} mouse striatal cells showed that mHTT causes alterations in early endosome motility due to upregulation of HAP40. HTT-HAP40 complex is a direct

downstream effector of a key regulator of endocytosis, Rab5. HAP40 upregulation leads to the displacement of early endosomes from microtubules and their preferential association with actin filaments, thereby causing reduced motility (Pal et al., 2006). Furthermore, HTT was shown to induce axonal transport in neurons by linking vesicles with $p150^{Glued}$ dynactin subunit via HAP1. However, the polyQ within mHTT induces transport deficits by disrupting the dynein motor complex, which results in the reduced transport of BDNF and increased vulnerability of striatal neurons to death (Gauthier et al., 2004). In the presence of mHTT, HAP1 interacts with $p150^{Glued}$ with increased strength, leading to a displacement of molecular motors from microtubules and halting of transport (Gunawardena et al., 2003). Importantly, HTT together with HAP1 were identified as regulators of autophagosome transport. However, mHTT has stronger association with HAP1 than HTT, affecting fusion of autophagosome and lysosome (Li et al., 1995; Wong and Holzbaur, 2014). Furthermore, fragments of HTT N-terminus form aggregates. These aggregates accumulate and physically block the transport of organelles, such as mitochondria (Borrell-Pagès et al., 2006).

1.2.4 Dynamics

Another key aspect underlying efficient distribution of mitochondria is the fact that mitochondria are exceptionally dynamic organelles. In neurons, as well as in many other cell types, mitochondria can be observed as short tubular structures, which move, divide, and fuse, thus forming an interconnected network (Kageyama et al., 2011). This dynamic remodeling of mitochondria is achieved by balancing two opposing forces – fusion and fission. The primary intention behind these two processes is to regulate organelle size, shape, number, as well as the beforementioned distribution (Itoh et al., 2013; Knott and Bossy-Wetzel, 2008).

Fusion and fission are regulated by evolutionary conserved, large GTPases of the dynamin family of proteins. Fission is mainly regulated by the dynamin-related protein 1 (DRP1), which is mostly localized in the cytoplasm, but a small part shuttles to the outer mitochondrial membrane (OMM), thus facilitating mitochondrial division. Like dynamin, Dynamin 1 (Dnm1), yeast DRP1 ortholog, assembles into ring and spiral-shaped multimeric complexes, which enables lipid membrane constriction. This postulated model also applies to DRP1, suggesting that DRP1 forms rings or spirals, which surround the OMM with the help of mitochondrial fission 1 protein (FIS1) and other cofactors (Ingerman et al., 2005). While Fis1 is essential for mitochondrial fission in yeast, knockdown of FIS1 in HeLa cells did not interfere with the localization of DRP1 to mitochondria (Lee et al., 2004). However, some data suggest

that FIS1 directly interacts with DRP1 and plays a role in the regulation of excessive fission induced by oxidative stress (Qi et al., 2013).

In contrast to fission, mitochondrial fusion requires machinery for both the fusion of inner and outer membrane. This machinery consists of three major participators – also from the family of GTPase proteins – two OMM-localized proteins Mitofusin 1 and 2 (MFN1 and 2) and one inner mitochondrial membrane (IMM) localized protein optic atrophy 1 (OPA1) (Chen et al., 2003; Olichon et al., 2002). Another role of OPA1 is the maintenance of cristae microarchitecture (Pernas and Scorrano, 2016). OPA1 exists in two major isoforms, long and short. The long form OPA1 (L-OPA1) contains a transmembrane domain, which anchors it in the IMM. The short form (S-OPA1) is produced by proteolytic processing of L-OPA1, where the transmembrane domain is detached.

Cardiolipin (CL) is a mitochondria-specific phospholipid, which acts as a specific binding site for L-OPA1. Moreover, CL has been shown to be involved in mitochondrial fission, where it stimulates the oligomerization of DRP1 and oligomerization induced GTP hydrolysis (Ban et al., 2018, 2017; Kameoka et al., 2018). Moreover, both HTT and mHTT bind directly to CL. Mutant huntingtin binds with increased affinity, which may contribute to the HD pathogenesis (Kegel et al., 2009).

HTT was described to have interactions with many components of the fusion and fission machinery. Expression levels of several of these proteins were altered in post mortem brain tissue of HD patients, possibly due to interaction with mHTT. While the expression of OPA1, TOMM40, MFN1, and MFN2 was decreased, the expression of DRP1 and FIS1 was increased (Shirendeb et al., 2011). Furthermore, Shirendeb et al. also described the direct interaction of mHTT (but not HTT) and DRP1 in BACHD mouse model (Shirendeb et al., 2012). These interactions may explain the impairment of mitochondrial fusion/fission machinery often observed as the fragmentation of mitochondrial networks in HD cell lines.

1.2.5 Protein Import

Human mitochondria contain about 1500 different proteins. While majority of these proteins is expressed on the cytosolic ribosomes, about 1% of the proteins is still expressed on ribosomes in the matrix. Mitochondrial proteins synthesized in the matrix were most probably derived from the prokaryotic ancestor of mitochondria and are essential for the function of mitochondria, as these proteins represent components of the oxidative phosphorylation

machinery (Pagliarini et al., 2008). Thereby, the rest, which is expressed in cytosol, remains to be translocated into mitochondria. This protein import relies on a system of mitochondrial complexes, which consist of translocases of the outer membrane (TOM) and translocases of the inner membrane (TIM) (Chacinska et al., 2009).

Cells from presymptomatic R6/2 HD mice and grade 2 HD patients exhibited protein import defect, which was caused by the interaction of mHTT and TIM23. In addition, inhibition of mitochondrial protein import in primary neurons triggered neuronal death, and the augmentation of mitochondrial import rescued neurons from mHTT-induced death (Yano et al., 2014).

1.2.6 Transcriptional dysregulation

In the past, mHTT was reported to cause dysregulation of transcription through interference with transcription factors, occupation of promoters, and by direct binding to DNA (Benn et al., 2008; Steffan et al., 2000). In contrast to HTT, mHTT in addition to being found in the cytosol can also be found in the nucleus (Cha, 2000). Mutant HTT was shown to repress the transcription of the PGC-1α gene by interfering with the CREB/TAF4-dependent transcriptional pathway, which is important for the modulation of PGC-1α gene expression (Cui et al., 2006). The PGC1-α co-activator is a key player in the transcriptional control of mitochondrial biogenesis and respiratory function, as it targets several transcriptional factors, such as NRF-1 and NRF-2 among others (Scarpulla, 2011).

HTT is also involved in cell survival and apoptotic signaling. HTT prevents cell death by desensitizing cells to a variety of pro-apoptotic stimuli, such as serum withdrawal, death receptors, and pro-apoptotic Bcl-2 homologs (Rigamonti et al., 2000). However, mHTT makes neuronal cells more susceptible to cell death by increasing transcriptional activity and nuclear levels of p53 (Bae et al., 2005). Furthermore, mHTT mitigates p53 binding to DRP1, which induces DRP1-mediated mitochondrial and neuronal damage (Guo et al., 2013). Evidence also suggests that p53 can regulate autophagic activity and specifically mitophagy (Wang et al., 2014).

So far, the dysregulation of these two previously mentioned transcription factors has been thoroughly studied in HD, mainly for their participation in mitochondrial impairment, apoptosis, and neurodegeneration (Oliveira, 2010). Recently, a novel role for Heat Shock transcription Factor 1 (HSF1) as a converging mechanism that integrates responses mediated by both PGC1-α and p53 has been proposed. However, levels of HSF1 and its activity are

heavily reduced in cell and mouse models of HD, as well as in the striatum of patients with HD (Chafekar and Duennwald, 2012; Gomez-Pastor et al., 2017; Hay et al., 2004; Labbadia et al., 2011; Maheshwari et al., 2014; Riva et al., 2012). HSF1 has been previously linked to mitochondrial dysfunctions and PGC-1α expression. It is thereby possible that the depletion of HSF1 could be a contributing factor to impairment of PGC-1a expression in HD (Intihar et al., 2019).

1.3 Related Diseases

The deposition of misfolded aggregated proteins is a common denominator for most of the late-onset, progressive neurodegenerative disorders, such as Parkinson, Alzheimer's, HD, as well as transmissible spongiform encephalopathies (Brundin et al., 2010). The disease-causing proteins are characteristic for the disease and are thereby diverse in their primary sequence, as well as in their native state. Whether it is huntingtin in HD, β amyloid and tau in AD, α synuclein in PD and prion protein (PrP) in transmissible spongiform encephalopathies, all these proteins share a common feature – they remain soluble for a long time and then start to assemble in amyloid-like fibrils in aged neurons (Münch and Bertolotti, 2012).

Hydrophobic amino acid side chains, which are buried inside of a protein under native conditions, get exposed on the exterior surface of a protein. Exposition to this new environment makes them prone to self-aggregation, which promotes further association with soluble protein monomers. Once formed, such aggregates can become transmissible and are called prions (Prusiner, 1998). The ability of recruiting and incorporating soluble protein into aggregates in a process called "seeding" and is shared amongst mentioned proteins. However, the exact mechanism of PrP propagation and transmission probably differs from α-synuclein, tau, and huntingtin, most likely due to their distinctive localization (Brundin et al., 2010).

There are mechanisms that will help cells cope with the continuous synthesis of mutant, aggregation-prone proteins for decades. During this latent period, these mechanisms, such as ubiquitin-proteasome system (UPS) and autophagy, will slow down the formation of aggregation-inducing nuclei (Dimcheff et al., 2003; Heiseke et al., 2010). However, the aggregation-prone proteins will eventually leave the lag phase, escape the governing quality control mechanisms, and cells will start to exhibit signs of neuropathology.

2 Mutant Huntingtin and Mitochondria Quality Control

2.1 Autophagy

Autophagy was described in mammalian cells almost 60 years ago as a means of delivering cytoplasmic components and organelles to the lysosome for degradation (Deter et al., 1967; Klionsky, 2007; Mizushima, 2007). Autophagy can be divided into three general types – macroautophagy, microautophagy, and chaperone-mediated autophagy. However, the term autophagy usually refers to the process of macroautophagy, if not specified otherwise. Despite autophagy being further classified into more subtypes, including selective types of autophagy, it is generally considered as a nonselective degradation system, when speaking of nutrient-deprivation-induced autophagy. This event is characterized mainly by the formation of a cup-shaped membrane called isolation membrane (or phagophore), which engulfs a random portion of cytoplasm. Interestingly, the origin of the membrane is questionable, as one theory presumes regions of the rough endoplasmic reticulum (ER) devoid of ribosomes as the place of origin, and the other states that isolation membrane is a structure free of Golgi and ER markers that origins *de novo*. The isolation membrane grows and its both ends fuse together, forming a double membrane vesicle called autophagosome (Martinez-Vicente, 2017). The content of such vesicle is later degraded, as the outer membrane of the autophagosome fuses with the lysosomal membrane. This feature puts autophagy in contrast to the ubiquitin-proteasome degradation system, which degrades only specifically marked proteins.

Basal autophagy needs to be maintained at steady levels to preserve cellular homeostasis. Neither low nor high levels represent a benefit. On the contrary, upregulated autophagy may be linked to senescence or shortened lifespan (Benedetto and Gems, 2019; Bjedov et al., 2020). However, autophagy is drastically upregulated when cells are facing stress conditions, such as nutrient deprivation, oxidative stress, hypoxia etc., and removes damaging cytoplasmic components and pathogens, while providing missing nutrients (Martinez-Vicente, 2017).

As mentioned above, autophagy can be further categorized based on its selectivity. Selective autophagy might be induced by a different set of signals and requires specific adaptor proteins to target the substrate (Martinez-Vicente, 2017). There is plethora of substrates recognized by selective autophagy, and the specific type of selective autophagy is named after its targeted substrate, e.g. ribosomes and ribophagy, peroxisomes and pexophagy, or mitochondria and mitophagy (Dunn et al., 2005; Kim et al., 2007; Kraft et al., 2008).

2.1.1 Core Autophagy Machinery

The autophagic machinery consists of evolutionary conserved autophagy related (Atg) proteins that were first identified in yeast (Tsukada and Ohsumi, 1993). So far, more than 30 of these proteins have been identified, of which 18 have been described as fundamental for autophagosome formation (Kabeya et al., 2007; Suzuki et al., 2007). Based on their function, these proteins were assorted into five respective groups: 1) The Atg1 protein kinase complex (Atg1, Atg13, Atg17, Atg29, and Atg31), 2) The Vps34 phosphatidylinositol 3-kinase complex (PI3K) (Atg6/Vps30 (Beclin 1 in mammals), Atg14, Vps15, and Vps34), 3) Atg9 and the Atg2-Atg18 complex, 4) The Atg8 conjugation system (Atg3, Atg4, Atg7, and Atg8), 5) The Atg12 conjugation system (Atg5, Atg7, Atg10, Atg12, and Atg16) (Noda et al., 2009).

In *Saccharomyces cerevisiae*, most of these fundamental proteins sequester to a perivacuolar site called the autophagosome assembly site, or pre-autophagosomal structure (PAS) (Kabeya et al., 2007; Kawamata et al., 2008; Suzuki et al., 2007, 2001).

Atg1 protein kinase complex is essential for the initiation of starvation-induced autophagy. In budding yeast, Atg1 forms a pentameric complex consisting of Atg1, Atg13, Atg17, Atg29, and Atg31, whereas its mammalian homolog Unc-51-like kinase (ULK1) forms a tetrameric complex consisting of ULK1, ATG13, ATG101, and FIP200. The kinase activity of the Atg1 complex is regulated by several kinases that sense nutrient status, such as target of rapamycin (TOR) kinase complex 1 and AMP-activated protein kinase (Noda and Fujioka, 2015). Under growing conditions, Atg13 is hyperphosphorylated. However, it gets promptly dephosphorylated due to Tor kinase inactivation caused by nitrogen starvation or rapamycin treatment. In response to the dephosphorylation, Atg13 binds to Atg1 and activates its kinase activity. Atg17 constitutively assembles into a complex with Atg29 and Atg31 (Kabeya et al., 2005; Kamada et al., 2000; Kawamata et al., 2008).

The recruitment of the PI3K complex I to the PAS is determined by Atg14, Atg9, and Atg13 (Obara et al., 2006; Suzuki et al., 2007). Subsequent production of phosphatidylinositol 3-phosphate at the PAS results in the recruitment of Atg2 and Atg18 (Obara et al., 2008). As Atg9, Atg2, and Atg18 relocate to the growing edge of the phagophore, ATG2 tethers the edge of IM to ER, especially at the place of COPII vesicle formation (ER exit site; ERES) (Graef et al., 2013; Suzuki et al., 2013). Furthermore, recent research presented evidence that Atg2 possesses a hydrophobic cavity in its conserved N-terminal region that can accommodate phospholipid acyl chains, suggesting that Atg2 allows phospholipids to be transferred from the ER membrane to the cytoplasmic leaflet of IM (Osawa et al., 2020, 2019; Valverde et al., 2019).

Nonetheless, some of these phospholipids need to be further transferred to the luminal leaflet of IM to allow its growth. Atg9 is the only transmembrane protein in the core autophagy machinery and colocalizes with Atg2 at the edge of IM, where it mediates bidirectional transport of phospholipids between the IM inner and outer leaflet (Matoba et al., 2020).

Among the 18 Atg proteins of the core autophagy machinery, 8 establish two ubiquitin-like conjugation systems: the Atg8 and Atg12 systems (Ohsumi, 2001). The Atg12 system comprises five Atg proteins: Atg5, Atg7, Atg10, Atg12, and Atg16 (Mizushima et al., 1999, 1998; Shintani et al., 1999). Atg7 acts as an E1-like enzyme that activates Atg12 (Mizushima et al., 1998). Atg12 is afterwards transferred to an E2-like enzyme - Atg10 (Shintani et al., 1999). Glycine at the C-terminal of Atg12 is then conjugated to the side chain of Lys149 of Atg5 (Mizushima et al., 1998). Interestingly, there have not been reported any E3-like enzymes for this conjugation reaction. Also, there are no processing or deconjugating enzymes for Atg12, and the Atg12-Atg5 conjugate forms constitutively *in vivo*. This conjugate further groups into a complex with a dimeric protein, Atg16 (Atg16L in plants and mammals), through noncovalent bonding of Atg5 and Atg16 (Fujioka et al., 2010; Mizushima et al., 2003, 1999).

The Atg8 conjugation system composes of four Atg proteins: Atg3, Atg4, Atg7, and Atg8 (microtubule-associated protein light chain 3; LC3 in mammals) (Ichimura et al., 2000; Kabeya et al., 2000). First, the C-terminus of a newly synthesized Atg8 is processed by Atg4, a cysteine protease, exposing new C-terminus conforming of glycine at its end (Kirisako et al., 2000). Such protein is then activated by Atg7, an E1-like enzyme used by both conjugating systems, and passed on to Atg3, an E2-like enzyme. The glycine at the C-terminus of Atg8 can then be conjugated to the amine moiety of phosphatidylethanolamine (PE) (Ichimura et al., 2000). Here, the Atg12-Atg5-Atg16 complex, the product of the Atg12 system formed in the last step, steps into the light. It acts as an E3-like enzyme and promotes the conjugation of Atg8 to PE (Hanada et al., 2007). Conjugation of Atg8 and PE is reversible, and the deconjugation can be carried out by Atg4 again (Kirisako et al., 2000).

2.2 Mitophagy

Autophagy does not only serve to compensate for nutrient deprivation. On the contrary, cargo-specific autophagy operates under conditions rich in nutrients and ensures the elimination of superfluous or dysfunctional organelles to maintain their size, number, and quality control, as well as the elimination of protein aggregates that could otherwise have toxic effect.

The term mitophagy was coined by Lemasters and colleagues and refers to the engulfment of mitochondria by a vesicular structure containing the autophagosome marker, LC3 (Atg8 in yeast). First evidence of mitophagy were provided by early electron microscopy (EM) studies performed on mammalian hepatocytes, where increased mitochondrial sequestration into lysosomes was observed (Kim et al., 2007; Lemasters, 2005).

Mitophagy in both yeast and mammalian cells follows mitochondrial fission, which separates elongated mitochondrial networks into individual mitochondria of feasible size for their encapsulation (Nowikovsky et al., 2007; Twig et al., 2008; Westermann, 2010). Mitochondrial fission also provides selective partition of damaged mitochondrial material targeted for removal by mitophagy. Apart from quality control, mitophagy secures a steady-state turnover of mitochondria to meet altering metabolic demands and to maintain the number of mitochondria during specific developmental stages of mammalian cells, such as red blood cell differentiation (Schweers et al., 2007). Based on the proteins that are utilized, mitophagy is classified as receptor-mediated and ubiquitin-mediated mitophagy.

2.2.1 Receptor Mediated Mitophagy

In yeast, mitophagy is induced during nitrogen deprivation or when grown to stationary phase (Kanki and Klionsky, 2008; Okamoto et al., 2009; Tal et al., 2007). The main mediator of mitophagy in this organism is Atg32, a protein anchored to OMM via its single transmembrane domain (Kanki et al., 2009; Okamoto et al., 2009). While Atg32 is dispensable for most autophagy-related mechanisms, such as bulk autophagy, ER-phagy, pexophagy, and cytoplasm-to-vacuole targeting pathway, it is specifically important for mitophagy. Once mitophagy is induced, transcriptional levels of Atg32 increase, and as the protein accumulates on the OMM, it forms a complex with Atg8 and Atg11. Whereas no homologs of Atg32 were found in mammalian cells, BCL2L13/Bcl-rambo acts as a functional counterpart of the yeast receptor (Murakawa et al., 2015).

In mammals, mitophagy is induced by different stimuli. Probably the most potent trigger of mitophagy in mammals is mitochondrial membrane potential disruption (Elmore et al., 2001). As well as Atg32 in yeast, mitophagy receptors are expected to sequester on the OMM. Indeed, treatment with ionophores depolarizing mitochondrial membrane, such as Carbonyl cyanide m-chlorophenyl hydrazone (CCCP) and antimycin A, promotes accumulation of mitophagy receptors on the OMM. These receptors are integral membrane proteins that comprise a conserved LC3-interacting region (LIR) motif in its cytosolic domain, which promotes binding to LC3. There are two main types of mitophagy receptors – first group containing BNIP3

(BCL2/adenovirus E1B 19 kDa protein-interacting protein 3) and NIX/BNIP3L (BCL2 Interacting Protein 3 Like), and second group containing FUNDC1 (FUN14 Domain Containing 1) (Liu et al., 2012; Murakawa et al., 2015; Sandoval et al., 2008; Schweers et al., 2007).

BNIP3 functions as a mitophagy receptor under hypoxic conditions (Tracy et al., 2007). Usually, BNIP3 is expressed as an inactive monomer in the cytosol. However, under stress conditions, BNIP3 forms a homodimer and gets integrated into the OMM (Chen et al., 1999). Mutations, which hinder the ability to form homodimers but have no effect on mitochondrial localization, disrupt mitophagy, implying that homodimerization of BNIP3 is essential for efficient elimination of mitochondria by mitophagy (Hanna et al., 2012). NIX shows great amount of homology to BNIP3, as they share 53-56% of the amino acid sequence (Chen et al., 1999). NIX deficient mice suffer from anemia with reduced mature erythrocytes that showed mitochondrial retention and decreased lifespan (Sandoval et al., 2008). Cell nucleus, mitochondria, and other intracellular organelles get degraded during late phase of erythrocyte maturation to allow free space for hemoglobin to deliver as much oxygen as possible. NIX expression levels are highly increased during this phase, which ensures mitochondrial clearance (Novak et al., 2010).

FUNDC1 is an integral protein of the OMM that plays a key role as a receptor for hypoxia-induced mitophagy. FUNDC1 uses LIR motif to interact with LC3 as well. Mutations in this motif disrupts its ability to interact with LC3, thereby causing mitophagy impairment. Phosphorylation by Src kinase at Tyr18 and casein kinase-2 at Ser13 in the LIR motif also prevent FUNDC1 induced mitophagic activity (Chen et al., 2014). However, Src kinase is inactivated under hypoxic conditions and FUNDC1 gets dephosphorylated, thereby upregulating mitophagy. Bcl-xL, an anti-apoptotic protein of the Bcl-2 family, also inhibits mitophagy through its interaction with PGAM5, a mitochondrial phosphatase that dephosphorylates FUNDC1 at Ser13 (Wu et al., 2014). PGAM5 knock-out mice develop Parkinson's disease-like symptoms, as PGAM5 aids Parkin recruitment due to stabilization of serine-threonine kinase important for the induction of mitophagy, phosphatase and tensin homolog induced putative protein kinase 1 (PINK1), on mitochondria (Lu et al., 2014). This report may suggest a closer cooperative mechanism between FUNDC1 and PINK1/Parkin mitophagy that needs to be further elucidated.

2.2.2 Ubiquitin-mediated Mitophagy

Receptor-mediated mitophagy often operates in a very specific manner, e.g. the function of NIX in the maturation of reticulocytes. In contrast, PINK1/Parkin pathway is considered to be the major player in the maintenance of mitochondrial quality and elimination of damaged mitochondria.

Under physiological conditions, PINK1 is imported into IMM via its N-terminal mitochondria targeting sequence (MTS), which is subsequently cleaved by the matrix processing peptidase (MPP) (Greene et al., 2012). The transmembrane domain is then cleaved between Ala103 and Phe104 by the presenilin-associated rhomboid like (PARL) protease (Jin et al., 2010; Meissner et al., 2011). The rest of the protein is then promptly degraded according to the N-rule (Yamano and Youle, 2013). However, upon the dissipation of the mitochondrial membrane potential, PINK1 cannot be transported completely and accumulates on the OMM (Lazarou et al., 2012). Accumulated PINK1 forms dimers and undergoes autophosphorylation at Ser228 and Ser402, activating itself and leading to downstream phosphorylation events that include the recruitment of an E3-ligase Parkin to mitochondria (Okatsu et al., 2012). However, this signal itself is not sufficient to induce mitophagy. Thereby PINK1 also phosphorylates free ubiquitin as well as ubiquitin chains at Ser65, which serves as a major signal promoting mitophagy (Okatsu et al., 2012). After Parkin's full activation, it polyubiquitinates several proteins of the OMM mainly via K48- and K63-linkages. The K48-linkage is generally considered to the activating agent for degradation by the UPS system. K48-chains ensure the isolation of mitochondria through inhibiting fusion and promoting fission. K63-linkage is thought to function in the recruitment of adaptor proteins like sequestosome1 (SQSTM1, also known as p62) (Narendra et al., 2010). Adaptor proteins interconnect polyubiquitinated mitochondria and Atg8-like proteins such as LC3 and gamma-aminobutyric acid receptor-associated proteins (GABARAPs) (Stolz et al., 2014). Originally, SQSTM1 was identified as the main PINK1/Parkin-mediated mitophagy adaptor. However, later studies reported SQSTM1/p62 to be dispensable for mitophagy yet necessary for clustering of impaired mitochondria (Narendra et al., 2010). A more recent study by Lazarou et al., showed that out of five adaptors identified in mitophagy only two (optineurin, OPTN; nuclear dot protein 52 kDa, NDP52) were primary adaptors essential for mitophagy. These two primary adaptor proteins were recruited to mitochondria in the absence of Parkin. As mentioned above, Parkin-mediated mitophagy is induced by the PINK1-mediated phosphorylation of Ser65 in the ubiquitin-like (UBL) domain of Parkin, but also Ser65 of ubiquitin. Therefore, PINK1-dependent generation of phospho-ubiquitin results in the

recruitment of OPTN and NDP52 via their ubiquitin binding domains. While adaptor proteins are generally associated with the attaching of LC3 to ubiquitinated cargo, both OPTN and NDP52 were indicated in autophagy machinery recruitment upstream of LC3 (Lazarou et al., 2015). However, SQSTM1/p62 is still being implied to have a key role as a mitophagy adaptor protein due to its increased expression via the Nrf2 and TFEB pathways during PINK1/Parkin mitophagy (Ivankovic et al., 2016). Furthermore, both HTT and mHTT were indicated to interact with SQSTM/p62, depicting them as conserved binding partners, thereby increasing its significance to HD-related PINK/Parkin mitophagy (Martinez-Vicente et al., 2010).

Differences in expression levels of adaptor proteins suggest varying importance in different human tissues. Particularly interesting are the expression levels of OPTN, which are highest in brain and testis (Lazarou et al., 2015). OPTN is a primary adaptor protein, and its abnormal interaction with mHTT would result in low levels of free OPTN and therefore defective mitophagy. Low rates of mitophagy caused by decreased levels of free OPTN could possibly explain why mainly brain and testis are affected in HD.

2.2.3 mHTT Impairs Mitophagy

HTT is engaged in several steps of mitophagy, acting as a scaffold protein that promotes physical proximity of protein complexes involved in the initiation of mitophagy and recruiting adaptor proteins to promote sequestration of damaged mitochondria by nascent autophagosomes. However, these functions are affected when the extended polyQ tract in HTT is present, resulting in unsuccessful loading of autophagosomes and therefore accumulation of dysfunctional mitochondria and increased oxidative stress (Khalil et al., 2015; Martinez-Vicente et al., 2010).

2.2.3.1 mHTT and ULK1

The C-terminal domain of HTT is similar to the structure of yeast Atg11, an autophagic protein that acts as a scaffold, allowing HTT to interact with human homologs of Atg11 interaction partners, such as the ULK1 kinase complex, adaptor proteins, and the Atg8 family of proteins (Ochaba et al., 2014). In mammalian cells, mitophagy is initiated through events including the formation of the ULK1-Atg13-FIP200 complex, which's activity is inhibited by the mammalian TOR complex 1 (mTORC1). Starvation or rapamycin treatment results in mTORC1 inhibition and thus the activation of ULK1. Furthermore, both mTORC1 and HTT comprise several HEAT repeats and HTT is thereby able to compete with mTORC1 for ULK binding. The ULK1-HTT complex is exclusive to the mTORC1 complex and the displacement of mTORC1 allows total activation of selective autophagy (Rui et al., 2015). However, mHTT exhibits

reduced affinity to ULK1 compared to HTT, which interferes with the shift of ULK1 from MTORC1 to the HTT scaffolding complex (Franco-Iborra et al., 2021).

2.2.3.2 mHTT and p62

Second major problem uprises when successfully formed autophagosomes are expected to uptake their cargo (Martinez-Vicente et al., 2010). Indeed, autophagosomes fail to load with lipid droplets and mitochondria in HD (Fig. 2). Colocalization assay performed on HdhQ111 cells showed significantly reduced translocation of mitochondria to LC3-positive autophagosomes (Khalil et al., 2015). The Atg11-like C-terminal HTT fragment also allows it to interact with SQSTM1/p62. As Ochaba et al. described, this fragment copurified with SQSTM1/p62, as this adaptor protein is an ortholog of yeast Atg19, a protein known to interact with Atg11 (Ochaba et al., 2014). Thereby, an abnormal interaction of SQSTM1/p62 and mHTT may cause such hinderance in the process of mitophagy.

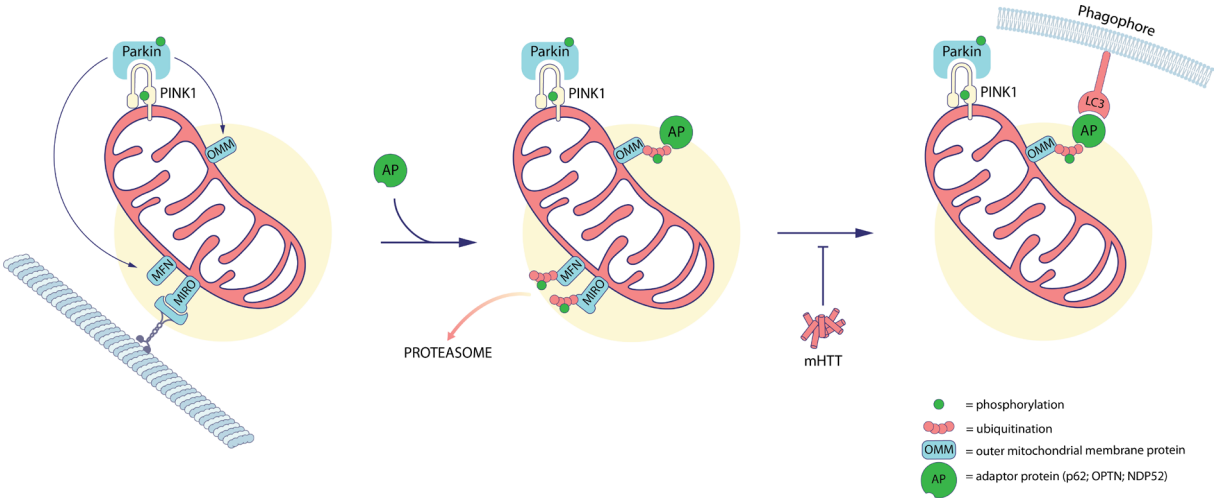

Fig. 2. mHTT impairs PINK1-Parkin mitophagy at the cargo sequestration step. When exposed to stress conditions, PINK1 gets stabilized on the OMM, which results in the recruitment of E3 ubiquitin ligase Parkin. After its accumulation on mitochondria, Parkin ubiquitinates several components of the OMM. At the same moment, PINK1 further phosphorylates both Parkin and ubiquitin, which generates a positive feedback loop. Under physiological conditions, adaptor proteins, such as SQSTM1/p62, OPTN, and NDP52 recognize phosphoubiquitin marks on OMM proteins, leading to subsequent translocation of mitochondria onto autophagosome through the binding of the adaptor protein and autophagosome marker LC3. However, this step is hindered in HD due to an abnormal interaction of mHTT and adaptor proteins. Besides Parkin, PINK1 also phosphorylates other proteins, as for example the motor-adaptor protein MIRO and Mitofusin 1 and 2. As these

proteins are a substrate for parkin as well, they get modified and undergo proteasomal degradation, which modulates certain aspects of mitochondrial dynamics and motility. LC3 - microtubule-associated protein light chain 3, MFN – mitofusin, MIRO - mitochondrial Rho GTPase, mHTT – mutated huntingtin, NDP52 – nuclear dot protein 52, OPTN – optineurin, PINK1 - PTEN-induced putative kinase 1, SQSTM1/p62 - sequestosome 1. Image taken from Sonsky et al., 2021 (Šonský et al., 2021)

2.2.4 Targeting Mitophagy *In Vitro*

The fact that impaired mitophagy, which results in the accumulation of dysfunctional mitochondria in neurons, markedly increases the pathogenesis of several neurodegenerative diseases, unveils the truth that modulating mitophagy may have implications for therapeutical use. Although mitophagy has attracted substantial research interest in the recent past, we still lack understanding of the molecular mechanisms due to the limited availability of suitable chemical substances that induce mitophagy.

Current conventional approaches utilize mitochondrial uncouplers (for example, Carbonyl cyanide 4-(trifluoromethoxy)phenylhydrazone (FCCP) or CCCP) that cause collapse of mitochondrial membrane potential ($\Delta\Psi_m$) or antimycin A and oligomycin that impair respiration to induce mitophagy. While both approaches certainly do induce mitophagy, they do so in a physiologically noncompliant manner that limits our insight into the delicate regulatory mechanisms.

2.2.4.1 Nrf2 Inducing Drugs

Nuclear transcription factor E2-related factor 2 (Nrf2) is a transcription factor that has attracted interest for improving mitochondrial function and health. Genetically or pharmacologically increased Nrf2 activity results in numerous positive effects on mitochondria (Dinkova-Kostova and Abramov, 2015). Nrf2 supervises the expression of several cytoprotective genes that contain antioxidant response elements (AREs) in their promoter regions. Two of them with notable relevance to both general and selective autophagy are SQSTM1/p62 and NDP52 (Jain et al., 2010; Jo et al., 2014). Hence, the recently increasing effort to induce mitophagy via the Nrf2 pathway.

2.2.4.1.1 Sulforaphane

Sulforaphane (1-isothiocyanoate-4-[methylsulfinyl]-butane, SFN) is an isothiocyanate compound selectively inducing phase II detoxication enzymes and is naturally produced by certain cruciferous vegetable, such as SAGA broccoli (*Brassica oleracea italica*) (Fahey and

Talalay, 1999; Zhang et al., 1992). SFN induces Nrf2 activity by disabling the interaction with its negative regulator Kelch-like ECH-associated protein 1 (Keap1), a redox-sensitive protein serving as an adaptor for the cullin 3–Rbx1 ubiquitin ligase complex, which promotes ubiquitination and degradation of Nrf2 by the proteasome (McMahon et al., 2003). Due to the electrophilic nature of SFN, it can interact with protein thiols, generating thionoacyl adducts. This allows SFN to covalently modify sensor Cys residues in Keap1, affecting the Nrf2/Keap1 complex and thereby stabilizing Nrf2 by preventing its degradation in proteasome (Hong et al., 2005; McMahon et al., 2003). Despite the Nrf2-mediated upregulation of SQSTM1/p62 and NDP52, SFN interferes with mitochondria targeted ubiquitination, which has negative impact on recruitment of the aforementioned adaptor proteins. SFN is overall a very reactive compound and is capable of irreversibly altering plethora of redox sensitive proteins, which may jeopardize the Nrf2-mediated effects on mitochondrial biogenesis and quality control (Georgakopoulos et al., 2017).

2.2.4.1.2 HB299/PMI

Relatively recently identified activator of mitophagy is a small molecule compound called the p62/SQSTM1-mediated mitophagy inducer (PMI). PMI activates mitophagy independently of $\Delta\Psi_m$ collapse or without recruiting Parkin to mitochondria (East et al., 2014). In contrast to the routinely used compounds, PMI represents a more suitable tool to selectively induce mitophagy without compromising the bio-energetic state of the cell. PMI activates Nrf2 by disrupting the protein-protein interaction (PPI) between Nrf2 and Keap1 (Wells, 2015). This interaction is based on the 'hinge and latch' principle, where a high affinity $_{79}$ETGE$_{82}$ motif and a lower affinity $_{26}$QDIDLG$_{31}$ 'latch' motif in the N-terminal Neh2 domain of Nrf2 interact with two spots in KEAP1. In order to proceed with the ubiquitination of Lys residues in the Neh2 domain, KEAP1 first interacts with the high affinity 'hinge' motif and forms an open conformation, and then it interacts with the 'latch' motif, forming a closed conformation of the Keap1-Nrf2 complex (Baird et al., 2013). After forming the closed conformation, the Cullin 3 complex can promote the proteasomal degradation of Nrf2 (Furukawa and Xiong, 2005). PMI binds to the low affinity DLG motif, thereby preventing Keap1 from binding and forming the closed conformation (Bertrand et al., 2015).

2.2.4.1.3 MIND4-17

Nonetheless, PMI is not commercially available for purchase, and more mitophagy inducing compounds need to be identified. After reviewing several compounds, one of them appeared as highly convenient for this cause. MIND4-17 is a thiazole-containing compound that was able

to induce Nrf2 activation response in neuronal and non-neuronal cells. Furthermore, application of this compound reduced production of reactive oxygen species (ROS) and nitrogen intermediates and exhibited neuroprotectivity in *ex vivo* HD rat corticostriatal brain slices and *Drosophila* models of HD (Quinti et al., 2016). Yet, its effect on mitophagy has not been studied. MIND4-17 comprises an electron-withdrawing group containing a sulfur atom and electron-deficient aromatic system, through which it can covalently modify an important stress-sensor cysteine (Cys151) in the Broad complex, Tramtrack, and Bric-à-Brac (BTB) domain of KEAP1. Substituting the S atom with an O or C atom resulted in a completely inactive analog, showing the essentiality of the S atom for inducer activity. Furthermore, during the quantitative cysteine reactivity profiling, only four from a subset of >300 reactive cysteine-containing peptides exhibited increased change in reactivity after treatment with MIND4-17, implicating its high specificity (Quinti et al., 2017). Such specific and non-toxic upregulation of Nrf2 activity could compensate for the defective mitophagy (Fig. 3) (Šonský et al., 2021).

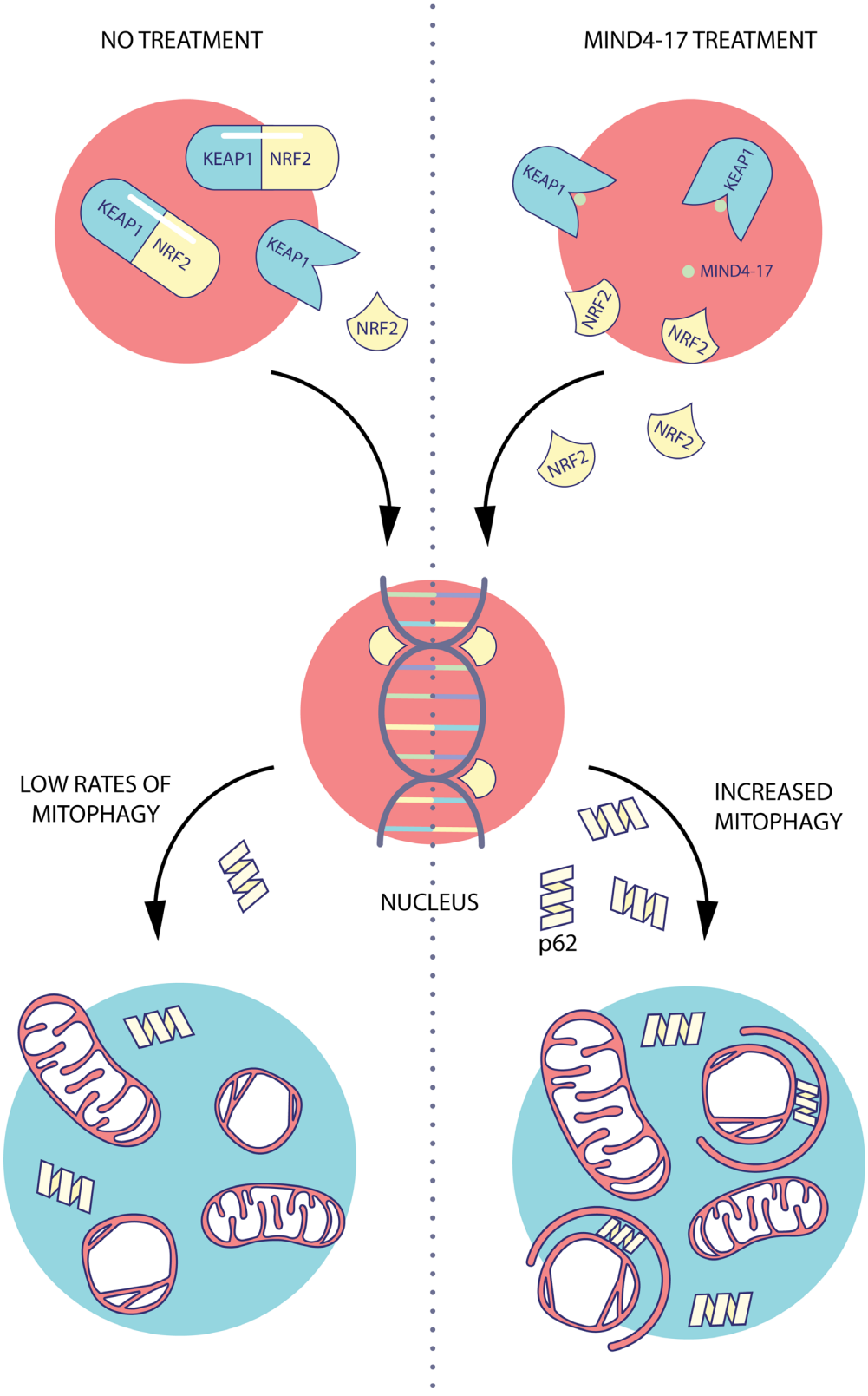

Fig. 3. Proposed working model of MIND4-17. Image taken from Sonsky et al., 2021 (Šonský et al., 2021)

3 Aims of the Thesis

The first aim of the thesis was to assess, whether the small molecule compound MIND4-17 would be able to increase the flux of autophagy using immunoblotting techniques, and whether it would be possible to study autophagy and specifically mitophagy in fibroblasts from HD patients.

The second aim was to identify effect of the MIND4-17 treatment on mitochondria. Using spectrophotometry and Seahorse analyzer, we set to determine the rate of mitochondrial respiration. Next, we examined effect of the treatment on mitochondrial morphology using electron and fluorescent microscopy.

Third aim was to observe specific improvement in mitophagy. For that purpose, the goal was to prepare cells expressing recombinant EGFP-LC3 protein, pCLBW cox8 EGFP mCherry protein, and pTRE-Tight-MitoTimer protein.

4 Materials and Methods

4.1 Material

4.1.1 Cell Lines

Cultivated cell lines consisted of a set of human skin fibroblasts (HSF) from 3 patients (P1-P3) diagnosed with HD obtained via skin biopsy after their informed consent. Group of control fibroblast cell lines resided of HSF from 3 healthy donors (C1-C3). All of the control cell lines expressed less than 35 CAG in the IT15 gene and were devoid of any HD associated symptoms.

4.1.2 Chemicals

- Acetic acid (Penta, CZ)
- Acetyl CoA (Sigma-Aldrich, USA)
- Amino persulfate (APS)
- Antibiotic-antimycotic (Biosera, Fr)
- ATP (Sigma-Aldrich, USA)
- bromophenol blue (Sigma-Aldrich, USA)
- BSA (Sigma-Aldrich, USA)
- CCCP (Sigma-Aldrich, USA)
- Chloroquine (Sigma-Aldrich, USA)
- Coomassie brilliant Blue R-250 (Sigma-Aldrich, USA)
- DCPIP (Sigma-Aldrich, USA)
- decyl ubiquinone (Sigma-Aldrich, USA)
- DMEM (PAN-Biotech, GE)
- DMSO (Sigma-Aldrich, USA)
- Doxycycline (Sigma-Aldrich, USA)
- DTNB (Sigma-Aldrich, USA)
- EDTA (Sigma-Aldrich, USA)
- Ethanol (Penta, CZ)
- FBS (Sigma-Aldrich, USA)
- Glycerol (Penta, CZ)
- Glycine (Sigma-Aldrich, USA)
- HCl (Penta, CZ)
- Isopropanol (Penta, CZ)
- KCN (Sigma-Aldrich, USA)
- $KMnO_4$ (Sigma-Aldrich, USA)
- Methanol (Penta, CZ)
- MIND4-17 (Sigma-Aldrich, USA)
- N'N'-methylene-bis-acrylamide (Sigma-Aldrich, USA)
- NaCl (Penta, CZ)
- NADH (Sigma-Aldrich, USA)
- PIC (Sigma-Aldrich, USA)
- PMSF (Sigma-Aldrich, USA)
- Precision Plus Protein™ Dual Color Standards (Bio-Rad, USA)
- Rotenone (Sigma-Aldrich, USA)
- SDS (Sigma-Aldrich, USA)
- Skimmed milk powder (Laktino, CZ)
- Sodium succinate (Sigma-Aldrich, USA)
- SuperSignal™ West Femto Maximum Sensitivity Substrate (Thermo Fisher, USA)
- TEMED (Sigma-Aldrich, USA)

- Tet system approved FBS (Sigma-Aldrich, USA)
- Tricine (Sigma-Aldrich, USA)
- Tris-HCl (Sigma-Aldrich, USA)
- Trisma base (Sigma-Aldrich, USA)
- Cytochrome *c* (Sigma-Aldrich, USA)
- Oxalacetate (Sigma-Aldrich, USA)
- DBH2 (Sigma-Aldrich, USA)
- Malonate (Sigma-Aldrich, USA)
- Triton X-100 (Sigma-Aldrich, USA)
- Trypsin (Sigma-Aldrich, USA)
- Tween-20 (Sigma-Aldrich, USA)
- Oligomycin (Sigma-Aldrich, USA)
- 2-deoxy-D-glucose (Sigma-Aldrich, USA)
- Glucose (Sigma-Aldrich, USA)
- FCCP (Sigma-Aldrich, USA)
- Ampicilin (Sigma-Aldrich, USA)
- D5030 medium (Sigma-Aldrich, USA)
- RNAse-free water (Top-Bio, CZ)
- L-glutamine (Sigma-Aldrich, USA)
- Mitotracker^{TM} Red CMXRos (Thermo Fisher, USA)
- Kanamycin (Sigma-Aldrich, USA)
- β-mercaptoethanol (Sigma-Aldrich, USA)

4.1.3 Antibodies

Table 1: Primary and secondary antibodies and their concentration used in immunoblotting.

Primary antibodies and their concentration	Secondary antibodies and their concentration
Anti-LC3B (ab192890, Abcam) – 1/2000	anti-mouse IgG peroxidase conjugate (A8924, Sigma Aldrich) – 1/5000
Anti-SQSTM1/p62 antibody (ab109012, Abcam) – 1/10000	anti-rabbit IgG peroxidase conjugate (A0545, Sigma Aldrich) – 1/5000
Anti-NDP52 antibody (ab68588, Abcam) – 1 µg/ml	
Anti-Optineurin antibody (ab213556, Abcam) – 1/1000	
Anti-GAPDH (ab8245) – 1/10000	

4.1.4 Prepared Solutions

- 10x Running buffer – 250 mM Tris Base; 1.92 mM glycine; 1% (v/v) SDS
- 2x Separating buffer – 0.75 M HCl, pH 8.8; 0.2% (v/v) SDS
- 2x Stacking buffer – 0.25 M Tris-HCl, pH 6.8; 0.2% (v/v) SDS
- Anode buffer (SDS-PAGE) – 100mM Tris-HCl, pH 8,9
- Bleaching solution for gels - 25% (v/v) methanol; 10% (v/v) acetic acid; dH2O
- Cathode buffer (SDS-PAGE) - 100 mM Tris-Cl, pH 8.9; 100 mM tricine; 0,1 % SDS

- Dyeing solution – 0.25% (w/v) Coomassie brilliant Blue R-250; 45% (v/v), methanol; 10% (v/v) acetic acid
- Gel buffer (SDS-PAGE) stock - 3x concentrated – 3 M Tris-HCl, pH 8.45; 0.3 % SDS glycerol; 4 % (v/v) SDS; 2 % (v/v) β-mercaptoethanol; 0.01 % (v/v) bromophenol blue
- KPi – 119 mM KH_2PO_4, pH 7.8; 119 mM K2HPO4, pH 7.8
- PBS [10x concentrated: 56mM Na_2HPO_4, Lonza (SWI) 1.54M NaCl, 10mM KH_2PO_4, pH 7.4]
- RIPA buffer – 50 mM Tris-Cl, pH 7.4; 150 mM NaCl; 1 mM PMSF; 1 mM
- Sample buffer (SDS-PAGE) 4x concentrated – 50 mM Tris-HCl, pH 6.8; 12 % (v/v)
- T + E (Trypsin + EDTA solution) Biosera (Francie) - [10x concentrated; 0.5% (w/v) trypsin, 0.2% (w/v) EDTA in PBS solution]
- TBS buffer (stock - 10x concentrated) – 20mM Tris-Cl; 130mM NaCl; pH 7.6
- TBST buffer – 1x TBS, pH 7.5; 0,1% Tween20
- Transfer buffer – 25mM Tris-Cl; 1.92mM glycine; 10% (v/v) methanol; 0,02% SDS

4.1.5 Commercial Kits

- EndoFree Plasmid Maxi Kit (Qiagen)
- Seahorse XF Cell Mito Stress Test Kit (Agilent)
- Seahorse XF Glycolysis Stress Test Kit (Agilent)
- Neon Transfection System (Thermo Fisher)

4.1.6 Instruments

- Analytical balance — AND HA-120M
- Automatic pipettes (1-5000 µL) — Nichipet, Nichiryo
- Centrifuge — Hettich Rotofix 32R
- Confocal microscope — LSXM Leica SP8X, Leica
- Electron microscope — Jeol JEM 1400+
- Electrophoresis power supply — Bio-Rad Basic power supply
- Gel documentation system — Syngene G:BOX
- Incubator — SANYO CO_2
- Magnetic stirrer — MM2A, Laboratory instruments Prague
- Phase contrast microscope — Nikon Eclipse Ti2-U
- Seahorse instrument — Seahorse XFe24 Analyzer
- Spectrophotometer — Shimadzu UV-2401 PC, UV-2600 PC
- Thermoblock — LABNet
- Transfer system — Trans-blot Turbo
- Vortex — Velp Scientifica

4.2 Methods

4.2.1 Fibroblasts Cultivation

Fibroblasts were cultivated in 25 cm^2 and 75 cm^2 cell culture flasks respectively. In 25 cm^2 flasks, cells were cultivated in 5 mL (10 mL in 75 cm^2 flasks) of DMEM growth medium with 1% (w/v) ATB (Biosera), 10% iFBS, 25 mM glucose (4.5 g/l) and 2mM L-glutamine (0.580 g/l). At 90-100% confluency, cells were passaged using following procedure: the entire medium was aspirated with a Pasteur pipette and the cultivating surface was rinsed with 3-5 mL of PBS. Then, 0.5 mL of 1% (w/v) T + E solution (1.5 mL for 75 cm^2 flask) was added to the cells, covering the whole surface, and the flask was placed into an incubator (37°C; 5% CO_2; SanyoCO_2 incubator, Sanyo). After approximately 5 mins, the flask was inspected under a phase contrast microscope (Nikon Eclipse T*i*2-U) to confirm that the cells had started to round up and detach. If not, the cells were returned to the incubator for a shorter period. After the cells had started to detach, 10 mL (20 mL for 75 cm^2 flask) of fresh, 37°C preheated DMEM growth medium with 1% (w/v) ATB, 10% iFBS was added. The content was then thoroughly resuspended and evenly split into two 25 cm^2 (75 cm^2) flasks, which were transferred to an incubator (37°C; 5% CO_2; SanyoCO_2 incubator, Sanyo).

4.2.2 Cryopreservation of Fibroblasts

Cell culture medium from fibroblasts grown to 70-80% confluency was removed, and the cultivation surface of the flask was gently washed with 3-5 mL PBS. To initiate cell detachment, 0.5 mL of 1% (w/v) T + E dissociation reagent was added to 25 cm^2 flask (1.5 mL to 75 cm^2 flask). Cells were then placed into an incubator (37°C; 5% CO_2; SanyoCO_2 incubator, Sanyo) for approximately 5 mins and were checked under a phase contrast microscope (Nikon Eclipse T*i*2-U) on whether they had started to dissociate from flask surface. Afterwards, 5 mL of DMEM medium (10 mL to 75 cm^2 flask) with 1% (w/v) ATB and 10% iFBS was added to neutralize the effect of the dissociation reagent. Small aliquot of cells was removed to perform a cell count. The rest of the cell suspension was transferred to a 15 mL centrifuge tube and was centrifuged (300g, 23°C, 5 min, Universal 32R centrifuge, Hettich). The supernatant was discarded, and the cell pellet was then resuspended in freeze DMEM medium with 1% (w/v) ATB, 10% iFBS, 10% DMSO. Cells were pipetted into 2 mL cryotubes at 1-4x10^6 cells per each. Cryotubes were then placed inside a freezing container (Corning® CoolCell™) and left at -80°C for 24 h/ overnight. Frozen tubes were transferred into a liquid nitrogen storage vessel and preserved at -196°C.

4.2.3 Cell Storing and Thawing

Human skin fibroblasts were stored at -196°C in cryotubes containing 1.8 mL of DMEM medium with 1% (w/v) ATB, 10% (w/v) iFBS and 10% (w/v) DMSO. First, content of the cryotube was thawed in 37°C (Heratherm™ IMC 18, Thermo Fisher Scientific) and then transferred into a 75 cm^2 cell culture flask. Afterwards, 10 mL of DMEM medium with 1% (w/v) ATB and 10% (w/v) iFBS was added to the flask, which was then placed into an incubator (37°C; 5% CO_2; SanyoCO_2 incubator, Sanyo). After several hours, the DMSO containing cell culture medium was replaced with 10 mL of fresh DMEM medium with 1% (w/v) ATB, 10% iFBS and cells were placed back into an incubator (37°C; 5% CO_2; SanyoCO_2 incubator, Sanyo).

4.2.4 Cell Harvesting for SDS Page

First, the cell culture medium was aspirated, and cells were then gently washed twice with 3-5 mL of ice-cold PBS. Cells were then treated with 1.5 mL of 1% (w/v) T + E solution. After approximately 5 min, 5 mL of cold DMEM medium with 1% (w/v) ATB, 10% iFBS was added into the flask, cells were scraped with a cold plastic cell scraper and the cell suspension from two 75 cm^2 flasks was gently transferred into a pre-cooled centrifuge tube. Cells were then centrifuged (600g, 4°C, 10 min; Universal 32R centrifuge, Hettich), supernatant was discarded, and cells were resuspended in 1 mL of PBS. This suspension was gently transferred into a cooled Eppendorf tube, centrifuged (600g, 4°C, 10 min; Universal 32R centrifuge, Hettich) and supernatant was again discarded. Sample pellet was stored at -80°C for later use.

4.2.5 Preparation of Cell Lysate

Harvested cell pellet was resuspended in RIPA buffer (RIPA + 1% (w/v) PIC), stored on ice for 20 min and once in every 5 min mixed on vortex. Sample was then centrifuged (4°C, 51 000g, 20 min, Thermo Scientific Heraeus Biofuge Stratos Centrifuge, Thermo Fisher Scientific) and supernatant was collected in fresh Eppendorf tube. 2 µL were used for the determination of protein concentration using the bicinchoninic acid (BCA) assay.

4.2.6 Determination of Protein Concentration

First, 10 µL of each standard and samples was pipetted into a microplate well in doublets. Then, 200 µl of working reagent was added to each well, and the microplate well was mixed thoroughly on a plate shaker for 30 s. Afterwards, the plate was incubated at 37°C for 30 min and then cooled down to RT. After it reached RT, absorbance was measured at 562 nm on a plate reader (BioTek PowerWave, BioTek).

4.2.7 SDS Page

First, glass plates and spacers were assembled into gel casting apparatus. Then, components for the preparation of 12% separating gel (Table 3) were mixed on ice. The mixture was poured in between the glass plates to a level approximately 2 cm below the top and covered with ddH_2O. After one hour, the ddH_2O on the top of the polymerized gel was replaced with 4% stacking gel (Table 3), and a comb was inserted to the top. The gel was then left to polymerize for at least 30 min. Afterwards, the comb was removed, and the gel was placed into an assembled electrophoretic apparatus. Both chambers of the apparatus were then filled with running buffers. Prepared samples and 4 µL of marker (Precision Plus Protein™ Dual Color Standards; Biorad) were loaded into the wells of the gel. The electrophoresis was performed at 40V for 30 min and then at 90V for approximately 1.5 h.

Table 2: Mix of Agents and Their Concentrations Used for 12% Separating and 4% Stacking Polyacrylamide Gel

Component	Separating gel 12%	Stacking gel 4%
ddH_2O	4.2 mL	5.8 mL
3xGB	3.3 mL	3.3 mL
48% Acrylamide	2.4 mL	0.8 mL
APS	50 µL	120 µL
TEMED	5 µL	12 µL

For the separation of LC3B-I and LC3B-II, different gel mixture was used (Table 4). After the gel polymerized and was placed into an electrophoretic apparatus, both chambers were filled with 1x running buffer. The electrophoresis was performed at constant 120V for approximately 1 h.

Table 3: Mix of Agents and Their Concentrations Used for 12% Separating and 4% Stacking Polyacrylamide Gel for Glycine SDS Page.

Component	Separating gel 12%	Stacking gel 4%
ddH_2O ddH_2O	2.3 mL	1.6 mL
48% Acrylamide	2.5 mL	0.3 mL
2x Separating buffer	5 mL	X
2x Stacking buffer	X	2 mL

10% APS	0.1 mL	0.04 mL
TEMED	0.01 mL	0.004 mL

4.2.8 Semi-dry Western Blot

After running an SDS Page gel, the gel was immediately equilibrated in transfer buffer for 30 min on a 3D shaker at 20 rpm. Meanwhile, a PVDF membrane of approximately same size as the gel was activated for 15 s in 100% methanol, incubated in ddH_2O for 5 min, and then in transfer buffer for 15 min. Three pieces of blotting paper were completely saturated by soaking in transfer buffer, placed on anode, and rolled over with a roller to remove air bubbles. On top of the papers was placed the PVDF membrane, on top of which was stacked the gel. Another three soaked blotting papers were placed on the whole aligned stack and gently rolled over to exclude air bubbles. The whole stack was gently sealed with the cathode plate, and the transfer ran at 1.3 A for 7 min (Trans Turbo Blot; BioRad,USA). After the end of the transfer, the PVDF membrane was dried out and then immunodetected with specific antibodies (see below).

4.2.9 Gel Staining and Drying

After the protein transfer, the gel was stained overnight on a 3D shaker at 20 rpm. Next day, the gel was bathed in destaining solution, till only the protein bands were visible. Afterwards, the gel was washed with ddH_2O, placed on a Whatman paper, and dried at 80°C for 1 h (Scie-Plas gel dryer, UK).

4.2.10 Immunodetection

Dried out PVDF membrane was activated in methanol, washed in ddH_2O for 10 min, and placed in blocking solution with agitation for 2 h. Then, the membrane was rinsed three times with 1xTBS for 10 min, incubated with primary antibody (Table 2) for 2 h, and washed three times with TBST for 10 min. Afterwards, the membrane was incubated with secondary antibody (Table 2) for 1 h, washed three times with TBST for 10 min, and then with 1xTBS for 10 min. Proteins were detected using SuperSignal™ West Femto Maximum Sensitivity Substrate (Thermo Scientific) and photographed using the G:Box system with GeneSys software (Syngene).

4.2.11 Analysis of Respiratory Chain Enzymes Activity

Enzymatic activity of respiratory chain enzymes was measured according to slightly modified protocol by Rustin (Rustin et al., 1994) in cuvettes (optical path of 1cm, 37°C) using a split

beam spectrophotometer Shimadzu UV-2401PC. The final volume of each sample was 1 mL, and each sample was measured twice. For one assay approximately 100 µg of protein was used.

4.2.11.1 Complex I

The rotenone-sensitive *NADH:ubiquinone oxidoreductase* (Complex I, NQR) activity can be estimated by measuring the rotenone-sensitive NADH oxidation at 340 nm in the presence of an electron recipient – decylubiquinone. To perform this assay, mitochondria need to be exposed to distilled water for 3 min leading to hypotonic lysis. Activity was measured in the presence of 50 mM TRIS/HCl (pH 8.1), 2.5 mg/ml BSA, 0.3 mM KCN, 50 µM decyl ubiquinone (Q_{10}). The reaction was initiated by adding 0,1 mM NADH. Obtained activity values were adjusted by reducing the values of activity measured in the presence of 3µM rotenone.

Final activity (SA – Specific Activity) was measured according to the formula:

$SA = dA * 10^6 / \varepsilon * v * c$

dA arithmetic average of both measured values after the reduction of activity in the presence of rotenone

ε molar absorption coefficient $6.22 * 10^3$ $dm^3/cm/mol$

v sample volume in µl

c sample protein concentration in mg/ml

SA was expressed as nmol/min/mg of protein.

4.2.11.2 Complex II

The estimation of *succinate:ubiquinone reductase* (Complex II, SQR) activity was obtained by measuring the rate of succinate-dependent reduction of dichlorophenol indophenol in the presence of decylubiquinone. Activity was measured in the presence of 10 mM KPi (pH 7.8), 2 mM EDTA, 1 mg/ml BSA, 3 µM rotenone, 10 mM sodium succinate, 0.2 mM ATP, 0.3 mM KCN, 80 µM DCPIP (2,6-dichlorophenol indophenol), 1 µM antimycin A. The reaction was initiated by adding 50 µM decyl ubiquinone. Decrease of absorbance at 600 nm in the consequence of DCPIP reduction was observed over the period of 3 min. The reaction was stopped by adding complex II specific inhibitor – 10 mM malonate.

Final activity (SA – Specific Activity) was measured according to the formula:

$SA = dA * 10^6 / \varepsilon * v * c$

dA arithmetic average of both measured values after the reduction of activity in the presence of malonate.

ε molar absorption coefficient $21.6 * 10^3$ $dm^3/cm/mol$

v sample volume in µl

c sample protein concentration in mg/ml

SA was expressed as nmol/min/mg of protein.

4.2.11.3 Complex III

Activity of the *ubiquinol: cytochrome c oxidoreductase complex* (complex III, QCCR) was measured in a reaction mixture containing 50 mM KPi (pH 7.8), 2 mM EDTA, 1 mg/ml BSA, 0.03 mM KCN, 40 µM cytochrome c and sample. Reaction was initiated by addition of 50 µM ubiquinol (DBH2). An increase of absorbance values at 550 nm caused by the reduction of cytochrome c was documented for 3 min. Afterwards, 1µM antimycin A was added to the cuvette and activity was measured for 1 min.

Final activity (SA – Specific Activity) was measured according to the formula:

$SA = dA * 10^6 / \varepsilon * v * c$

dA arithmetic average of both measured values after the reduction of activity in the presence of antimycin

ε molar absorption coefficient $6.22 * 10^3$ $dm^3/cm/mol$

v sample volume in µl

c sample protein concentration in mg/ml

SA was expressed as nmol/min/mg of protein

4.2.11.4 Complex IV

100 µl of fibroblasts suspension was solubilized by incubation with 10 µl of 15% laurylmaltoside (15min, 4°C), then centrifuged at 10 000g, 10 min, 4°C and supernatant was used for enzyme activity measurement.

Activity of the cytochrome *c* oxidase (complex IV, COX) was observed in a reaction mixture containing 40 mM KPi (pH 7.0), 1 mg/ml BSA, 25 µM reduced cytochrome *c* and sample and was pronounced as a decrease in absorbance at 550 nm.

Final activity (SA – Specific Activity) was measured according to the formula:

$SA = dA * 10^6 / \varepsilon * v * c$

dA arithmetic average of measured values

ε molar absorption coefficient $19.6 * 10^3$ $dm^3/cm/mol$

v sample volume in µl

c sample protein concentration in mg/ml

SA was expressed as nmol/min/mg of protein.

4.2.11.5 Citrate synthase

100 µl of fibroblasts suspension was solubilized by incubation with 10 µl of 15% laurylmaltoside (15min, 4°C), then centrifuged at 10 000g, 10 min, 4°C and supernatant was used for enzyme activity measurement.

Activity of citrate synthase (CS) was measured in the presence of 100 mM TRIS/HCl (pH8.1), 0.1 mM DTNB (5,5-dithio-bis-(2-nitrobenzoic acid)), sample, and 0.5 mM acetyl coenzyme A. Reaction was initiated by the addition of 0.5 mM oxalacetate after a 2 min background measurement at 412 nm. The activity was calculated after the reduction of background values.

Final activity (SA – Specific Activity) was measured according to the formula:

$SA = dA * 10^6 / \varepsilon * v * c$

dA arithmetic average of both measured values after the deduction of the background

ε molar absorption coefficient $13.6 * 10^3$ $dm^3/cm/mol$

v sample volume in µl

c sample protein concentration in mg/ml

SA was expressed as nmol/min/mg of protein.

4.2.12 Seahorse XF^{e}24 Extracellular Flux Analyzer

The Agilent Seahorse XF^{e}24 Analyzer is an instrument that calculates rate of change of dissolved oxygen and pH in the media covering living cells cultured in a special 24-well plate format microplate in real time. These changes are measured as the oxygen consumption rate (OCR) and the extracellular acidification rate (ECAR) of live cells in a non-invasive manner. OCR data are reported as pmol/min, and ECAR data are reported as mpH/min. A sterile disposable cartridge comprising 24 fluorescent biosensors (one for each well) is used to perform the measurement. During a measurement cycle, up to 4 different reagents can be injected into each well – commonly used are compounds such as oligomycin, rotenone, antimycin A, FCCP, glucose, and 2-deoxy-D-glucose (Table 5), which evoke certain reactions of cells in the culture. Between the measurement of every analyte level, the media is gently mixed. The assay kit includes a designated 24-well cell culture microplate and a fluorescent sensor-containing cartridge.

Table 4: Reagents Commonly Used in XF^{e}24 Assay, Their Concentration, and Their Effects

Agent	**Concentration**	**Function**
Oligomycine	1.5 µM	F_OF_1-ATPase inhibitor
Rotenone	2 µM	Complex I of ETC inhibitor
Antimycin A	1 µM	Complex III of ETC inhibitor
FCCP	0.7 µM	Oxidative phosphorylation uncoupler (allows H^+ transport trough IMM)
2-D-deoxyglucose	100 mM	Inhibitor of glucose metabolism

Two main protocols can be followed in order to perform the assay on XF^{e}24 analyzer, the Seahorse XF Mito Stress Test (Fig. 4) and the Glycolysis Stress Test (Fig. 5). Based on oxygen consumption and/or changes of pH in used media, the Seahorse XF^{e}24 analyzer can quantify metabolic profile of an examined cell line.

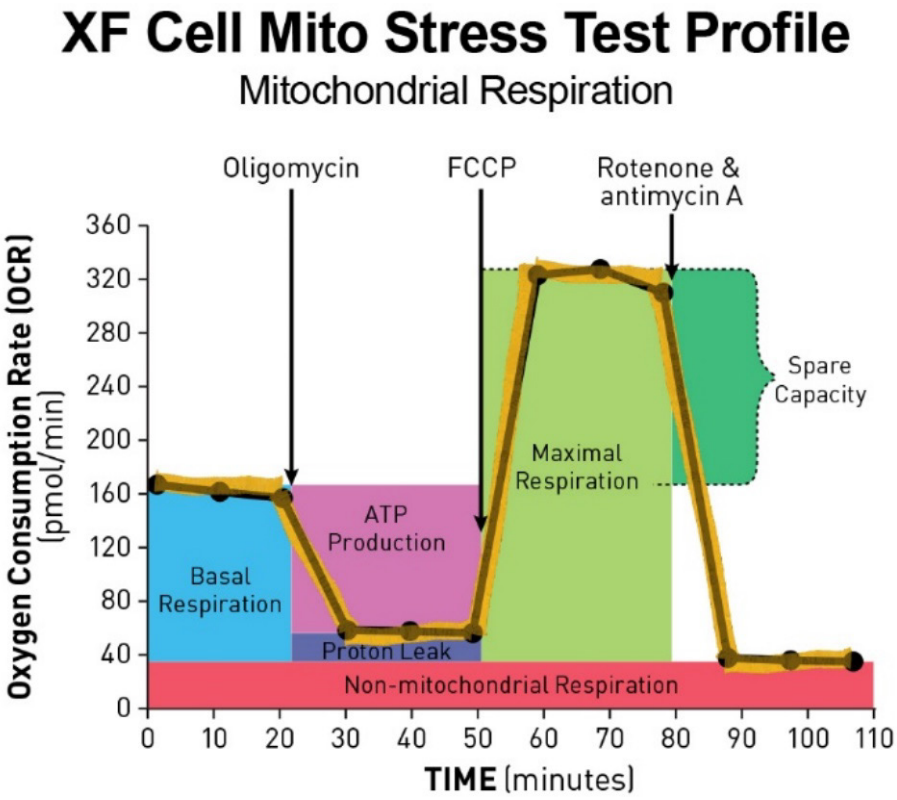

Fig. 4. Seahorse XF Mito Stress Test

Image taken from: Seahorse XF Cell Mito Stress Test Kit User Guide

(https://hpst.cz/metabolicka-analyza-seahorse-xf/spotrebni-material-pro-seahorse-xfe/seahorse-xf-cell-mito-stress)

During the first part of the measurement, cells consume oxygen to meet the ATP demand of cells resulting from generating mitochondrial membrane potential. However, after injecting the ATP synthase inhibitor oligomycin, the electron flow through electron transport chain (ETC) decreases, leading to a decrease in mitochondrial respiration, and thereby OCR. Next follows the injection of FCCP, an uncoupling agent disrupting the proton gradient and thereby the mitochondrial membrane potential. As a result, oxygen consumption by complex IV reaches maximal values. Such FCCP-generated OCR can then be used to subtract spare respiratory capacity, which is defined as the difference between maximal and basal respiration and showing the ability of the cell to react to elevated energy demand or stress. The last injection is a

combination of rotenone, a complex I inhibitor, and antimycin A, a complex III inhibitor. This injection completely ceases mitochondrial respiration and enables measurement of nonmitochondrial respiration driven by processes mitochondrial surroundings.

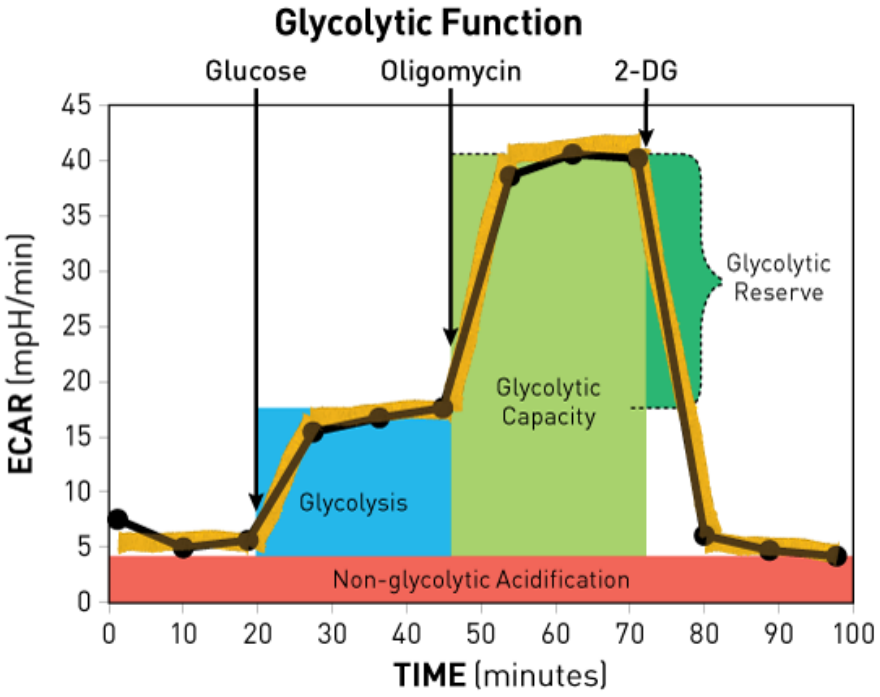

Fig. 5. Seahorse XF Glycolysis Stress Test

Image taken from: Image taken from: Seahorse XF Cell Mito Stress Test Kit User Guide (https://www.agilent.com/cs/library/usermanuals/public/XF_Glycolysis_Stress_Test_Kit_User_Guide.pdf)

First, ECAR is measured in a medium without glucose or pyruvate, so that cells cannot use the glycolytic pathway. Following the first injection, which is a saturating concentration of glucose, cells start to catabolize it and produce pyruvate, ATP, NADH, water, and protons. The production of protons into the medium results in an increase of ECAR, displaying the rate of glycolysis under basal conditions. Next, oligomycin is injected, inhibiting mitochondrial ATP production. This results in a shift in energy production to glycolysis, increasing ECAR and displaying maximum capacity of cellular glycolysis. The final injection of 2-DG results in an inhibition of glycolysis due to competitive binding to hexokinase, the first glycolytic pathway enzyme. The decrease in ECAR after this injection confirms that the measured ECAR was a result of glycolysis.

4.2.12.1 Analysis of mitochondrial respiration and glycolytic function

A day prior to the measurement by the XF^{e}24 analyzer (420109, Agilent Seahorse), cells were seeded into 24-well cell culture microplate. Before the actual seeding, wells were coated with 100 µl of 1x poly-L-lysine for 10 min and then washed twice with miliQ water. Number of cells per well was 30 000 contained in 100 µl of cultivation media, and each cell line was seeded in pentaplicates. Four wells were filled only with 100 µl cultivation media and no cells for background measurements. Right after the cells were seeded, they were left to sit for 1h at RT and then moved into an incubator (37°C; 5% CO_2; SanyoCO_2 incubator, Sanyo). After the cells fully adhered, another 150 µl of cultivation media (optionally containing 1 µM MIND4-17) were added into the wells, and the microplate was then moved back into the incubator for another 23 h (37°C; 5% CO_2; SanyoCO_2 incubator, Sanyo). After the seeding was done, the sensor-containing cartridge was hydrated with Seahorse XF24 Calibrant pH 7.4 overnight in an incubator without CO_2. Next day, the microplate was checked under a microscope (Nikon Eclipse T*i*2-U) for potential contamination of empty wells with cells. Then, fresh assay medium (D5030 medium (Sigma-Aldrich); 2mM L-Glutamine, pH 7.4) and agents (Table 5) were prepared. Before measurement, the cultivation media was removed from the cultivation microplate, and cells were twice washed with 1 mL of pre-warmed assay media. Next, wells were filled with 450 µl of pre-warmed assay, and the microplate was incubated at 37 °C, without CO_2, for at least 60 minutes prior to loading microplate in XFe24 analyzer. In the meanwhile, ports in the sensor cartridge were loaded with appropriate reagents in specified volume: port A was filled with 50 µl of 10 mM glucose, port B was filled with 55 µl of 1.5 µM oligomycin, port C was filled with 61 µl of 0.7 µM FCCP, and port D was filled with 67 µl of 2 µM rotenone and 1 µM antimycin A diluted in 100 mM 2-DG (pH7,4). Then the assay continued in the XF^{e}24 analyzer following manufacturer's instructions. OCR chart showed oxygen consumption in pmols per minute. ECAR chart displayed the pH changes in mpH (milli pH units) per minute.

4.2.13 Electron Microscopy

First, cells grown to 70% confluence were fixed in cell culture flasks with 2% solution of KMnO4 in PBS for 15 min at RT and washed twice with PBS. Afterwards, cells were incubated for 15 minutes at RT – first in 50% ethanol and then in 70% ethanol. Majority of the ethanol was discarded, and cells were transferred into a clean labeled Eppendorf tube and were centrifuged in the residual ethanol (500g, 5min, RT). Next steps were carried out in the cooperation with our colleagues at the Laboratory of electron microscopy at Institute of Pathology of the First Faculty of Medicine and General University Hospital in Prague, where

the cells were further dehydrated, twice incubated with propylene oxide for 15 min, embedded in durcupan epoxy and cut into thin slices ranging from 600-900 A. Cells were then analyzed with a transmission electron microscope (Jeol JEM 1400+; Jeol Ltd.).

4.2.14 Immunocytochemistry

Cells grown on special glass coverslips (Ibidi) were fixed in 4% paraformaldehyde solution at RT for 20 min and mixed gently every 5 minutes. Cells were washed twice with PBS and permeabilized using 0.1% Triton X-100 for 20 min at RT. Next, cells were washed twice with PBS and incubated in blocking solution (10% donkey serum in PBS) for 1 h. Afterwards, cells were incubated overnight at 4°C with primary antibodies (Table 6) in 10% donkey serum in PBS containing 0.1% Triton X-100. Next morning, cells were washed with PBS three times followed by an incubation with secondary antibodies (Table 6) in 10% donkey serum in PBS containing 0.1% Triton X-100 for two hours at RT. Following the incubation, cells were washed with PBS three times, coverslips were mounted with ProLong^{TM} Gold antifade Mountant with DAPI (Invitrogen) and sealed around edges with transparent nail polish to prevent drying and movement. For analysis, a confocal microscope (LSXM Leica SP8X, Leica) equipped with Arg/HeNe laser was used.

Table 5: List of Antibodies Used in Immunocytochemistry

Primary antibodies and their concentration	Secondary antibodies and their concentration
Anti-LC3B (ab192890, Abcam) – 1 µg/mL	Alexa Fluor 488 (A-21121, Thermo Fisher – 1 µg/mL
Anti-TOMM20 (ab56783, Abcam) – 5%	Alexa Fluor 555 (A-31572, Thermo Fisher) – 4 µg/mL

4.2.15 Plasmid Preparation

Plasmid containing (Table 7) bacterial culture from glycerol stock were plated on a LB agar (15 g/l) containing ampicillin (100 µg/ml) or kanamycin (50 µg/ml) using the quadrant streaking method to separate single colonies. Plates were incubated overnight at 37°C. Next day, colonies grown on plates were examined. Single distinctive colonies were picked and inoculated into 5 ml of LB media containing ampicillin (100 µg/ml) or kanamycin (50 µg/ml) and incubated at 37°C and 250 rpm for 8h. Plasmids were isolated using EndoFree Plasmid Maxi Kit (Qiagen) and the next steps were carried out according to the manufacturer's instructions.

Table 6: List of plasmids used in this thesis.

Plasmid name	Plasmid number (Addgene)
pEGFP-LC3 (human)	24920
pCLBW cox8 EGFP mCherry	78520
pTRE-Tight-MitoTimer	50547
pCAG-rtTA	163601

4.2.16 Electroporation

A mixture of plasmid (15 µg) and 2-4x10^5 cells in 100 µl of resuspension buffer (Thermo Fisher) were aspirated into the Neon™ Tip (Thermo Fisher). In the case of pTRE-Tight-MitoTimer, cells were co-transfected with 7.5 µg of pTRE-Tight-MitoTimer and 7.5 µg of pCAG-rtTA. The tip was then securely inserted into the Neon™ tube (Thermo Fisher) containing 3 mL of Electrolytic Buffer (Thermo Fisher) and already placed in the Neon™ Pipette Station (Thermo Fisher). The content was electroporated (pulse: 12.5 kV/cm, time constant: 4.4 – 5.0 msec). Electroporated cells were transferred onto special glass coverslips (Ibidi) with chambers filled with cell culture media without antibiotics and left to sit for 24 h. Cell culture media purposed for cells co-transfected with pTRE-Tight-MitoTimer and pCAG-rtTA contained Tet system-approved FBS instead of typical iFBS. Expression of these two plasmids had to be induced by doxycycline (4 µg/ml; at least 4h). Cells were then stained with 200 nM Mitotracker™ Red CMXRos (Thermo Fisher) for 20 min and further processed (Fixation, permeabilization and mounting (See 4.2.15)). For analysis, a confocal microscope (LSXM Leica SP8X, Leica) equipped with Arg/HeNe laser was used.

4.2.17 Data Handling

Captured immunoblot data were analyzed using the ImageJ software (LOCI, University of Wisconsin), where the luminescence intensity of separate bands was quantified. The values of intensity were then processed in Microsoft Excel. Confocal microscopy images were deconvoluted and Costes maps were produced using Huygens Software (Scientific Volume Imaging). Colocalization was analyzed using ImageJ software (LOCI, University of Wisconsin). Data from spectrophotometry and Seahorse XF^e24 Analyzer were processed in Microsoft Excel. Statistical analysis was performed in Microsoft Excel and RStudio (RStudio, Inc).

5 Results

5.1 MIND4-17 Impacts Autophagic Flux and Levels of Adaptor Proteins

To determine the potential of MIND4-17 to induce mitophagy, we examined levels of the autophagosome marker LC3B and some of the autophagy adaptor proteins involved in the step of cargo sequestration – SQSTM1/p62, OPTN, and NDP52. Cells were treated with 10 µM MIND4-17 for 24 hours. After 24 hours, cells were harvested, and protein expression was analyzed by western blot.

Expression of the autophagosome marker LC3B was significantly increased in cells treated with MIND4-17 compared to vehicle treated control cells (Fig. 6 A and F; Data in Table S1). Yet, to verify, whether this increase in expression is related to an increase in the autophagy flow, we needed to prevent the fusion of autophagosome and lysosome and observe specifically the cleaved and lipidated LC3B-II form. To achieve such goal, we treated the cells with 10 µM chloroquine (CQ) for additional 2 hours. Instead of using tricine-SDS-PAGE, we had to use the glycine-SDS-page and a PVDF membrane with pores of smaller diameter to successfully separate the two forms of LC3B.

Indeed, we observed higher LC3B-II levels in cells treated with MIND4-17 and CQ, even compared to cells exposed to CQ alone, indicating that MIND4-17 treatment enhances autophagic flux (Fig. 6 B).

Furthermore, an increase in expression of SQSTM1/p62 in response to MIND4-17 treatment was observed (Fig. 6 C and F; Data in Table S1). Also, the expression of primary adaptor proteins was altered after the treatment with MIND4-17. While NDP52 expression levels increased after the treatment (Fig. 6 D and F; Data in Table S1), OPTN expression was slightly repressed in MIND4-17 treated patients' cells (Fig. 6 E and F; Data in Table S1).

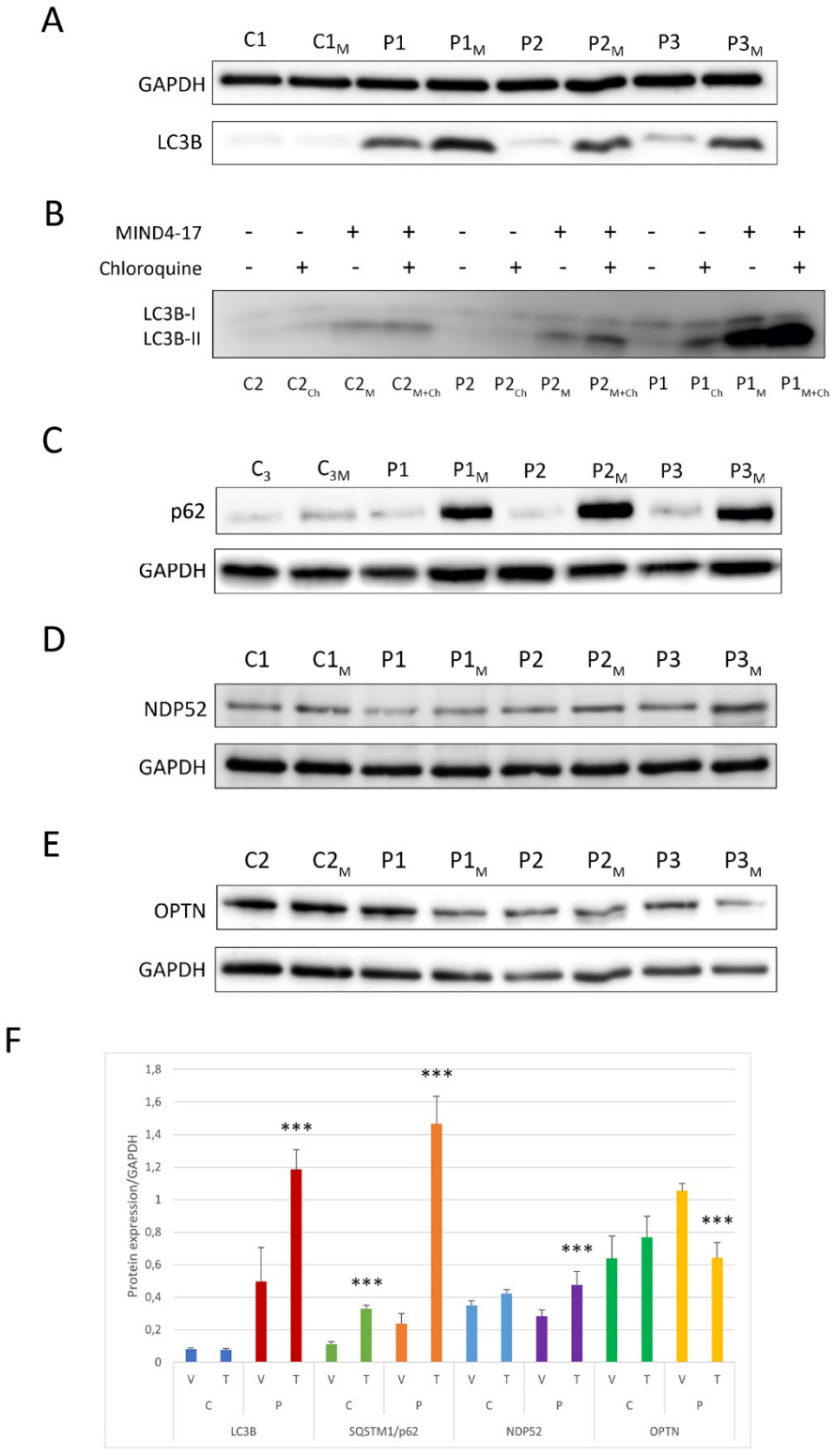

Fig. 6. Western blot analysis of autophagic flux in cultivated fibroblasts from HD patients and controls. (A) Levels of LC3B before and after MIND4-17 treatment. (B) Levels of LC3B-I and LC3B-II before and after MIND4-17 and chloroquine treatment. (C) Levels of SQSTM1/p62 before and after MIND4-17 treatment. (D) Levels of NDP52 before and after MIND4-17 treatment. (E) Levels of OPTN before and after MIND4-17

treatment. (F) Chart showing expression of proteins. LC3B marks total LC3B expression. Quantitative analysis was performed using ImageJ software (LOCI, University of Wisconsin). Statistical analysis was accomplished using a Student's t-test (*P<0.01 versus cells treated with vehicle (dimethylsulfoxide, DMSO); **P<0.01 versus cells treated with vehicle; ***P<0.001 versus cells treated with vehicle). Data from at least 3 independent experiments were averaged and were presented as mean ± S.D. C – control cells treated with vehicle, C_M – control cells treated with 10 μM MIND4-17 for 24 h, C_{Ch} – control cells treated with 10 μM chloroquine for 2 h, C_{M+Ch} – Control cells treated with 10 μM MIND4-17 for 24 h and 10 μM chloroquine for 24 h, P – patient cells treated with vehicle, P_M – patient cells treated with 10 μM MIND4-17 for 24h, P_{Ch} – patient cells treated with 10 μM chloroquine for 2 h, P_{M+Ch} – patient cells treated with c MIND4-17 for 24h and 10 μM chloroquine for 2 h.

5.2 MIND4-17 Does Not Negatively Affect Mitochondrial Morphology

To determine whether MIND4-17 treatment alters mitochondrial morphology, we performed transmission electron microscopy analysis in fibroblasts. We found regularly shaped mitochondria (Fig. 7 A (C1 and $C1_M$)), where the shape could have been subjected to the plane of cut. Mitochondria contained in cells from HD patients were typically more swollen and had slightly altered cristae microarchitecture (Fig. 7 A (P1-$P2_M$)). While MIND4-17 treatment did not seem to have any major effect (Fig. 7 A ($C1_M$, $P1_M$, and $P2_M$)) on the ultrastructure of mitochondria, we found ring-shaped structures that engulfed cytoplasmic components in one MIND4-17 treated patient line (Fig. 7 B). Such structures were highly reminiscent to autophagosomes.

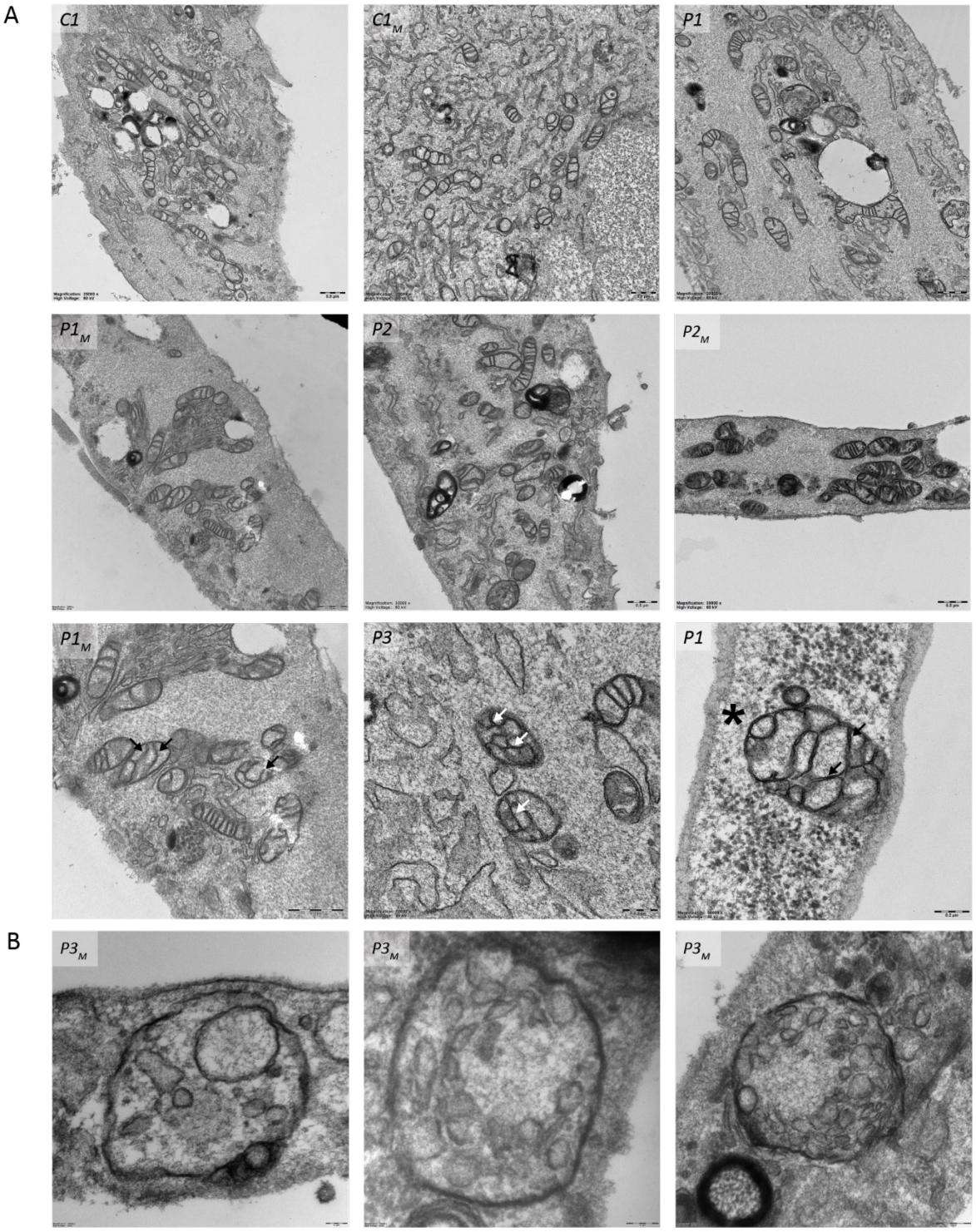

Fig. 7. (A) Mitochondrial ultrastructure in cultivated fibroblasts of HD patients and controls analyzed by transmission electron microscopy (TEM). Arrowheads show altered cristae in swollen mitochondria. Asterisk marks swollen mitochondrion. Scale bar: 0.5 μM and in last two images 0.2 μM. (B) TEM images of HD patient cell line treated with MIND4-17 exhibiting the presence of autophagosome reminiscent structures. Scale bar: 0.1 μM in the first two images and 0.2 μM in the third. C – control cell line; C_M – control cell line treated with 10 μM MIND4-17 for 24 h; P – patient cell line; P_M – patient cell line treated with 10 μM MIND4-17 for 24 h.

5.3 Mitochondrial Network is Compromised in MIND4-17 Treated Cells

Mitochondria are dynamic organelles and form interconnected networks. In order to analyze the effect of MIND4-17 treatment on the forming of mitochondrial networks, we stained mitochondria with the MitoTracker™ Red CMXRos fluorescent marker. First, we observed fragmented networks in HD patient's cells opposed to long tubular mitochondria in control cells. Indeed, mitochondrial fragmentation is common to many pathologies including HD. Furthermore, we observed that mitochondria in both control and patient cell lines tended to accumulate around nucleus and get more fragmented upon MIND4-17 treatment.

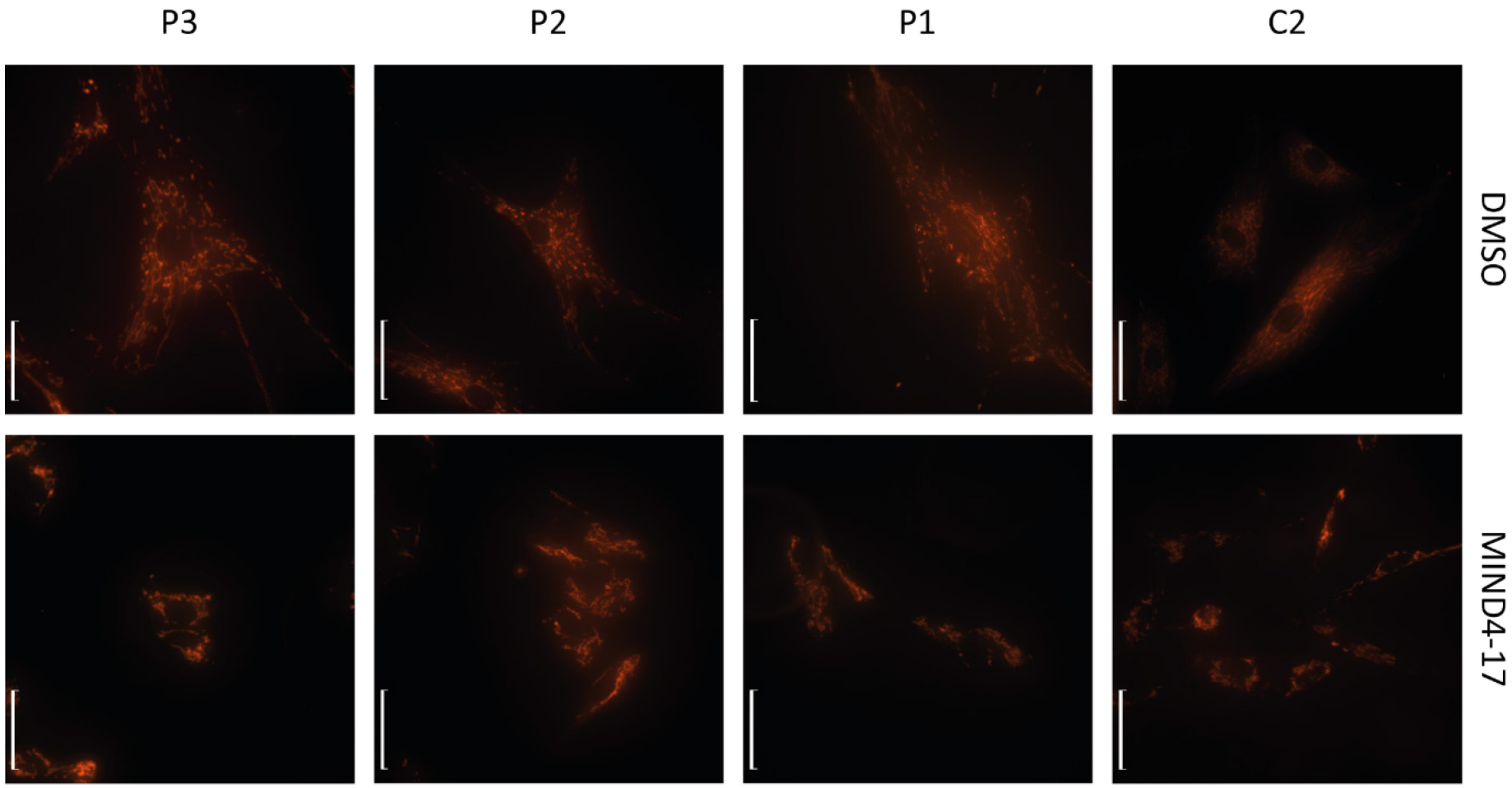

Fig. 8. Mitochondrial networks in fibroblasts of HD patients and controls stained with MitoTracker™ Red CMXRos fluorescent marker. Cells were treated with vehicle (dimethyl sulfoxide, DMSO) or 10 μM MIND4-17 for 24h and stained with 10 nM MitoTrackerTM Red CMXRos for 10 min. Scale bar: 50 μM. C- control cells, P – patients' cells

5.4 The Effect of MIND4-17 on Mitochondrial Function

Next, to evaluate whether MIND4-17 treatment had any impact on mitochondrial respiration, we first measured the activity of respiratory chain enzymes spectrophotometrically. Then, we measured mitochondrial respiration using the Seahorse XFe24 Extracellular Flux Analyzer.

Spectrophotometric analysis did not show any statistically significant changes between treated and untreated cells except for the change of Complex I activity in patients (Fig. 9; Data in table S2). The activity of Complex I in patients' cells increased after MIND4-17 treatment. Although control cells followed similar trend, the change was not as significant due to increased variances.

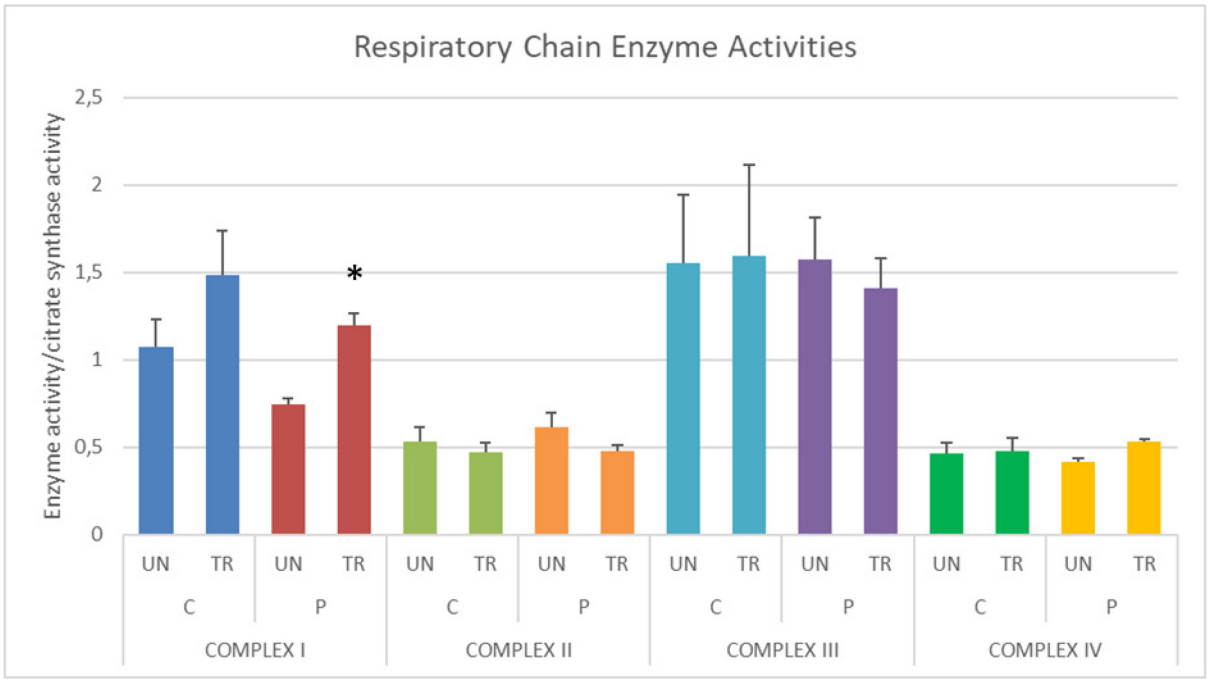

Fig. 9. Spectrophotometric analysis of respiratory chain complexes in fibroblasts from HD patients and controls after treatment with MIND4-17. Enzyme activities were normalized to the activity of citrate synthase. Data from three independent experiments were averaged and were presented as mean ± SD. Activity of Complex I in patients significantly increases upon MIND4-17 treatment (Student's t-test, $^{*}P<0.05$ versus untreated patients). C – control cells, P – patients' cells, UN – cells treated with vehicle (DMSO), T – cells treated with 10 µM MIND4-17 for 24h.

Analysis of mitochondrial respiration revealed that MIND4-17 treatment had visible effect on respiration, which is mainly noticeable after FCCP treatment (Fig. 10 A). Quantification of obtained data (Fig. 10 B; data in Table S3) showed that MIND4-17 treatment in patients' cells significantly decreased routine respiration and maximal capacity. Routine respiration, ATP production, maximal capacity, and spare capacity of patients' cells was significantly increased

compared to control cells. These differences were evened out to some extent after MIND4-17 treatment.

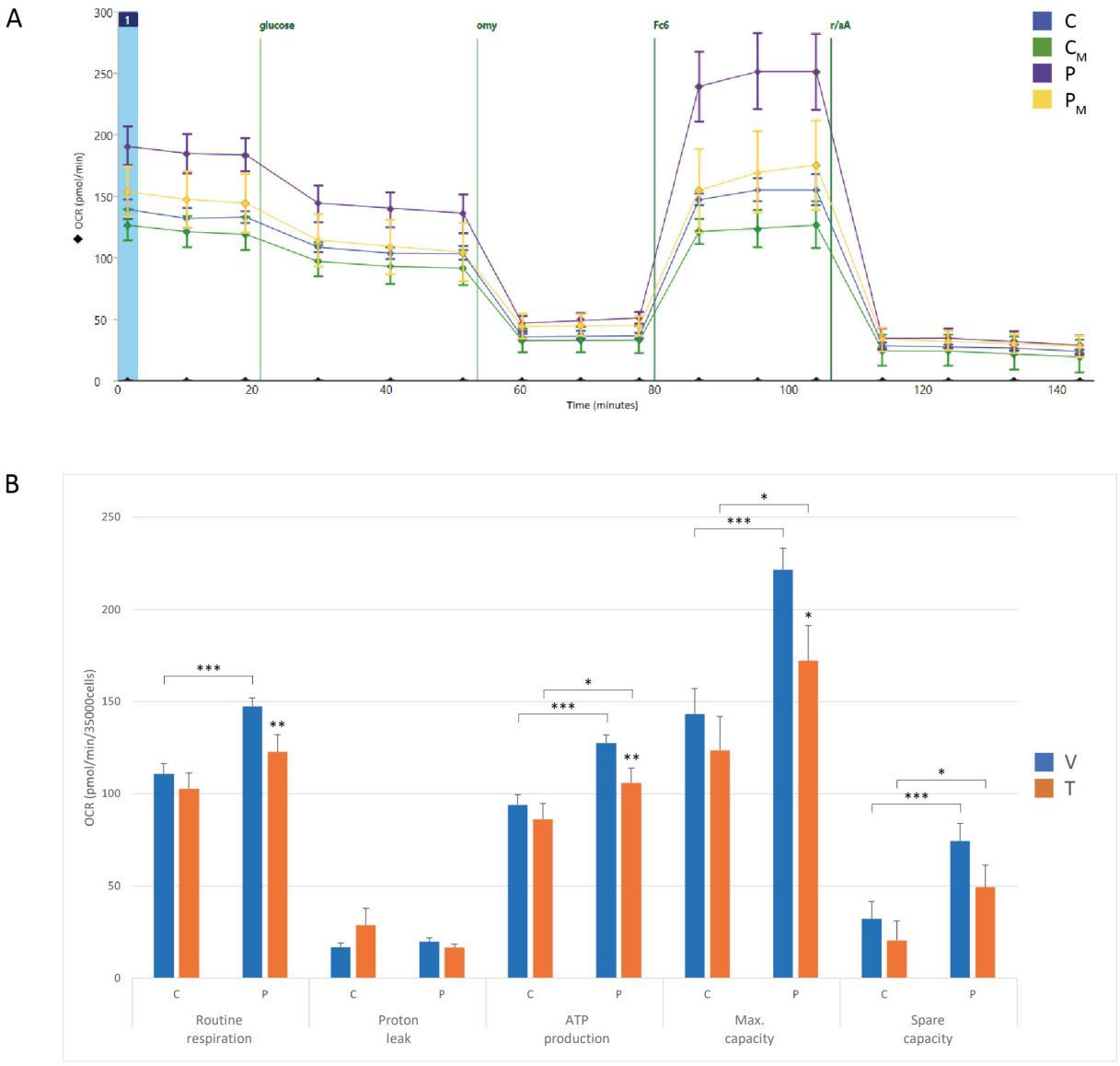

Fig. 10. Seahorse XFe24 Extracellular Flux Analysis of mitochondrial respiration in fibroblasts from HD patients and controls. (A) A representative chart showing Oxygen consumption ratio (OCR) of control and patients' cell lines. Error bars represent mean ± SD. n = 5. C – control cells treated with vehicle (DMSO), C_M – control cells treated with 10 µM MIND4-17 for 24 h, P – patients's cells treated with vehicle (DMSO), P_M – patients' cells treated with 10 µM MIND4-17 for 24 h. (B) Comparison of routine (basal) respiration, proton leak, ATP production, maximal capacity, and spare capacity. Statistical analysis was performed using ANOVA test with Tukey post-hoc test (n≥15). Routine respiration in patients' cells decreased significantly upon MIND4-17 treatment ($^{**}P$<0.01). ATP production in patients' cells decreased significantly upon MIND4-17 ($^{**}P$<0.01). Maximal capacity in patients' cells decreased significantly upon MIND4-17 treatment ($^{*}P$<0.05). Routine respiration increased significantly in patients' cells not treated with MIND4-17 ($^{***}P$<0.001 versus control). ATP production increased significantly in patients' cells not treated with MIND4-17 ($^{***}P$<0.001 versus control). ATP

production increased significantly in patients' cells treated with MIND4-17 ($^{*}P<0.05$ versus MIND4-17 treated control). Maximal capacity increased significantly in patients' cells not treated with MIND4-17 ($^{***}P<0.001$ versus control). Maximal capacity increased significantly in patients' cells treated with MIND4-17 ($^{*}P<0.05$ versus MIND4-17 treated control). Spare capacity increased significantly in patients' cells not treated with MIND4-17 ($^{***}P<0.001$ versus control). Spare capacity increased significantly in patients' cells treated with MIND4-17 ($^{*}P<0.05$ versus MIND4-17 treated control). C – control, P – patient, V – treated with vehicle (DMSO), T – treated with 10 μM MIND4-17 for 24h.

Glycolytic rates were obtained from ECAR measurements, which were measured simultaneously with OCR. Glycolysis and glycolytic capacity were calculated by subtracting the non-glycolytic acidification from respective values. Glycolytic reserves were calculated as the difference between glycolysis and glycolytic capacity. While there were many significant changes in mitochondrial respiration, we did not observe any significant changes in glycolytic rates (Fig. 11; data in Table S4).

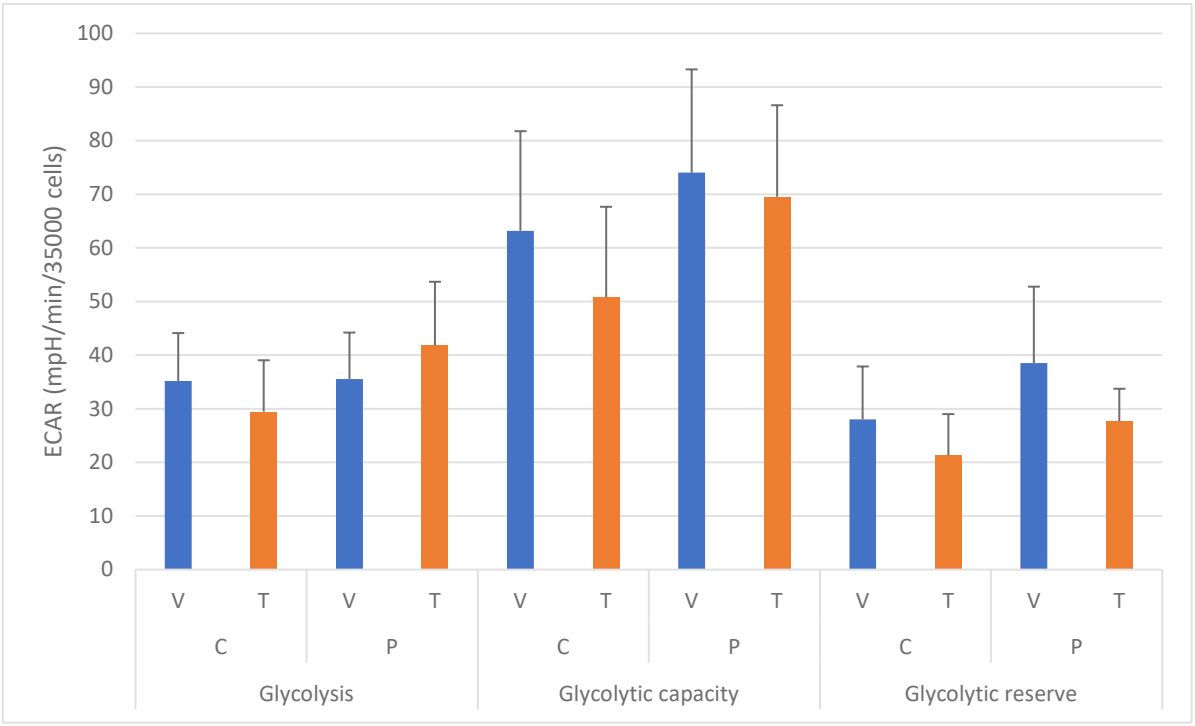

Fig. 11. Seahorse XFe24 Extracellular Flux Analysis of Glycolytic Rates in Fibroblasts from HD patients and Controls. C – control cells, P – patients' cells, V – vehicle, T – treatment with 10 μM MIND4-17 for 24h

5.5 The Targeting of Mitochondria to Autophagosomes is Increased by MIND4-17

Next, we investigated whether MIND4-17 treatment can compensate for the compromised step of mitophagy, which is loading of autophagosomes with mitochondria. First, we tried to use immunolabeling to visualize the colocalization of autophagosomes and mitochondria. However, the labeling of LC3B was quite unspecific (Fig. S1). Next, we decided to transfect cells either with pEGFP-LC3 or pCLBW cox8 EGFP mCherry or co-transfect them with pTRE-Tight-MitoTimer and pCAG-rtTA. However, the signal generated by the pCLBW cox8 EGFP mCherry plasmid expression was mostly diffuse throughout the cells. While some of the cells had properly labeled mitochondria, as all cells should have, the results were inconsistent (Fig. S2). The co-transfection with pTRE-Tight-MitoTimer and pCAG-rtTA was successful, producing clear signal on mitochondria. However, the confocal microscope was not able to maintain saved focus plane and positions, as it was supposed to. Thereby, we do not have any images except for the first captured frames (data not shown). Besides, it would be more suitable to analyze the intensities with flow cytometry, which we plan to do in the future. Therefore, we leaned towards the transfection with the pEGFP-LC3 plasmid, which generated successful results (Fig. 12 A). Our observations confirmed data from previous studies, as HD patients' cells exhibited decreased colocalization of mitochondria and autophagosomes compared to control cells (Fig. 12 B), implying insufficient targeting of defective mitochondria to autophagosomes. However, treatment with MIND4-17 significantly increased colocalization of LC3-positive autophagic membranes and mitochondria in both control and patients' cells (Fig. 12 B; Data in table S5). This suggests that MIND4-17 treatment helps to bypass the mHTT-caused perturbation of cargo sequestration.

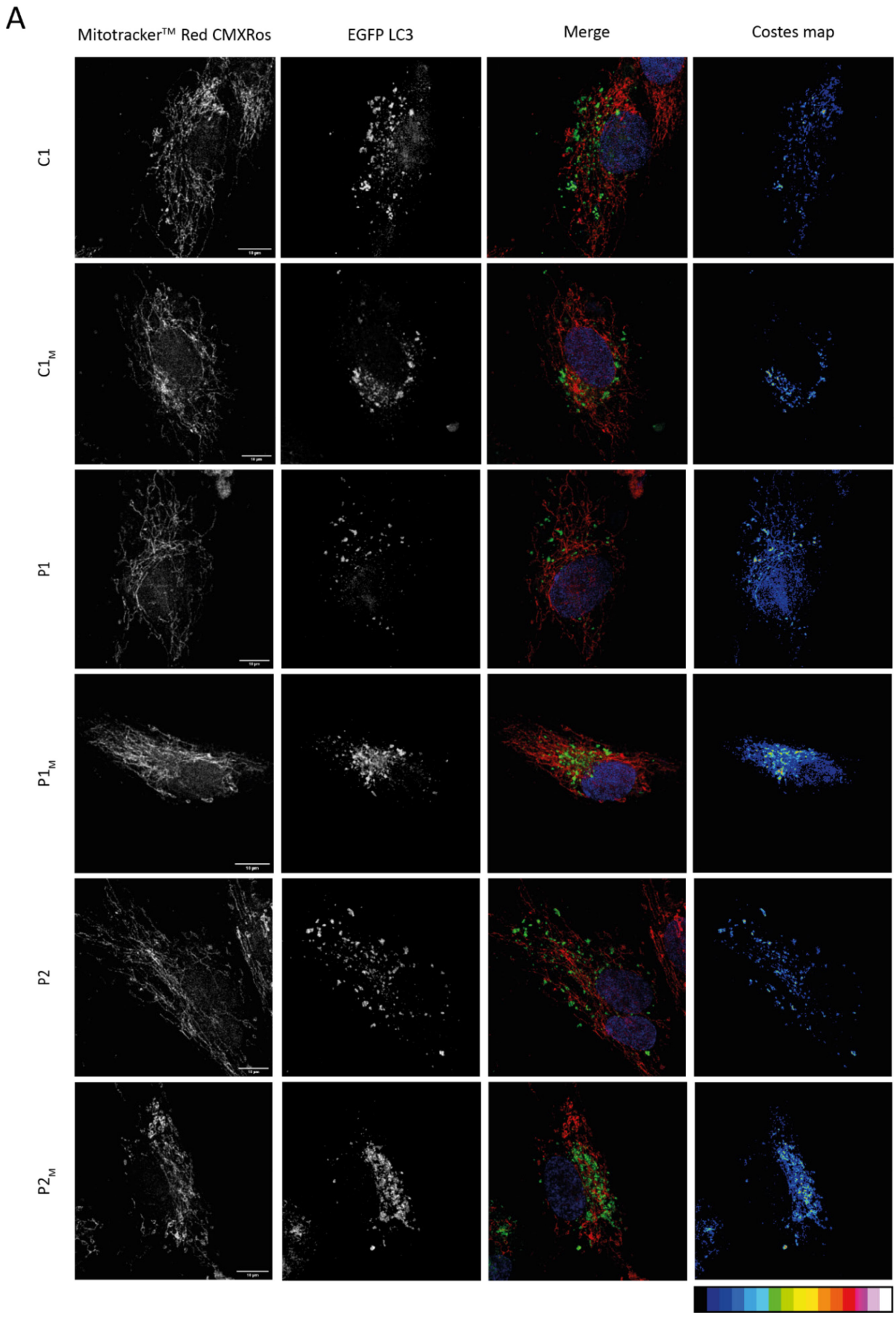
A
Mitotracker™ Red CMXRos
EGFP LC3
Merge
Costes map
C1
C1M
P1
P1M
P2
P2M

B

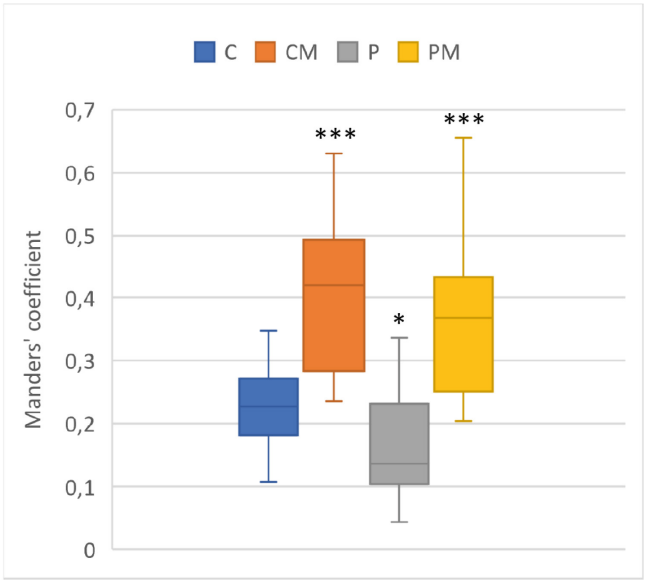

Fig. 12. Colocalization of autophagosomes and mitochondria is altered in cells from patients suffering from HD but is increased by MIND4-17 treatment. (A) Representative confocal microscopy images showing the effect of MIND4-17 on colocalization of mitochondria and autophagosomes. Cells were transfected by electroporation with EGFP-LC3 and treated by dimethyl sulfoxide (DMSO) or 10 µM MIND4-17 for 24h. Mitochondria were immunostained by an anti-TOMM20 antibody and nuclei were stained with DAPI. Fourth column shows Costes maps, which translate the level of colocalization into colors shown in the look up table below. Blacks mean the lowest values, white the highest values. Scale bar: 10µM. (B) Quantitative analyses displaying the Manders' overlap coefficient between EGFP-LC3 and mitochondria. Statistical analysis was performed using the Student's t-test (n<15, $^{***}P<0.001$ versus untreated cells, $^{*}P<0.05$ versus untreated control cells)

6 Discussion

The unique morphology and bioenergetic demands of post-mitotic neurons make maintenance of neuronal homeostasis a difficult task. Mitochondrial impairments represent an early hallmark of neuronal dysfunction implied in many neurodegenerative diseases, including HD. Thereby, accumulation of damaged mitochondria poses a major threat to neurons. Many previous studies have shown that deregulation of mitophagy is also fundamental to the process of neurodegeneration. It needs to be acknowledged that while mitophagy eliminates damaged mitochondria and therefore mediates neuroprotection, neither low rates nor high rates of mitophagy will benefit the cell. On the contrary, uncontrolled mitophagy may even trigger neuronal cell death (Doxaki and Palikaras, 2021; Sharma et al., 2019; Subramaniam, 2020).

Despite the recent progress in understanding the mechanisms underlying the process of mitophagy, efforts to modulate mitophagy are still very obscured, as the vast majority of available mitophagy inducers are mito-toxins causing $\Delta\Psi_m$ dissipation (Hirose et al., 1974; Tsiper et al., 2012).

Here we report that MIND4-17, a highly selective small-molecule activator of NRF2, was able to alter expression of autophagosome marker LC3B-II and autophagy adaptor proteins SQSTM1/p62, NDP52, and OPTN. SQSTM1/p62 contains ARE in the promoter of its gene. This element is responsible for induction of SQSTM1/p62 expression, which is caused by MIND4-17-mediated increase in the levels of NRF2. Moreover, the induction of SQSTM1/p62 creates a positive feedback loop, in which SQSTM1/p62 further inhibits the interaction between KEAP1 and NRF2, leading to an additional increase in ARE-driven gene expression (Jain et al., 2010). The first primary adaptor protein, NDP52 contains three AREs in its promoter region that can react to increased activation of Nrf2 (Jo et al., 2014). While the trend was not as strong as the one we observed with the analysis of SQSTM1/p62, we still identified a significant increase in the expression of NDP52. In contrast, the second primary adaptor protein we tested, OPTN, exhibited slightly reduced expression levels in patient cells after MIND4-17 treatment. OPTN shows strong homology in primary sequence and on domain organization levels with NFκB essential modulator (NEMO) and is therefore also known as the NEMO-related protein (NRP) (Schwamborn et al., 2000). OPTN may thereby respond to levels of tumor necrosis factor α (TNFα), which are decreased due to the anti-inflammatory effects of the NRF2 activation (Quinti et al., 2017; Sudhakar et al., 2009). While LC3 does not seem to contain an ARE (based on available literature), increased activation of NRF2 led to a fundamental increase in LC3II expression in patients' cells. Similar effect was also observed in other studies implying

that LC3 expression levels change based on levels of NRF2 (Lastres-Becker et al., 2016; Li et al., 2014). Moreover, we observed further accumulation of LC3B-II after a treatment with CQ, implying increased autophagic flux. CQ is a compound, which raises the lysosomal pH and therefore inhibits the fusion between autophagosomes and lysosomes (Mauthe et al., 2018).

Next, we decided to assess the effect of MIND4-17 on mitochondrial morphology. Electron microscopy did not reveal any detrimental results. However, we were able to spot autophagosomes in patients' cells treated with MIND4-17. Intriguingly, Mitotracker^{TM} Red CMXRos staining revealed that mitochondrial networks get more fragmented and accumulate around nucleus after 24 h long incubation with MIND4-17. In fact, the upregulation of SQSTM1/p62 may be related to the clustering. SQSTM1/p62 was previously described as responsible for aggregation of dysfunctional mitochondria into tight clusters to minimize the surface area, which is exposed to other cellular components (Narendra et al., 2010). Such sequestration of ubiquitinated mitochondria by SQSTM1/p62 seems to be analogous to the SQSTM1/p62-mediated clustering of ubiquitinated proteins. Several studies have presented evidence that SQSTM1/p62 binds ubiquitin through its UBA domain and polymerizes via its PB1 domain, thereby enabling the aggregation of misfolded proteins (Bjørkøy et al., 2005; Komatsu et al., 2007; Nezis et al., 2008). While the implications for mitochondrial aggregation in pathophysiology remain to be further unveiled, the reduction of surface area of dysfunctional mitochondria may lower their uptake of substrates and decrease the transmission of mitochondrial ROS across the cell. Moreover, clustering of dysfunctional mitochondria could avoid having them transported to cell compartments with high bioenergetic demands, such as synapses. Another theory depicts SQSTM1/p62 as sensory protein, which detects defective mitophagy, as SQSTM1/p62 clustering of ubiquitinated cargo has been described to be responsible for cell death in certain cell types where its degradation by autophagy was absent (Komatsu et al., 2007; Narendra et al., 2010).

To further determine the impact of MIND4-17 treatment on mitochondrial functions, we measured activity of respiratory chain complexes. MIND4-17 treatment caused a significant increase in the activity of Complex I in patients' cells. First underlying reason might be that NRF2 increases $\Delta\Psi_m$, which directly affects respiratory chain. Second and more probable underlying reason might be the ability of NRF2 to increase substrate availability for complex I (NADH). NRF2-deficient mice exhibited almost two-fold decrease in the pool of mitochondrial NADH, which could be caused by decreased efficiency of the tricarboxylic acid (TCA) cycle (Holmström et al., 2013). Moreover, the so-called "master regulation of mitochondrial

biogenesis", PGC-1α, interacts with both nuclear respiratory factors NRF1 and NRF2, stimulating their powerful induction (Wu et al., 1999). NRF1 also binds to promoter regions of mitochondrial respiratory chain subunits, therefore regulating their expression (Evans and Scarpulla, 1990). Given that NRF1 contains four ARE in its promoter region, this is an indirect effect of NRF2 as well (Piantadosi et al., 2008). Furthermore, DJ-1/PARK7, a mitochondrial protein maintaining the activity of complex I, has been shown to stabilize NRF2 by preventing association with its negative regulator, KEAP1, thereby promoting cytoprotection (Clements et al., 2006). Although the neuroprotectivity mediated by either pharmacological or genetic activation of NRF2 is independent of DJ-1, consequences of the relationship between NRF2 and DJ-1 for mitochondria remains to be investigated (Gan et al., 2010).

Surprising results were observed when we evaluated oxygen consumption in untreated cells. Patients' cells repeatedly exhibited increased respiration, which is contradictory to previous studies of respiration in HD cells. Other studies in different cell types with HD pathology describe a decrease in respiration. However, there is a study which showed that oxygen consumption in juvenile HD fibroblasts was not significantly changed (Aladdin et al., 2019). At this point, we cannot tell, what the cause of this phenomenon is. It could be caused by some pathological behavior, changes in $\Delta\Psi_m$, or cells could be simply trying to overcompensate some deficiencies. Nonetheless, this phenomenon needs to be further studied. On the other hand, MIND4-17 treatment significantly decreased oxygen consumption in HD patients' cells, restoring the values closer to original oxygen consumption levels of control cells. These data are in agreement with observations made by Holmström et. al, where genetically constitutively upregulated NRF2 (caused by Keap1-KO) decreased basal oxygen consumption by ~35% as well as minimized the effect of FCCP on maximal respiration compared to their WT counterparts (Holmström et al., 2013).

While changes in expression of autophagy markers suggested increased autophagic flux, we still needed to study the effect of MIND4-17 on mitophagy specifically. In order to achieve that, we transfected cells with pEGFP-LC3 plasmid. Then we studied the colocalization of TOMM20 stained mitochondria and LC3-positive autophagosomes. First interesting results were delivered, when quantitative analysis of colocalization revealed that untreated patients' cells have decreased Manders' overlap coefficient by ~27% compared to untreated control cells. This is consistent with previous studies, which demonstrated that mHTT impairs cargo recognition by autophagosomes through the sequestration of proautophagic proteins, such as SQSTM1/p62, which results in disrupted loading of autophagosomes with mitochondria (Khalil

et al., 2015; Martinez-Vicente et al., 2010). Excitingly, MIND4-17 treatment resulted in a 1.85-fold increase of Manders' overlap coefficient in control cells and a 2.2-fold increase of Manders' overlap coefficient in patients' cells. These differences in colocalization suggest that the formation of mitochondria-containing autophagosomes is upregulated after NRF2 activation mediated by MIND4-17 treatment. Regarding the immunoblot data, we believe that the enormous increase of SQSTM1/p62 expression allows an escape from sequestration by mHTT. Hence, the increased amount of free SQSTM1/p62 accompanied by the increased amount of NDP52 could then together sufficiently serve to target ubiquitinated mitochondria into autophagosomes.

Based on these *in vitro* observations, it seems that the small-molecule compound MIND4-17 could serve as a potent mitophagy inducer. Being already well known for its neuroprotective effects, we can add modulation of mitochondrial quality control to the already wide scope of positive outcomes MIND4-17 can provide. Therefore, we highlight the therapeutic potential of NRF2 inducing drugs not only in the study of neurodegenerative diseases. Furthermore, we report that HD HSF can be used to study mitophagy. This proves useful especially since human HD striatal tissue is hardly accessible and postmortem HD brain tissue is not feasible for the study of cellular pathogenesis. It would also be interesting to study mitophagy in neural stem cells differentiated from HD induced pluripotent stem cells. However, one should bear in mind that there is no easy way to extrapolate results obtained from cell cultures to complex organisms. Even data obtained from the currently very advanced animal HD models need to meet the relational, qualitative, quantitative, and modal elements before one can assume any resemblance to the actual occurrence in the HD human brain.

7 Conclusion

Aims of this thesis were fullfilled. We proved that the small molecule compound, MIND4-17, could be used as a mitophagy inducer. We showed that fibroblasts from HD patients could serve as a suitable and "easily" accessible model to study mitophagy in the context of HD. Conlusions of this thesis are supported by these main results:

- Immunobloting techniques have shown increased autophagic flux in fibroblasts from HD patients after MIND4-17 treatment.
- Fluorescence microscopy revealed clustering of mitochondria around nucleus after MIND4-17 treatment in fibroblasts from HD patients and control cells.
- Electron microscopy did not show any significant changes on the level of mitochondrial ultrastructure.
- Spectrophotometric analysis of respiratory chain enzymes activities displayed increased activity of complex I in MIND4-17 treated fibroblasts from HD patients.
- Analysis on the Seahorse XFe24 Extracellular Flux Analysis revealed decrease in oxygen consumption after MIND4-17 treatment in both control fibroblasts and fibroblasts from HD patients. No significant changes in glycolytic rates were observed.
- MIND4-17 treatment increased colocalization of mitochondria and autophagosomes in both control fibroblasts and with higher rate in fibroblasts from HD patients.

8 References

Aladdin, A., Király, R., Boto, P., Regdon, Z., Tar, K., 2019. Juvenile Huntington's Disease Skin Fibroblasts Respond with Elevated Parkin Level and Increased Proteasome Activity as a Potential Mechanism to Counterbalance the Pathological Consequences of Mutant Huntingtin Protein. Int J Mol Sci 20, 5338. https://doi.org/10.3390/ijms20215338

Albin, R.L., Reiner, A., Anderson, K.D., Penney, J.B., Young, A.B., 1990. Striatal and nigral neuron subpopulations in rigid Huntington's disease: Implications for the functional anatomy of chorea and rigidity-akinesia. Annals of Neurology 27, 357–365. https://doi.org/10.1002/ana.410270403

Bae, B.-I., Xu, H., Igarashi, S., Fujimuro, M., Agrawal, N., Taya, Y., Hayward, S.D., Moran, T.H., Montell, C., Ross, C.A., Snyder, S.H., Sawa, A., 2005. p53 Mediates Cellular Dysfunction and Behavioral Abnormalities in Huntington's Disease. Neuron 47, 29–41. https://doi.org/10.1016/j.neuron.2005.06.005

Baird, L., Llères, D., Swift, S., Dinkova-Kostova, A.T., 2013. Regulatory flexibility in the Nrf2-mediated stress response is conferred by conformational cycling of the Keap1-Nrf2 protein complex. Proc Natl Acad Sci U S A 110, 15259–15264. https://doi.org/10.1073/pnas.1305687110

Ban, T., Ishihara, T., Kohno, H., Saita, S., Ichimura, A., Maenaka, K., Oka, T., Mihara, K., Ishihara, N., 2017. Molecular basis of selective mitochondrial fusion by heterotypic action between OPA1 and cardiolipin. Nat Cell Biol 19, 856–863. https://doi.org/10.1038/ncb3560

Ban, T., Kohno, H., Ishihara, T., Ishihara, N., 2018. Relationship between OPA1 and cardiolipin in mitochondrial inner-membrane fusion. Biochim Biophys Acta Bioenerg 1859, 951–957. https://doi.org/10.1016/j.bbabio.2018.05.016

Beal, M.F., Brouillet, E., Jenkins, B.G., Ferrante, R.J., Kowall, N.W., Miller, J.M., Storey, E., Srivastava, R., Rosen, B.R., Hyman, B.T., 1993. Neurochemical and histologic characterization of striatal excitotoxic lesions produced by the mitochondrial toxin 3-nitropropionic acid. J Neurosci 13, 4181–4192.

Benchoua, A., Trioulier, Y., Zala, D., Gaillard, M.-C., Lefort, N., Dufour, N., Saudou, F., Elalouf, J.-M., Hirsch, E., Hantraye, P., Déglon, N., Brouillet, E., 2006. Involvement of Mitochondrial Complex II Defects in Neuronal Death Produced by N-Terminus Fragment of Mutated Huntingtin. Mol Biol Cell 17, 1652–1663. https://doi.org/10.1091/mbc.E05-07-0607

Benedetto, A., Gems, D., 2019. Autophagy promotes visceral aging in wild-type C. elegans. Autophagy 15, 731–732. https://doi.org/10.1080/15548627.2019.1569919

Benn, C.L., Sun, T., Sadri-Vakili, G., McFarland, K.N., DiRocco, D.P., Yohrling, G.J., Clark, T.W., Bouzou, B., Cha, J.-H.J., 2008. Huntingtin Modulates Transcription, Occupies Gene Promoters In Vivo, and Binds Directly to DNA in a Polyglutamine-Dependent Manner. J Neurosci 28, 10720–10733. https://doi.org/10.1523/JNEUROSCI.2126-08.2008

Bertrand, H.C., Schaap, M., Baird, L., Georgakopoulos, N.D., Fowkes, A., Thiollier, C., Kachi, H., Dinkova-Kostova, A.T., Wells, G., 2015. Design, Synthesis, and Evaluation of Triazole Derivatives That Induce Nrf2 Dependent Gene Products and Inhibit the Keap1–Nrf2 Protein–Protein Interaction. J. Med. Chem. 58, 7186–7194. https://doi.org/10.1021/acs.jmedchem.5b00602

Bjedov, I., Cochemé, H.M., Foley, A., Wieser, D., Woodling, N.S., Castillo-Quan, J.I., Norvaisas, P., Lujan, C., Regan, J.C., Toivonen, J.M., Murphy, M.P., Thornton, J., Kinghorn, K.J., Neufeld, T.P., Cabreiro, F., Partridge, L., 2020. Fine-tuning autophagy maximises lifespan and is associated with changes in mitochondrial gene expression in Drosophila. PLoS Genet 16. https://doi.org/10.1371/journal.pgen.1009083

Bjørkøy, G., Lamark, T., Brech, A., Outzen, H., Perander, M., Øvervatn, A., Stenmark, H., Johansen, T., 2005. p62/SQSTM1 forms protein aggregates degraded by autophagy and has a protective

effect on huntingtin-induced cell death. J Cell Biol 171, 603–614. https://doi.org/10.1083/jcb.200507002
Borrell-Pagès, M., Zala, D., Humbert, S., Saudou, F., 2006. Huntington's disease: from huntingtin function and dysfunction to therapeutic strategies. Cell Mol Life Sci 63, 2642–2660. https://doi.org/10.1007/s00018-006-6242-0
Brouillet, E., Hantraye, P., Ferrante, R.J., Dolan, R., Leroy-Willig, A., Kowall, N.W., Beal, M.F., July 18. Chronic mitochondrial energy impairment produces selective striatal degeneration and abnormal choreiform movements in primates. 1995, 7105–7109. https://doi.org/10.1073/pnas.92.15.7105
Brundin, P., Melki, R., Kopito, R., 2010. Prion-like transmission of protein aggregates in neurodegenerative diseases. Nat Rev Mol Cell Biol 11, 301–307. https://doi.org/10.1038/nrm2873
Budd, S.L., Nicholls, D.G., 1996. Mitochondria, calcium regulation, and acute glutamate excitotoxicity in cultured cerebellar granule cells. J Neurochem 67, 2282–2291. https://doi.org/10.1046/j.1471-4159.1996.67062282.x
Cha, J.H., 2000. Transcriptional dysregulation in Huntington's disease. Trends Neurosci 23, 387–392. https://doi.org/10.1016/s0166-2236(00)01609-x
Chacinska, A., Koehler, C.M., Milenkovic, D., Lithgow, T., Pfanner, N., 2009. Importing Mitochondrial Proteins: Machineries and Mechanisms. Cell 138, 628–644. https://doi.org/10.1016/j.cell.2009.08.005
Chafekar, S.M., Duennwald, M.L., 2012. Impaired heat shock response in cells expressing full-length polyglutamine-expanded huntingtin. PLoS ONE 7, e37929. https://doi.org/10.1371/journal.pone.0037929
Chen, G., Cizeau, J., Vande Velde, C., Park, J.H., Bozek, G., Bolton, J., Shi, L., Dubik, D., Greenberg, A., 1999. Nix and Nip3 Form a Subfamily of Pro-apoptotic Mitochondrial Proteins*. Journal of Biological Chemistry 274, 7–10. https://doi.org/10.1074/jbc.274.1.7
Chen, G., Han, Z., Feng, D., Chen, Y., Chen, L., Wu, H., Huang, L., Zhou, C., Cai, X., Fu, C., Duan, L., Wang, X., Liu, L., Liu, X., Shen, Y., Zhu, Y., Chen, Q., 2014. A regulatory signaling loop comprising the PGAM5 phosphatase and CK2 controls receptor-mediated mitophagy. Mol Cell 54, 362–377. https://doi.org/10.1016/j.molcel.2014.02.034
Chen, H., Detmer, S.A., Ewald, A.J., Griffin, E.E., Fraser, S.E., Chan, D.C., 2003. Mitofusins Mfn1 and Mfn2 coordinately regulate mitochondrial fusion and are essential for embryonic development. J Cell Biol 160, 189–200. https://doi.org/10.1083/jcb.200211046
Clements, C.M., McNally, R.S., Conti, B.J., Mak, T.W., Ting, J.P.-Y., 2006. DJ-1, a cancer- and Parkinson's disease-associated protein, stabilizes the antioxidant transcriptional master regulator Nrf2. Proceedings of the National Academy of Sciences 103, 15091–15096. https://doi.org/10.1073/pnas.0607260103
Craufurd, D., Dodge, A., 1993. Mutation size and age at onset in Huntington's disease. J Med Genet 30, 1008–1011.
Cui, L., Jeong, H., Borovecki, F., Parkhurst, C.N., Tanese, N., Krainc, D., 2006. Transcriptional repression of PGC-1alpha by mutant huntingtin leads to mitochondrial dysfunction and neurodegeneration. Cell 127, 59–69. https://doi.org/10.1016/j.cell.2006.09.015
Deter, R.L., Baudhuin, P., de Duve, C., 1967. PARTICIPATION OF LYSOSOMES IN CELLULAR AUTOPHAGY INDUCED IN RAT LIVER BY GLUCAGON. J Cell Biol 35, C11–C16.
Dimcheff, D.E., Portis, J.L., Caughey, B., 2003. Prion proteins meet protein quality control. Trends Cell Biol 13, 337–340. https://doi.org/10.1016/s0962-8924(03)00125-9
Dinkova-Kostova, A.T., Abramov, A.Y., 2015. The emerging role of Nrf2 in mitochondrial function. Free Radic Biol Med 88, 179–188. https://doi.org/10.1016/j.freeradbiomed.2015.04.036
Doxaki, C., Palikaras, K., 2021. Neuronal Mitophagy: Friend or Foe? Frontiers in Cell and Developmental Biology 8.

Dunn, W.A., Cregg, J.M., Kiel, J.A.K.W., van der Klei, I.J., Oku, M., Sakai, Y., Sibirny, A.A., Stasyk, O.V., Veenhuis, M., 2005. Pexophagy: the selective autophagy of peroxisomes. Autophagy 1, 75–83. https://doi.org/10.4161/auto.1.2.1737

East, D.A., Fagiani, F., Crosby, J., Georgakopoulos, N.D., Bertrand, H., Schaap, M., Fowkes, A., Wells, G., Campanella, M., 2014. PMI: A ΔΨm Independent Pharmacological Regulator of Mitophagy. Chemistry & Biology 21, 1585–1596. https://doi.org/10/f6rfjz

Elmore, S.P., Qian, T., Grissom, S.F., Lemasters, J.J., 2001. The mitochondrial permeability transition initiates autophagy in rat hepatocytes. FASEB J 15, 2286–2287. https://doi.org/10.1096/fj.01-0206fje

Evans, M.J., Scarpulla, R.C., 1990. NRF-1: a trans-activator of nuclear-encoded respiratory genes in animal cells. Genes Dev 4, 1023–1034. https://doi.org/10.1101/gad.4.6.1023

Fahey, J.W., Talalay, P., 1999. Antioxidant Functions of Sulforaphane: a Potent Inducer of Phase II Detoxication Enzymes. Food and Chemical Toxicology 37, 973–979. https://doi.org/10.1016/S0278-6915(99)00082-4

Franco-Iborra, S., Plaza-Zabala, A., Montpeyo, M., Sebastian, D., Vila, M., Martinez-Vicente, M., 2021. Mutant HTT (huntingtin) impairs mitophagy in a cellular model of Huntington disease. Autophagy 17, 672–689. https://doi.org/10.1080/15548627.2020.1728096

Fujioka, Y., Noda, N.N., Nakatogawa, H., Ohsumi, Y., Inagaki, F., 2010. Dimeric coiled-coil structure of Saccharomyces cerevisiae Atg16 and its functional significance in autophagy. J Biol Chem 285, 1508–1515. https://doi.org/10.1074/jbc.M109.053520

Furukawa, M., Xiong, Y., 2005. BTB Protein Keap1 Targets Antioxidant Transcription Factor Nrf2 for Ubiquitination by the Cullin 3-Roc1 Ligase. Mol Cell Biol 25, 162–171. https://doi.org/10.1128/MCB.25.1.162-171.2005

Gan, L., Johnson, D.A., Johnson, J.A., 2010. Keap1-Nrf2 activation in the presence and absence of DJ-1. European Journal of Neuroscience 31, 967–977. https://doi.org/10.1111/j.1460-9568.2010.07138.x

Gauthier, L.R., Charrin, B.C., Borrell-Pagès, M., Dompierre, J.P., Rangone, H., Cordelières, F.P., De Mey, J., MacDonald, M.E., Lessmann, V., Humbert, S., Saudou, F., 2004. Huntingtin controls neurotrophic support and survival of neurons by enhancing BDNF vesicular transport along microtubules. Cell 118, 127–138. https://doi.org/10.1016/j.cell.2004.06.018

Georgakopoulos, N.D., Frison, M., Alvarez, M.S., Bertrand, H., Wells, G., Campanella, M., 2017. Reversible Keap1 inhibitors are preferential pharmacological tools to modulate cellular mitophagy. Scientific Reports 7, 1–14. https://doi.org/10.1038/s41598-017-07679-7

Gomez-Pastor, R., Burchfiel, E.T., Neef, D.W., Jaeger, A.M., Cabiscol, E., McKinstry, S.U., Doss, A., Aballay, A., Lo, D.C., Akimov, S.S., Ross, C.A., Eroglu, C., Thiele, D.J., 2017. Abnormal degradation of the neuronal stress-protective transcription factor HSF1 in Huntington's disease. Nat Commun 8, 1–17. https://doi.org/10.1038/ncomms14405

Graef, M., Friedman, J.R., Graham, C., Babu, M., Nunnari, J., 2013. ER exit sites are physical and functional core autophagosome biogenesis components. Mol Biol Cell 24, 2918–2931. https://doi.org/10.1091/mbc.E13-07-0381

Greene, A.W., Grenier, K., Aguileta, M.A., Muise, S., Farazifard, R., Haque, M.E., McBride, H.M., Park, D.S., Fon, E.A., 2012. Mitochondrial processing peptidase regulates PINK1 processing, import and Parkin recruitment. EMBO Rep 13, 378–385. https://doi.org/10/f4rn8b

Gu, M., Gash, M.T., Mann, V.M., Javoy-Agid, F., Cooper, J.M., Schapira, A.H., 1996. Mitochondrial defect in Huntington's disease caudate nucleus. Ann. Neurol. 39, 385–389. https://doi.org/10/dxjzjn

Gunawardena, S., Her, L.-S., Brusch, R.G., Laymon, R.A., Niesman, I.R., Gordesky-Gold, B., Sintasath, L., Bonini, N.M., Goldstein, L.S.B., 2003. Disruption of Axonal Transport by Loss of Huntingtin or Expression of Pathogenic PolyQ Proteins in Drosophila. Neuron 40, 25–40. https://doi.org/10.1016/S0896-6273(03)00594-4

Guo, X., Disatnik, M.-H., Monbureau, M., Shamloo, M., Mochly-Rosen, D., Qi, X., 2013. Inhibition of mitochondrial fragmentation diminishes Huntington's disease–associated neurodegeneration. J Clin Invest 123, 5371–5388. https://doi.org/10.1172/JCI70911

Hanada, T., Noda, N.N., Satomi, Y., Ichimura, Y., Fujioka, Y., Takao, T., Inagaki, F., Ohsumi, Y., 2007. The Atg12-Atg5 conjugate has a novel E3-like activity for protein lipidation in autophagy. J Biol Chem 282, 37298–37302. https://doi.org/10.1074/jbc.C700195200

Hanna, R.A., Quinsay, M.N., Orogo, A.M., Giang, K., Rikka, S., Gustafsson, Å.B., 2012. Microtubule-associated protein 1 light chain 3 (LC3) interacts with Bnip3 protein to selectively remove endoplasmic reticulum and mitochondria via autophagy. J Biol Chem 287, 19094–19104. https://doi.org/10.1074/jbc.M111.322933

Hay, D.G., Sathasivam, K., Tobaben, S., Stahl, B., Marber, M., Mestril, R., Mahal, A., Smith, D.L., Woodman, B., Bates, G.P., 2004. Progressive decrease in chaperone protein levels in a mouse model of Huntington's disease and induction of stress proteins as a therapeutic approach. Hum Mol Genet 13, 1389–1405. https://doi.org/10.1093/hmg/ddh144

Heiseke, A., Aguib, Y., Schatzl, H.M., 2010. Autophagy, prion infection and their mutual interactions. Curr Issues Mol Biol 12, 87–97.

Hirose, S., Yaginuma, N., Inada, Y., 1974. Disruption of Charge Separation Followed by that of the Proton Gradient in the Mitochondrial Membrane by CCCP. The Journal of Biochemistry 76, 213–216. https://doi.org/10.1093/oxfordjournals.jbchem.a130549

Hollenbeck, P.J., Saxton, W.M., 2005. The axonal transport of mitochondria. J Cell Sci 118, 5411–5419. https://doi.org/10.1242/jcs.02745

Holmström, K.M., Baird, L., Zhang, Y., Hargreaves, I., Chalasani, A., Land, J.M., Stanyer, L., Yamamoto, M., Dinkova-Kostova, A.T., Abramov, A.Y., 2013. Nrf2 impacts cellular bioenergetics by controlling substrate availability for mitochondrial respiration. Biol Open 2, 761–770. https://doi.org/10.1242/bio.20134853

Hong, F., Freeman, M.L., Liebler, D.C., 2005. Identification of sensor cysteines in human Keap1 modified by the cancer chemopreventive agent sulforaphane. Chem Res Toxicol 18, 1917–1926. https://doi.org/10.1021/tx0502138

Ichimura, Y., Kirisako, T., Takao, T., Satomi, Y., Shimonishi, Y., Ishihara, N., Mizushima, N., Tanida, I., Kominami, E., Ohsumi, M., Noda, T., Ohsumi, Y., 2000. A ubiquitin-like system mediates protein lipidation. Nature 408, 488–492. https://doi.org/10.1038/35044114

Ikeda, H., Yamaguchi, M., Sugai, S., Aze, Y., Narumiya, S., Kakizuka, A., 1996. Expanded polyglutamine in the Machado–Joseph disease protein induces cell death in vitro and in vivo. Nature Genetics 13, 196–202. https://doi.org/10.1038/ng0696-196

Ingerman, E., Perkins, E.M., Marino, M., Mears, J.A., McCaffery, J.M., Hinshaw, J.E., Nunnari, J., 2005. Dnm1 forms spirals that are structurally tailored to fit mitochondria. J Cell Biol 170, 1021–1027. https://doi.org/10.1083/jcb.200506078

Intihar, T.A., Martinez, E.A., Gomez-Pastor, R., 2019. Mitochondrial Dysfunction in Huntington's Disease; Interplay Between HSF1, p53 and PGC-1α Transcription Factors. Front. Cell. Neurosci. 13. https://doi.org/10.3389/fncel.2019.00103

Itoh, K., Nakamura, K., Iijima, M., Sesaki, H., 2013. Mitochondrial dynamics in neurodegeneration. Trends Cell Biol 23, 64–71. https://doi.org/10.1016/j.tcb.2012.10.006

Ivankovic, D., Chau, K.-Y., Schapira, A.H.V., Gegg, M.E., 2016. Mitochondrial and lysosomal biogenesis are activated following PINK1/parkin-mediated mitophagy. J. Neurochem. 136, 388–402. https://doi.org/10.1111/jnc.13412

Jain, A., Lamark, T., Sjøttem, E., Larsen, K.B., Awuh, J.A., Øvervatn, A., McMahon, M., Hayes, J.D., Johansen, T., 2010. p62/SQSTM1 Is a Target Gene for Transcription Factor NRF2 and Creates a Positive Feedback Loop by Inducing Antioxidant Response Element-driven Gene Transcription. J. Biol. Chem. 285, 22576–22591. https://doi.org/10.1074/jbc.M110.118976

Jenkins, B.G., Andreassen, O.A., Dedeoglu, A., Leavitt, B., Hayden, M., Borchelt, D., Ross, C.A., Ferrante, R.J., Beal, M.F., 2005. Effects of CAG repeat length, HTT protein length and protein context on cerebral metabolism measured using magnetic resonance spectroscopy in

transgenic mouse models of Huntington's disease. Journal of Neurochemistry 95, 553–562. https://doi.org/10/db9ztd
Jin, S.M., Lazarou, M., Wang, C., Kane, L.A., Narendra, D.P., Youle, R.J., 2010. Mitochondrial membrane potential regulates PINK1 import and proteolytic destabilization by PARL. J Cell Biol 191, 933–942. https://doi.org/10.1083/jcb.201008084
Jo, C., Gundemir, S., Pritchard, S., Jin, Y.N., Rahman, I., Johnson, G.V.W., 2014. Nrf2 reduces levels of phosphorylated tau protein by inducing autophagy adaptor protein NDP52. Nature Communications 5, 1–13. https://doi.org/10.1038/ncomms4496
Kabeya, Y., Kamada, Y., Baba, M., Takikawa, H., Sasaki, M., Ohsumi, Y., 2005. Atg17 functions in cooperation with Atg1 and Atg13 in yeast autophagy. Mol Biol Cell 16, 2544–2553. https://doi.org/10.1091/mbc.e04-08-0669
Kabeya, Y., Kawamata, T., Suzuki, K., Ohsumi, Y., 2007. Cis1/Atg31 is required for autophagosome formation in Saccharomyces cerevisiae. Biochem Biophys Res Commun 356, 405–410. https://doi.org/10.1016/j.bbrc.2007.02.150
Kabeya, Y., Mizushima, N., Ueno, T., Yamamoto, A., Kirisako, T., Noda, T., Kominami, E., Ohsumi, Y., Yoshimori, T., 2000. LC3, a mammalian homologue of yeast Apg8p, is localized in autophagosome membranes after processing. EMBO J 19, 5720–5728. https://doi.org/10.1093/emboj/19.21.5720
Kageyama, Y., Zhang, Z., Sesaki, H., 2011. Mitochondrial division: molecular machinery and physiological functions. Curr Opin Cell Biol 23, 427–434. https://doi.org/10.1016/j.ceb.2011.04.009
Kaltenbach, L.S., Romero, E., Becklin, R.R., Chettier, R., Bell, R., Phansalkar, A., Strand, A., Torcassi, C., Savage, J., Hurlburt, A., Cha, G.-H., Ukani, L., Chepanoske, C.L., Zhen, Y., Sahasrabudhe, S., Olson, J., Kurschner, C., Ellerby, L.M., Peltier, J.M., Botas, J., Hughes, R.E., 2007. Huntingtin Interacting Proteins Are Genetic Modifiers of Neurodegeneration. PLoS Genet 3, e82. https://doi.org/10.1371/journal.pgen.0030082
Kamada, Y., Funakoshi, T., Shintani, T., Nagano, K., Ohsumi, M., Ohsumi, Y., 2000. Tor-Mediated Induction of Autophagy via an Apg1 Protein Kinase Complex. J Cell Biol 150, 1507–1513.
Kameoka, S., Adachi, Y., Okamoto, K., Iijima, M., Sesaki, H., 2018. Phosphatidic Acid and Cardiolipin Coordinate Mitochondrial Dynamics. Trends in Cell Biology 28, 67–76. https://doi.org/10.1016/j.tcb.2017.08.011
Kanki, T., Klionsky, D.J., 2008. Mitophagy in yeast occurs through a selective mechanism. J Biol Chem 283, 32386–32393. https://doi.org/10.1074/jbc.M802403200
Kanki, T., Wang, K., Cao, Y., Baba, M., Klionsky, D.J., 2009. Atg32 is a mitochondrial protein that confers selectivity during mitophagy. Dev Cell 17, 98–109. https://doi.org/10.1016/j.devcel.2009.06.014
Kawamata, T., Kamada, Y., Kabeya, Y., Sekito, T., Ohsumi, Y., 2008. Organization of the Pre-autophagosomal Structure Responsible for Autophagosome Formation. Mol Biol Cell 19, 2039–2050. https://doi.org/10.1091/mbc.E07-10-1048
Kegel, K.B., Sapp, E., Alexander, J., Valencia, A., Reeves, P., Li, X., Masso, N., Sobin, L., Aronin, N., DiFiglia, M., 2009. Polyglutamine expansion in huntingtin alters its interaction with phospholipids. Journal of Neurochemistry 110, 1585–1597. https://doi.org/10.1111/j.1471-4159.2009.06255.x
Khalil, B., El Fissi, N., Aouane, A., Cabirol-Pol, M.-J., Rival, T., Liévens, J.-C., 2015. PINK1-induced mitophagy promotes neuroprotection in Huntington's disease. Cell Death Dis 6, e1617. https://doi.org/10.1038/cddis.2014.581
Kim, I., Rodriguez-Enriquez, S., Lemasters, J.J., 2007. Selective degradation of mitochondria by mitophagy. Arch Biochem Biophys 462, 245–253. https://doi.org/10.1016/j.abb.2007.03.034
Kirisako, T., Ichimura, Y., Okada, H., Kabeya, Y., Mizushima, N., Yoshimori, T., Ohsumi, M., Takao, T., Noda, T., Ohsumi, Y., 2000. The reversible modification regulates the membrane-binding state of Apg8/Aut7 essential for autophagy and the cytoplasm to vacuole targeting pathway. J Cell Biol 151, 263–276. https://doi.org/10.1083/jcb.151.2.263

Klionsky, D.J., 2007. Autophagy: from phenomenology to molecular understanding in less than a decade. Nat Rev Mol Cell Biol 8, 931–937. https://doi.org/10.1038/nrm2245
Knott, A.B., Bossy-Wetzel, E., 2008. Impairing the Mitochondrial Fission and Fusion Balance: A New Mechanism of Neurodegeneration. Ann N Y Acad Sci 1147, 283–292. https://doi.org/10.1196/annals.1427.030
Komatsu, M., Waguri, S., Koike, M., Sou, Y., Ueno, T., Hara, T., Mizushima, N., Iwata, J., Ezaki, J., Murata, S., Hamazaki, J., Nishito, Y., Iemura, S., Natsume, T., Yanagawa, T., Uwayama, J., Warabi, E., Yoshida, H., Ishii, T., Kobayashi, A., Yamamoto, M., Yue, Z., Uchiyama, Y., Kominami, E., Tanaka, K., 2007. Homeostatic Levels of p62 Control Cytoplasmic Inclusion Body Formation in Autophagy-Deficient Mice. Cell 131, 1149–1163. https://doi.org/10.1016/j.cell.2007.10.035
Koroshetz, W.J., Jenkins, B.G., Rosen, B.R., Beal, M.F., 1997. Energy metabolism defects in Huntington's disease and effects of coenzyme Q10. Annals of Neurology 41, 160–165. https://doi.org/10.1002/ana.410410206
Kowall, N.W., Ferrante, R.J., Martin, J.B., 1987. Patterns of cell loss in Huntington's disease. Trends in Neurosciences 10, 24–29. https://doi.org/10.1016/0166-2236(87)90120-2
Kraft, C., Deplazes, A., Sohrmann, M., Peter, M., 2008. Mature ribosomes are selectively degraded upon starvation by an autophagy pathway requiring the Ubp3p/Bre5p ubiquitin protease. Nat Cell Biol 10, 602–610. https://doi.org/10.1038/ncb1723
Labbadia, J., Cunliffe, H., Weiss, A., Katsyuba, E., Sathasivam, K., Seredenina, T., Woodman, B., Moussaoui, S., Frentzel, S., Luthi-Carter, R., Paganetti, P., Bates, G.P., 2011. Altered chromatin architecture underlies progressive impairment of the heat shock response in mouse models of Huntington disease. J Clin Invest 121, 3306–3319. https://doi.org/10.1172/JCI57413
Lastres-Becker, I., García-Yagüe, A.J., Scannevin, R.H., Casarejos, M.J., Kügler, S., Rábano, A., Cuadrado, A., 2016. Repurposing the NRF2 Activator Dimethyl Fumarate as Therapy Against Synucleinopathy in Parkinson's Disease. Antioxid Redox Signal 25, 61–77. https://doi.org/10.1089/ars.2015.6549
Lazarou, M., Jin, S.M., Kane, L.A., Youle, R.J., 2012. Role of PINK1 binding to the TOM complex and alternate intracellular membranes in recruitment and activation of the E3 ligase Parkin. Dev Cell 22, 320–333. https://doi.org/10.1016/j.devcel.2011.12.014
Lazarou, M., Sliter, D.A., Kane, L.A., Sarraf, S.A., Wang, C., Burman, J.L., Sideris, D.P., Fogel, A.I., Youle, R.J., 2015. The ubiquitin kinase PINK1 recruits autophagy receptors to induce mitophagy. Nature 524, 309–314. https://doi.org/10.1038/nature14893
Lee, Y., Jeong, S.-Y., Karbowski, M., Smith, C.L., Youle, R.J., 2004. Roles of the mammalian mitochondrial fission and fusion mediators Fis1, Drp1, and Opa1 in apoptosis. Mol Biol Cell 15, 5001–5011. https://doi.org/10.1091/mbc.e04-04-0294
Lemasters, J.J., 2005. Selective mitochondrial autophagy, or mitophagy, as a targeted defense against oxidative stress, mitochondrial dysfunction, and aging. Rejuvenation Res 8, 3–5. https://doi.org/10.1089/rej.2005.8.3
Li, S., Wang, W., Niu, T., Wang, H., Li, B., Shao, L., Lai, Y., Li, H., Janicki, J.S., Wang, X.L., Tang, D., Cui, T., 2014. Nrf2 Deficiency Exaggerates Doxorubicin-Induced Cardiotoxicity and Cardiac Dysfunction. Oxidative Medicine and Cellular Longevity 2014, e748524. https://doi.org/10.1155/2014/748524
Li, X.-J., Li, S.-H., Sharp, A.H., Nucifora, F.C., Schilling, G., Lanahan, A., Worley, P., Snyder, S.H., Ross, C.A., 1995. A huntingtin-associated protein enriched in brain with implications for pathology. Nature 378, 398–402. https://doi.org/10.1038/378398a0
Lin, M.T., Beal, M.F., 2006. Mitochondrial dysfunction and oxidative stress in neurodegenerative diseases. Nature 443, 787–795. https://doi.org/10.1038/nature05292
Liu, L., Feng, D., Chen, G., Chen, M., Zheng, Q., Song, P., Ma, Q., Zhu, C., Wang, R., Qi, W., Huang, L., Xue, P., Li, B., Wang, X., Jin, H., Wang, J., Yang, F., Liu, P., Zhu, Y., Sui, S., Chen, Q., 2012.

Mitochondrial outer-membrane protein FUNDC1 mediates hypoxia-induced mitophagy in mammalian cells. Nat Cell Biol 14, 177–185. https://doi.org/10.1038/ncb2422
Lu, W., Karuppagounder, S.S., Springer, D.A., Allen, M.D., Zheng, L., Chao, B., Zhang, Y., Dawson, V.L., Dawson, T.M., Lenardo, M., 2014. Genetic deficiency of the mitochondrial protein PGAM5 causes a Parkinson's-like movement disorder. Nat Commun 5, 4930. https://doi.org/10.1038/ncomms5930
MacDonald, M.E., Ambrose, C.M., Duyao, M.P., Myers, R.H., Lin, C., Srinidhi, L., Barnes, G., Taylor, S.A., James, M., Groot, N., MacFarlane, H., Jenkins, B., Anderson, M.A., Wexler, N.S., Gusella, J.F., Bates, G.P., Baxendale, S., Hummerich, H., Kirby, S., North, M., Youngman, S., Mott, R., Zehetner, G., Sedlacek, Z., Poustka, A., Frischauf, A.-M., Lehrach, H., Buckler, A.J., Church, D., Doucette-Stamm, L., O'Donovan, M.C., Riba-Ramirez, L., Shah, M., Stanton, V.P., Strobel, S.A., Draths, K.M., Wales, J.L., Dervan, P., Housman, D.E., Altherr, M., Shiang, R., Thompson, L., Fielder, T., Wasmuth, J.J., Tagle, D., Valdes, J., Elmer, L., Allard, M., Castilla, L., Swaroop, M., Blanchard, K., Collins, F.S., Snell, R., Holloway, T., Gillespie, K., Datson, N., Shaw, D., Harper, P.S., 1993. A novel gene containing a trinucleotide repeat that is expanded and unstable on Huntington's disease chromosomes. Cell 72, 971–983. https://doi.org/10.1016/0092-8674(93)90585-E
Maheshwari, M., Bhutani, S., Das, A., Mukherjee, R., Sharma, A., Kino, Y., Nukina, N., Jana, N.R., 2014. Dexamethasone induces heat shock response and slows down disease progression in mouse and fly models of Huntington's disease. Human Molecular Genetics 23, 2737–2751. https://doi.org/10.1093/hmg/ddt667
Mangiarini, L., Sathasivam, K., Seller, M., Cozens, B., Harper, A., Hetherington, C., Lawton, M., Trottier, Y., Lehrach, H., Davies, S.W., Bates, G.P., 1996. Exon 1 of the HD Gene with an Expanded CAG Repeat Is Sufficient to Cause a Progressive Neurological Phenotype in Transgenic Mice. Cell 87, 493–506. https://doi.org/10.1016/S0092-8674(00)81369-0
Martinez-Vicente, M., 2017. Neuronal Mitophagy in Neurodegenerative Diseases. Front. Mol. Neurosci. 10. https://doi.org/10.3389/fnmol.2017.00064
Martinez-Vicente, M., Talloczy, Z., Wong, E., Tang, G., Koga, H., Kaushik, S., de Vries, R., Arias, E., Harris, S., Sulzer, D., Cuervo, A.M., 2010. Cargo recognition failure is responsible for inefficient autophagy in Huntington's disease. Nat. Neurosci. 13, 567–576. https://doi.org/10.1038/nn.2528
Matoba, K., Kotani, T., Tsutsumi, A., Tsuji, T., Mori, T., Noshiro, D., Sugita, Y., Nomura, N., Iwata, S., Ohsumi, Y., Fujimoto, T., Nakatogawa, H., Kikkawa, M., Noda, N.N., 2020. Atg9 is a lipid scramblase that mediates autophagosomal membrane expansion. Nat Struct Mol Biol 27, 1185–1193. https://doi.org/10.1038/s41594-020-00518-w
McMahon, M., Itoh, K., Yamamoto, M., Hayes, J.D., 2003. Keap1-dependent proteasomal degradation of transcription factor Nrf2 contributes to the negative regulation of antioxidant response element-driven gene expression. J. Biol. Chem. 278, 21592–21600. https://doi.org/10.1074/jbc.M300931200
Meissner, C., Lorenz, H., Weihofen, A., Selkoe, D.J., Lemberg, M.K., 2011. The mitochondrial intramembrane protease PARL cleaves human Pink1 to regulate Pink1 trafficking. Journal of Neurochemistry 117, 856–867. https://doi.org/10.1111/j.1471-4159.2011.07253.x
Mizushima, N., 2007. Autophagy: process and function. Genes Dev 21, 2861–2873. https://doi.org/10.1101/gad.1599207
Mizushima, N., Kuma, A., Kobayashi, Y., Yamamoto, A., Matsubae, M., Takao, T., Natsume, T., Ohsumi, Y., Yoshimori, T., 2003. Mouse Apg16L, a novel WD-repeat protein, targets to the autophagic isolation membrane with the Apg12-Apg5 conjugate. J Cell Sci 116, 1679–1688. https://doi.org/10.1242/jcs.00381
Mizushima, N., Noda, T., Ohsumi, Y., 1999. Apg16p is required for the function of the Apg12p-Apg5p conjugate in the yeast autophagy pathway. EMBO J 18, 3888–3896. https://doi.org/10.1093/emboj/18.14.3888

Mizushima, N., Noda, T., Yoshimori, T., Tanaka, Y., Ishii, T., George, M.D., Klionsky, D.J., Ohsumi, M., Ohsumi, Y., 1998. A protein conjugation system essential for autophagy. Nature 395, 395–398. https://doi.org/10.1038/26506

Münch, C., Bertolotti, A., 2012. Propagation of the Prion Phenomenon: Beyond the Seeding Principle. Journal of Molecular Biology, Amyloid Structure, Function, and Molecular Mechanisms (Part II) 421, 491–498. https://doi.org/10.1016/j.jmb.2011.12.061

Murakawa, T., Yamaguchi, O., Hashimoto, A., Hikoso, S., Takeda, T., Oka, T., Yasui, H., Ueda, H., Akazawa, Y., Nakayama, H., Taneike, M., Misaka, T., Omiya, S., Shah, A.M., Yamamoto, A., Nishida, K., Ohsumi, Y., Okamoto, K., Sakata, Y., Otsu, K., 2015. Bcl-2-like protein 13 is a mammalian Atg32 homologue that mediates mitophagy and mitochondrial fragmentation. Nat Commun 6, 7527. https://doi.org/10.1038/ncomms8527

Narendra, D., Kane, L.A., Hauser, D.N., Fearnley, I.M., Youle, R.J., 2010. p62/SQSTM1 is required for Parkin-induced mitochondrial clustering but not mitophagy; VDAC1 is dispensable for both. Autophagy 6, 1090–1106. https://doi.org/10/ftnzft

Nezis, I.P., Simonsen, A., Sagona, A.P., Finley, K., Gaumer, S., Contamine, D., Rusten, T.E., Stenmark, H., Brech, A., 2008. Ref(2)P, the Drosophila melanogaster homologue of mammalian p62, is required for the formation of protein aggregates in adult brain. Journal of Cell Biology 180, 1065–1071. https://doi.org/10.1083/jcb.200711108

Noda, N.N., Fujioka, Y., 2015. Atg1 family kinases in autophagy initiation. Cell Mol Life Sci 72, 3083–3096. https://doi.org/10.1007/s00018-015-1917-z

Noda, N.N., Ohsumi, Y., Inagaki, F., 2009. ATG systems from the protein structural point of view. Chem Rev 109, 1587–1598. https://doi.org/10.1021/cr800459r

Novak, I., Kirkin, V., McEwan, D.G., Zhang, J., Wild, P., Rozenknop, A., Rogov, V., Löhr, F., Popovic, D., Occhipinti, A., Reichert, A.S., Terzic, J., Dötsch, V., Ney, P.A., Dikic, I., 2010. Nix is a selective autophagy receptor for mitochondrial clearance. EMBO Rep 11, 45–51. https://doi.org/10.1038/embor.2009.256

Nowikovsky, K., Reipert, S., Devenish, R.J., Schweyen, R.J., 2007. Mdm38 protein depletion causes loss of mitochondrial K+/H+ exchange activity, osmotic swelling and mitophagy. Cell Death Differ 14, 1647–1656. https://doi.org/10.1038/sj.cdd.4402167

Obara, K., Sekito, T., Niimi, K., Ohsumi, Y., 2008. The Atg18-Atg2 complex is recruited to autophagic membranes via phosphatidylinositol 3-phosphate and exerts an essential function. J Biol Chem 283, 23972–23980. https://doi.org/10.1074/jbc.M803180200

Obara, K., Sekito, T., Ohsumi, Y., 2006. Assortment of Phosphatidylinositol 3-Kinase Complexes—Atg14p Directs Association of Complex I to the Pre-autophagosomal Structure in Saccharomyces cerevisiae. Mol Biol Cell 17, 1527–1539. https://doi.org/10.1091/mbc.E05-09-0841

Ochaba, J., Lukacsovich, T., Csikos, G., Zheng, S., Margulis, J., Salazar, L., Mao, K., Lau, A.L., Yeung, S.Y., Humbert, S., Saudou, F., Klionsky, D.J., Finkbeiner, S., Zeitlin, S.O., Marsh, J.L., Housman, D.E., Thompson, L.M., Steffan, J.S., 2014. Potential function for the Huntingtin protein as a scaffold for selective autophagy. PNAS 111, 16889–16894. https://doi.org/10.1073/pnas.1420103111

Ohsumi, Y., 2001. Molecular dissection of autophagy: two ubiquitin-like systems. Nat Rev Mol Cell Biol 2, 211–216. https://doi.org/10.1038/35056522

Okamoto, K., Kondo-Okamoto, N., Ohsumi, Y., 2009. Mitochondria-anchored receptor Atg32 mediates degradation of mitochondria via selective autophagy. Dev Cell 17, 87–97. https://doi.org/10.1016/j.devcel.2009.06.013

Okatsu, K., Oka, T., Iguchi, M., Imamura, K., Kosako, H., Tani, N., Kimura, M., Go, E., Koyano, F., Funayama, M., Shiba-Fukushima, K., Sato, S., Shimizu, H., Fukunaga, Y., Taniguchi, H., Komatsu, M., Hattori, N., Mihara, K., Tanaka, K., Matsuda, N., 2012. PINK1 autophosphorylation upon membrane potential dissipation is essential for Parkin recruitment to damaged mitochondria. Nat Commun 3, 1016. https://doi.org/10.1038/ncomms2016

Olichon, A., Emorine, L.J., Descoins, E., Pelloquin, L., Brichese, L., Gas, N., Guillou, E., Delettre, C., Valette, A., Hamel, C.P., Ducommun, B., Lenaers, G., Belenguer, P., 2002. The human dynamin-related protein OPA1 is anchored to the mitochondrial inner membrane facing the inter-membrane space. FEBS Letters 523, 171–176. https://doi.org/10.1016/S0014-5793(02)02985-X

Oliveira, J.M.A., 2010. Nature and cause of mitochondrial dysfunction in Huntington's disease: focusing on huntingtin and the striatum. J Neurochem 114, 1–12. https://doi.org/10.1111/j.1471-4159.2010.06741.x

Ordway, J.M., Tallaksen-Greene, S., Gutekunst, C.-A., Bernstein, E.M., Cearley, J.A., Wiener, H.W., Dure, L.S., Lindsey, R., Hersch, S.M., Jope, R.S., Albin, Roger.L., Detloff, P.J., 1997. Ectopically Expressed CAG Repeats Cause Intranuclear Inclusions and a Progressive Late Onset Neurological Phenotype in the Mouse. Cell 91, 753–763. https://doi.org/10.1016/S0092-8674(00)80464-X

Osawa, T., Ishii, Y., Noda, N.N., 2020. Human ATG2B possesses a lipid transfer activity which is accelerated by negatively charged lipids and WIPI4. Genes Cells 25, 65–70. https://doi.org/10.1111/gtc.12733

Osawa, T., Kotani, T., Kawaoka, T., Hirata, E., Suzuki, K., Nakatogawa, H., Ohsumi, Y., Noda, N.N., 2019. Atg2 mediates direct lipid transfer between membranes for autophagosome formation. Nat Struct Mol Biol 26, 281–288. https://doi.org/10.1038/s41594-019-0203-4

Pagliarini, D.J., Calvo, S.E., Chang, B., Sheth, S.A., Vafai, S.B., Ong, S.-E., Walford, G.A., Sugiana, C., Boneh, A., Chen, W.K., Hill, D.E., Vidal, M., Evans, J.G., Thorburn, D.R., Carr, S.A., Mootha, V.K., 2008. A mitochondrial protein compendium elucidates complex I disease biology. Cell 134, 112–123. https://doi.org/10.1016/j.cell.2008.06.016

Pal, A., Severin, F., Lommer, B., Shevchenko, A., Zerial, M., 2006. Huntingtin–HAP40 complex is a novel Rab5 effector that regulates early endosome motility and is up-regulated in Huntington's disease. J Cell Biol 172, 605–618. https://doi.org/10.1083/jcb.200509091

Panov, A.V., Gutekunst, C.-A., Leavitt, B.R., Hayden, M.R., Burke, J.R., Strittmatter, W.J., Greenamyre, J.T., 2002. Early mitochondrial calcium defects in Huntington's disease are a direct effect of polyglutamines. Nat Neurosci 5, 731–736. https://doi.org/10/fkfcr7

Pernas, L., Scorrano, L., 2016. Mito-Morphosis: Mitochondrial Fusion, Fission, and Cristae Remodeling as Key Mediators of Cellular Function. Annual Review of Physiology 78, 505–531. https://doi.org/10.1146/annurev-physiol-021115-105011

Piantadosi, C.A., Carraway, M.S., Babiker, A., Suliman, H.B., 2008. Heme oxygenase-1 regulates cardiac mitochondrial biogenesis via Nrf2-mediated transcriptional control of nuclear respiratory factor-1. Circ Res 103, 1232–1240. https://doi.org/10.1161/01.RES.0000338597.71702.ad

Prusiner, S.B., 1998. Prions. Proc Natl Acad Sci U S A 95, 13363–13383.

Qi, X., Qvit, N., Su, Y.-C., Mochly-Rosen, D., 2013. A novel Drp1 inhibitor diminishes aberrant mitochondrial fission and neurotoxicity. J Cell Sci 126, 789–802. https://doi.org/10.1242/jcs.114439

Quinti, L., Casale, M., Moniot, S., Pais, T.F., Van Kanegan, M.J., Kaltenbach, L.S., Pallos, J., Lim, R.G., Naidu, S.D., Runne, H., Meisel, L., Rauf, N.A., Leyfer, D., Maxwell, M.M., Saiah, E., Landers, J.E., Luthi-Carter, R., Abagyan, R., Dinkova-Kostova, A.T., Steegborn, C., Marsh, J.L., Lo, D.C., Thompson, L.M., Kazantsev, A.G., 2016. SIRT2- and NRF2-Targeting Thiazole-Containing Compound with Therapeutic Activity in Huntington's Disease Models. Cell Chemical Biology 23, 849–861. https://doi.org/10.1016/j.chembiol.2016.05.015

Quinti, L., Naidu, S.D., Träger, U., Chen, X., Kegel-Gleason, K., Llères, D., Connolly, C., Chopra, V., Low, C., Moniot, S., Sapp, E., Tousley, A.R., Vodicka, P., Kanegan, M.J.V., Kaltenbach, L.S., Crawford, L.A., Fuszard, M., Higgins, M., Miller, J.R.C., Farmer, R.E., Potluri, V., Samajdar, S., Meisel, L., Zhang, N., Snyder, A., Stein, R., Hersch, S.M., Ellerby, L.M., Weerapana, E., Schwarzschild, M.A., Steegborn, C., Leavitt, B.R., Degterev, A., Tabrizi, S.J., Lo, D.C., DiFiglia, M., Thompson, L.M., Dinkova-Kostova, A.T., Kazantsev, A.G., 2017. KEAP1-modifying small

molecule reveals muted NRF2 signaling responses in neural stem cells from Huntington's disease patients. PNAS 114, E4676–E4685. https://doi.org/10.1073/pnas.1614943114
Rigamonti, D., Bauer, J.H., De-Fraja, C., Conti, L., Sipione, S., Sciorati, C., Clementi, E., Hackam, A., Hayden, M.R., Li, Y., Cooper, J.K., Ross, C.A., Govoni, S., Vincenz, C., Cattaneo, E., 2000. Wild-Type Huntingtin Protects from Apoptosis Upstream of Caspase-3. J. Neurosci. 20, 3705–3713. https://doi.org/10/gf7hpk
Riva, L., Koeva, M., Yildirim, F., Pirhaji, L., Dinesh, D., Mazor, T., Duennwald, M.L., Fraenkel, E., 2012. Polyglutamine Expanded Huntingtin Dramatically Alters the Genome-Wide Binding of HSF1. Journal of Huntington's Disease 1, 33–45. https://doi.org/10.3233/JHD-2012-120020
Rubinsztein, D.C., Barton, D.E., Davison, B.C.C., Ferguson-Smith, M.A., 1993. Analysis of the huntingtin gene reveals a trinucleotide-length polymorphism in the region of the gene that contains two CCG-rich stretches and a correlation between decreased age of onset of Huntington's disease and CAG repeat number. Human Molecular Genetics 2, 1713–1715. https://doi.org/10.1093/hmg/2.10.1713
Rui, Y.-N., Xu, Z., Patel, B., Chen, Z., Chen, D., Tito, A., David, G., Sun, Y., Stimming, E.F., Bellen, H.J., Cuervo, A.M., Zhang, S., 2015. Huntingtin functions as a scaffold for selective macroautophagy. Nat Cell Biol 17, 262–275. https://doi.org/10.1038/ncb3101
Saft, C., Zange, J., Andrich, J., Müller, K., Lindenberg, K., Landwehrmeyer, B., Vorgerd, M., Kraus, P.H., Przuntek, H., Schöls, L., 2005. Mitochondrial impairment in patients and asymptomatic mutation carriers of Huntington's disease. Movement Disorders 20, 674–679. https://doi.org/10.1002/mds.20373
Sandoval, H., Thiagarajan, P., Dasgupta, S.K., Schumacher, A., Prchal, J.T., Chen, M., Wang, J., 2008. Essential role for Nix in autophagic maturation of erythroid cells. Nature 454, 232–235. https://doi.org/10.1038/nature07006
Scarpulla, R.C., 2011. Metabolic control of mitochondrial biogenesis through the PGC-1 family regulatory network. Biochimica et Biophysica Acta (BBA) - Molecular Cell Research, Mitochondria and Cardioprotection 1813, 1269–1278. https://doi.org/10/ccfc6j
Schwamborn, K., Weil, R., Courtois, G., Whiteside, S.T., Israël, A., 2000. Phorbol Esters and Cytokines Regulate the Expression of theNEMO-related Protein, a Molecule Involved in a NF-κB-independent Pathway. J. Biol. Chem. 275, 22780–22789. https://doi.org/10.1074/jbc.M001500200
Schweers, R.L., Zhang, J., Randall, M.S., Loyd, M.R., Li, W., Dorsey, F.C., Kundu, M., Opferman, J.T., Cleveland, J.L., Miller, J.L., Ney, P.A., 2007. NIX is required for programmed mitochondrial clearance during reticulocyte maturation. Proceedings of the National Academy of Sciences 104, 19500–19505. https://doi.org/10.1073/pnas.0708818104
Sharma, M., Jarquín, U.N.R., Rivera, O., Kazantzis, M., Eshraghi, M., Shahani, N., Sharma, V., Tapia, R., Subramaniam, S., 2019. Rhes, a striatal-enriched protein, promotes mitophagy via Nix. PNAS 116, 23760–23771. https://doi.org/10.1073/pnas.1912868116
Shintani, T., Mizushima, N., Ogawa, Y., Matsuura, A., Noda, T., Ohsumi, Y., 1999. Apg10p, a novel protein-conjugating enzyme essential for autophagy in yeast. EMBO J 18, 5234–5241. https://doi.org/10.1093/emboj/18.19.5234
Shirendeb, U., Reddy, A.P., Manczak, M., Calkins, M.J., Mao, P., Tagle, D.A., Hemachandra Reddy, P., 2011. Abnormal mitochondrial dynamics, mitochondrial loss and mutant huntingtin oligomers in Huntington's disease: implications for selective neuronal damage. Hum Mol Genet 20, 1438–1455. https://doi.org/10.1093/hmg/ddr024
Shirendeb, U.P., Calkins, M.J., Manczak, M., Anekonda, V., Dufour, B., McBride, J.L., Mao, P., Reddy, P.H., 2012. Mutant huntingtin's interaction with mitochondrial protein Drp1 impairs mitochondrial biogenesis and causes defective axonal transport and synaptic degeneration in Huntington's disease. Hum Mol Genet 21, 406–420. https://doi.org/10.1093/hmg/ddr475
Sittler, A., Wälter, S., Wedemeyer, N., Hasenbank, R., Scherzinger, E., Eickhoff, H., Bates, G.P., Lehrach, H., Wanker, E.E., 1998. SH3GL3 associates with the Huntingtin exon 1 protein and

promotes the formation of polygln-containing protein aggregates. Mol Cell 2, 427–436. https://doi.org/10.1016/s1097-2765(00)80142-2
Šonský, I., Vodička, P., Vodičková Kepková, K., Hansíková, H., 2021. Mitophagy in Huntington's disease. Neurochemistry International 149, 105147. https://doi.org/10.1016/j.neuint.2021.105147
Steffan, J.S., Kazantsev, A., Spasic-Boskovic, O., Greenwald, M., Zhu, Y.-Z., Gohler, H., Wanker, E.E., Bates, G.P., Housman, D.E., Thompson, L.M., 2000. The Huntington's disease protein interacts with p53 and CREB-binding protein and represses transcription. Proceedings of the National Academy of Sciences 97, 6763–6768. https://doi.org/10.1073/pnas.100110097
Stolz, A., Ernst, A., Dikic, I., 2014. Cargo recognition and trafficking in selective autophagy. Nature Cell Biology 16, 495–501. https://doi.org/10/f543bk
Subramaniam, S., 2020. Exaggerated mitophagy: a weapon of striatal destruction in the brain? Biochem Soc Trans 48, 709–717. https://doi.org/10.1042/BST20191283
Sudhakar, C., Nagabhushana, A., Jain, N., Swarup, G., 2009. NF-κB Mediates Tumor Necrosis Factor α-Induced Expression of Optineurin, a Negative Regulator of NF-κB. PLoS One 4. https://doi.org/10.1371/journal.pone.0005114
Sun, N., Youle, R.J., Finkel, T., 2016. The Mitochondrial Basis of Aging. Molecular Cell 61, 654–666. https://doi.org/10.1016/j.molcel.2016.01.028
Suzuki, K., Akioka, M., Kondo-Kakuta, C., Yamamoto, H., Ohsumi, Y., 2013. Fine mapping of autophagy-related proteins during autophagosome formation in Saccharomyces cerevisiae. J Cell Sci 126, 2534–2544. https://doi.org/10.1242/jcs.122960
Suzuki, K., Kirisako, T., Kamada, Y., Mizushima, N., Noda, T., Ohsumi, Y., 2001. The pre-autophagosomal structure organized by concerted functions of APG genes is essential for autophagosome formation. EMBO J 20, 5971–5981. https://doi.org/10.1093/emboj/20.21.5971
Suzuki, K., Kubota, Y., Sekito, T., Ohsumi, Y., 2007. Hierarchy of Atg proteins in pre-autophagosomal structure organization. Genes Cells 12, 209–218. https://doi.org/10.1111/j.1365-2443.2007.01050.x
Tabrizi, S.J., Cleeter, M.W., Xuereb, J., Taanman, J.W., Cooper, J.M., Schapira, A.H., 1999. Biochemical abnormalities and excitotoxicity in Huntington's disease brain. Ann Neurol 45, 25–32. https://doi.org/10.1002/1531-8249(199901)45:1<25::aid-art6>3.0.co;2-e
Tabrizi, S.J., Schobel, S., Gantman, E.C., Mansbach, A., Borowsky, B., Konstantinova, P., Mestre, T.A., Panagoulias, J., Ross, C.A., Zauderer, M., Mullin, A.P., Romero, K., Sivakumaran, S., Turner, E.C., Long, J.D., Sampaio, C., 2022. A biological classification of Huntington's disease: the Integrated Staging System. The Lancet Neurology 21, 632–644. https://doi.org/10.1016/S1474-4422(22)00120-X
Tal, R., Winter, G., Ecker, N., Klionsky, D.J., Abeliovich, H., 2007. Aup1p, a yeast mitochondrial protein phosphatase homolog, is required for efficient stationary phase mitophagy and cell survival. J Biol Chem 282, 5617–5624. https://doi.org/10.1074/jbc.M605940200
Tracy, K., Dibling, B.C., Spike, B.T., Knabb, J.R., Schumacker, P., Macleod, K.F., 2007. BNIP3 is an RB/E2F target gene required for hypoxia-induced autophagy. Mol Cell Biol 27, 6229–6242. https://doi.org/10.1128/MCB.02246-06
Tsiper, M.V., Sturgis, J., Avramova, L.V., Parakh, S., Fatig, R., Juan-García, A., Li, N., Rajwa, B., Narayanan, P., Jr, C.W.Q., Robinson, J.P., Davisson, V.J., 2012. Differential Mitochondrial Toxicity Screening and Multi-Parametric Data Analysis. PLOS ONE 7, e45226. https://doi.org/10.1371/journal.pone.0045226
Tsukada, M., Ohsumi, Y., 1993. Isolation and characterization of autophagy-defective mutants of Saccharomyces cerevisiae. FEBS Lett 333, 169–174. https://doi.org/10.1016/0014-5793(93)80398-e
Twig, G., Elorza, A., Molina, A.J.A., Mohamed, H., Wikstrom, J.D., Walzer, G., Stiles, L., Haigh, S.E., Katz, S., Las, G., Alroy, J., Wu, M., Py, B.F., Yuan, J., Deeney, J.T., Corkey, B.E., Shirihai, O.S.,

2008. Fission and selective fusion govern mitochondrial segregation and elimination by autophagy. EMBO J 27, 433–446. https://doi.org/10.1038/sj.emboj.7601963
Valverde, D.P., Yu, S., Boggavarapu, V., Kumar, N., Lees, J.A., Walz, T., Reinisch, K.M., Melia, T.J., 2019. ATG2 transports lipids to promote autophagosome biogenesis. J Cell Biol 218, 1787–1798. https://doi.org/10.1083/jcb.201811139
Wang, D.B., Kinoshita, C., Kinoshita, Y., Morrison, R.S., 2014. p53 and Mitochondrial Function in Neurons. Biochim Biophys Acta 1842, 1186–1197. https://doi.org/10.1016/j.bbadis.2013.12.015
Wanker, E.E., 2002. Hip1 and Hippi participate in a novel cell death-signaling pathway. Dev Cell 2, 126–128. https://doi.org/10.1016/s1534-5807(02)00121-1
Wells, G., 2015. Peptide and small molecule inhibitors of the Keap1-Nrf2 protein-protein interaction. Biochem Soc Trans 43, 674–679. https://doi.org/10.1042/BST20150051
Westermann, B., 2010. Mitochondrial fusion and fission in cell life and death. Nat Rev Mol Cell Biol 11, 872–884. https://doi.org/10.1038/nrm3013
Wong, Y.C., Holzbaur, E.L.F., 2014. The Regulation of Autophagosome Dynamics by Huntingtin and HAP1 Is Disrupted by Expression of Mutant Huntingtin, Leading to Defective Cargo Degradation. J Neurosci 34, 1293–1305. https://doi.org/10.1523/JNEUROSCI.1870-13.2014
Wu, H., Xue, D., Chen, G., Han, Z., Huang, L., Zhu, C., Wang, X., Jin, H., Wang, J., Zhu, Y., Liu, L., Chen, Q., 2014. The BCL2L1 and PGAM5 axis defines hypoxia-induced receptor-mediated mitophagy. Autophagy 10, 1712–1725. https://doi.org/10.4161/auto.29568
Wu, Z., Puigserver, P., Andersson, U., Zhang, C., Adelmant, G., Mootha, V., Troy, A., Cinti, S., Lowell, B., Scarpulla, R.C., Spiegelman, B.M., 1999. Mechanisms controlling mitochondrial biogenesis and respiration through the thermogenic coactivator PGC-1. Cell 98, 115–124. https://doi.org/10.1016/S0092-8674(00)80611-X
Yamano, K., Youle, R.J., 2013. PINK1 is degraded through the N-end rule pathway. Autophagy 9, 1758–1769. https://doi.org/10.4161/auto.24633
Yano, H., Baranov, S.V., Baranova, O.V., Kim, J., Pan, Y., Yablonska, S., Carlisle, D.L., Ferrante, R.J., Kim, A.H., Friedlander, R.M., 2014. Inhibition of mitochondrial protein import by mutant huntingtin. Nat Neurosci 17, 822–831. https://doi.org/10.1038/nn.3721
Zhang, Y., Talalay, P., Cho, C.G., Posner, G.H., 1992. A major inducer of anticarcinogenic protective enzymes from broccoli: isolation and elucidation of structure. Proc Natl Acad Sci U S A 89, 2399–2403.
Zuccato, C., Ciammola, A., Rigamonti, D., Leavitt, B.R., Goffredo, D., Conti, L., MacDonald, M.E., Friedlander, R.M., Silani, V., Hayden, M.R., Timmusk, T., Sipione, S., Cattaneo, E., 2001. Loss of huntingtin-mediated BDNF gene transcription in Huntington's disease. Science 293, 493–498. https://doi.org/10.1126/science.1059581

9 Supplementary Data

Table S1: Data from chart showing analysis of immunoblot data normalized for GAPDH (Fig. 6)

Protein	Cell Type	Treatment	Average of Values	±SD
LC3B	controls	Vehicle	0,08	0,01
LC3B	controls	MIND4-17	0,08	0,02
LC3B	patients	Vehicle	0,50	0,42
LC3B	patients	MIND4-17	1,19	0,24
SQSTM1/p62	controls	Vehicle	0,11	0,03
SQSTM1/p62	controls	MIND4-17	0,33	0,05
SQSTM1/p62	patients	Vehicle	0,24	0,13
SQSTM1/p62	patients	MIND4-17	1,47	0,34
NDP52	controls	Vehicle	0,35	0,06
NDP52	controls	MIND4-17	0,42	0,04
NDP52	patients	Vehicle	0,28	0,08
NDP52	patients	MIND4-17	0,48	0,17
OPTN	controls	Vehicle	0,64	0,28
OPTN	controls	MIND4-17	0,77	0,26
OPTN	patients	Vehicle	1,05	0,09
OPTN	patients	MIND4-17	0,64	0,19

Table S2: Data from chart showing analysis of respiratory chain activities normalized for citrate synthase (Fig. 9)

Complex	Cell Type	Treatment	Average of Values	±SD
Complex I	controls	Vehicle	1,07	0,33
Complex I	controls	MIND4-17	1,49	0,51
Complex I	patients	Vehicle	0,75	0,07
Complex I	patients	MIND4-17	1,20	0,14
Complex II	controls	Vehicle	0,54	0,16
Complex II	controls	MIND4-17	0,47	0,11
Complex II	patients	Vehicle	0,62	0,16
Complex II	patients	MIND4-17	0,48	0,06
Complex III	controls	Vehicle	1,55	0,78
Complex III	controls	MIND4-17	1,60	1,04
Complex III	patients	Vehicle	1,58	0,47
Complex III	patients	MIND4-17	1,41	0,35
Complex IV	controls	Vehicle	0,47	0,13
Complex IV	controls	MIND4-17	0,48	0,16
Complex IV	patients	Vehicle	0,41	0,05
Complex IV	patients	MIND4-17	0,53	0,03

Table S3: Data from chart showing analysis of oxygen consumption measured by Seahorse XFe24 analyzer (Fig. 10)

Measurement	Cell Type	Treatment	Average of Values (pmol/min/35000 cells)	±SD
Routine respiration	controls	vehicle	110,79	11,11
Routine respiration	controls	MIND4-17	102,76	16,90
Routine respiration	patients	vehicle	147,40	8,97
Routine respiration	patients	MIND4-17	122,55	18,85
Proton leak	controls	vehicle	16,93	4,58
Proton leak	controls	MIND4-17	28,88	18,20
Proton leak	patients	vehicle	19,93	4,01
Proton leak	patients	MIND4-17	16,68	3,92
ATP production	controls	vehicle	93,86	10,99
ATP production	controls	MIND4-17	86,13	16,73
ATP production	patients	vehicle	127,48	8,50
ATP production	patients	MIND4-17	105,87	15,86
Maximal capacity	controls	vehicle	143,19	27,60
Maximal capacity	controls	MIND4-17	123,48	36,53
Maximal capacity	patients	vehicle	221,59	23,70
Maximal capacity	patients	MIND4-17	171,97	38,10
Spare capacity	controls	vehicle	32,40	18,37
Spare capacity	controls	MIND4-17	20,72	20,84
Spare capacity	patients	vehicle	74,19	19,06
Spare capacity	patients	MIND4-17	49,43	23,35

Table S4: Data from chart showing analysis of extracellular acidification ratio measured by Seahorse XFe24 analyzer (Fig. 11)

Measurement	Cell Type	Treatment	Average of Values (mpH/min/35000 cells)	±SD
Glycolysis	controls	vehicle	35,18	17,86
Glycolysis	controls	MIND4-17	29,45	19,17
Glycolysis	patients	vehicle	35,53	17,35
Glycolysis	patients	MIND4-17	41,87	23,62
Glycolytic capacity	controls	vehicle	63,20	37,13
Glycolytic capacity	controls	MIND4-17	50,80	33,71
Glycolytic capacity	patients	vehicle	74,03	38,57
Glycolytic capacity	patients	MIND4-17	69,53	34,14
Glycolytic reserve	controls	vehicle	28,02	19,74
Glycolytic reserve	controls	MIND4-17	21,36	15,29
Glycolytic reserve	patients	vehicle	38,49	28,55
Glycolytic reserve	patients	MIND4-17	27,66	12,13

Table S5: Data from chart showing analysis of Manders' overlap coefficient (Fig. 12)

Measurment	Cell Type	Treatment	Average of Values	±SD
Manders' overlap coefficient	controls	vehicle	0,23	0,07
Manders' overlap coefficient	controls	MIND4-17	0,42	0,12
Manders' overlap coefficient	patients	vehicle	0,17	0,08
Manders' overlap coefficient	patients	MIND4-17	0,37	0,11

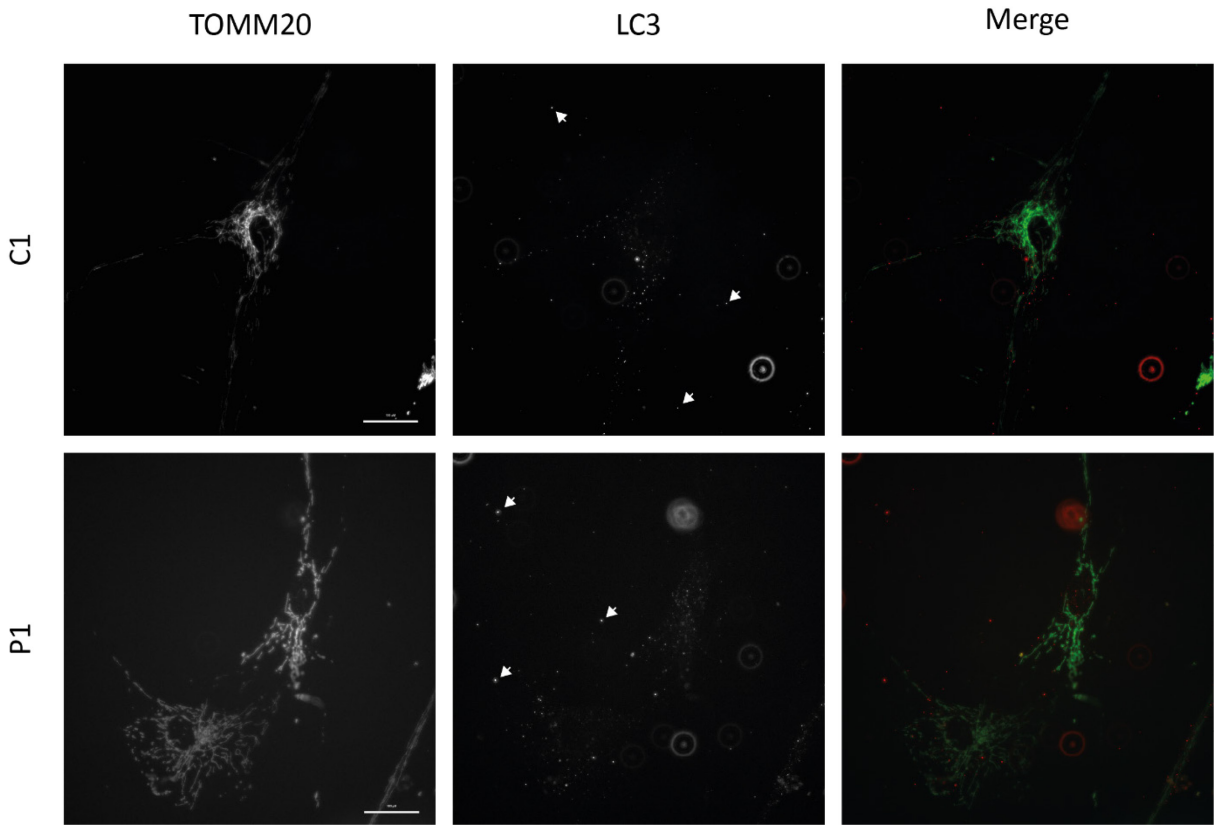

Fig. S1. Unspecific labeling of LC3 antibody. Cells were stained with anti-TOMM20 and anti-LC3 antibodies. Arrowheads show unspecific signal of anti-LC3 antibody outside cells. Scale bar: 100 µM. C – control fibroblasts, P – fibroblasts from HD patients

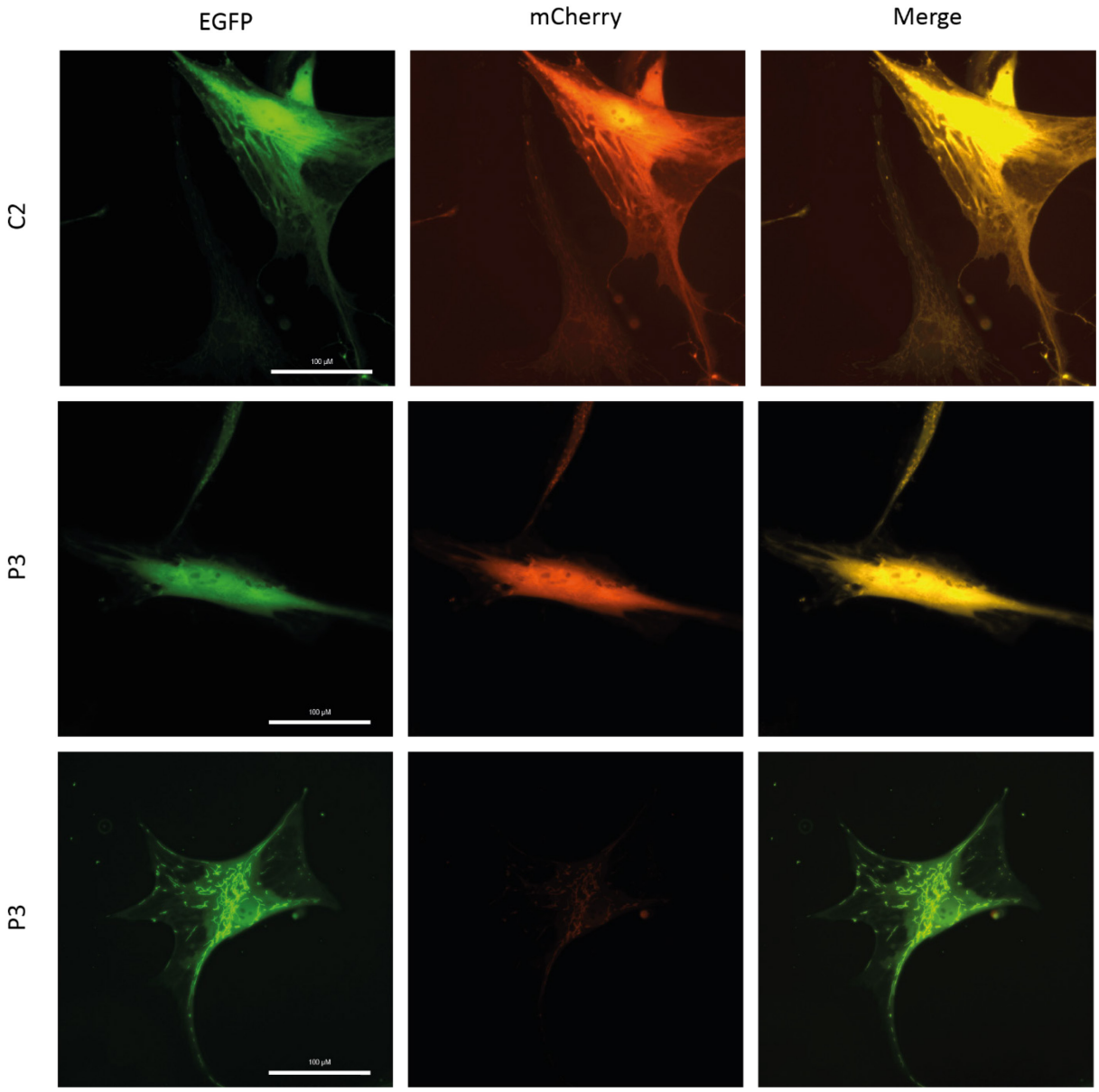

Fig. S2. Analysis of pCLBW cox8 EGFP mCherry expression. Majority of cells exhibited diffuse signal in both emission spectra (First two rows). In some cells, the protein successfully marked only mitochondria (Third row). However, the signal was often significantly weaker compared to the diffuse signal in most cells (First row of images). Scale bar: 100 µM. C – control fibroblasts, P – fibroblasts from HD patients